The Role Of Vascular Interfaces In Age-Related Macular Degeneration

PhD Thesis

Ferenc Balazs Sallo, MD

Semmelweis University,
School of Doctoral Studies
Academic Medical Sciences Programme 2/10

Supervisor:	Prof Dr György Salacz, MD, PhD
Opponents:	Prof Dr Bálint Kovács MD, PhD Dr András Papp MD, PhD
Examination Board	
Chairman:	Prof Dr Imre Oláh MD, PhD, DSc
Members:	Dr Ágnes Füst MD, PhD Dr Ágnes Kerényi MD, PhD Dr Péter Vámosi MD, PhD

Budapest

2009

CONTENTS page

ABBREVIATIONS USED IN THIS THESIS

[α-32P]dCTP	phosphorous isotope 32 - labelled deooxycytidine triphosphate
A2E	N-retinylidene- N-retinyl-ethanolamine
ABCA1	ATP-binding cassette transporter
AMD	age-related macular degeneration
ANSI	American National Standards Institute
apo A1	apolipoprotein A1
apo B	apolipoprotein B
apo E	apolipoprotein E
BCEA	bivariate contour ellipse area
BCVA	best corrected visual acuity
BlamD	basal laminar deposit(s)
BlinD	basal linear deposit(s)
BM	basement membrane
bp	base pair
BrM	Bruch's Membrane
C5	Complement factor 5
C57BL/6	C57 black 6 (a common inbred strain of laboratory mouse)
CCD	charge coupled device
CD	cluster of differentiation
CD36	cluster of differentiation 36 (membrane surface protein)
cDNA	complementary deoxyribonucleic acid
CETP	cholesteryl ester transfer protein
CH	choriocapillaris
CMBB	coated membrane-bound bodies
CNV	choroidal neovascularisation
cSLO	confocal scanning laser ophthalmoscope
CVL	coated vesicle-like bodies
dB	decibel
DC	dendritic cell
DD	disc diameter

EC	esterified cholesterol
ECM	extracellular matrix
ED	electron density
EM	electron microscopy
F1	first generation (of a hybrid)
FAF	fundus autofluorescence
FBM	fibrous banded material
FMM	fine matrix mapping
GA	Geographic Atrophy
GAG	glycosaminoglycan
GmbH	Gesellschaft mit beschränkter Haftung
HDL	high-density lipoprotein
HFA	Humphrey Field Analyzer
HFC	high-fat and cholesterol (diet)
HLA-DR	a major histocompatibility complex class II cell surface receptor
IC	International classification
ICL	inner collagenous layer (of BrM)
IPM	inter-photoreceptor matrix
kDa	kiloDalton
λ	wavelength
λ_{ex}	excitation wavelength
LASER	light amplification by stimulated emission of radiation
LCAT	Lecithin-cholesterol acyltransferase
LDL	low-density lipoprotein
LDL-R	LDL receptor
LF	lipofuscin
LLP	lipoprotein-like particle
LM	light microscopy
LpL	lipoprotein lipase
Ltd.	Limited (company)
MHC	major histocompatibility complex
MPS	Macular Photocoagulation Study

mRNA	messenger ribonucleic acid
NV	neovascularisation
OCL	outer collagenous layer (of BrM)
OPL	outer plexiform layer (of the retina)
OTAP	osmium-tannic acid-paraphenylenediamine
PAL	phase alternating line
PBS	phosphate buffered saline
PCR	polymerase chain reaction
PED	pigment epithelial detachment
PG	proteoglycan
POS	photoreceptor outer segment
QFDE	quick freeze/deep-etch
QRT-PCR	quantitative reverse transcription polymerase chain reaction
RAP	retinal angiomatous proliferation
RPE	Retinal Pigment Epithelium
RR	Relative Risk
RT-PCR	reverse transcription polymerase chain reaction
SCI	stereo colour image
SD	standard deviation
SG	small granule
SLO	scanning laser ophthalmoscope
SMase	sphyngomyelinase
SMC	smooth muscle cell
SPSS	Statistical Package for the Social Sciences
SR-BI	Scavenger receptor class B, type I
SR-BII	Scavenger receptor class B, type II
SVHS	super video home system
TEM	transmission electron microscopy
TGF-β	transforming growth factor β
TNF-α	tumor necrosis factor α
UC	unesterified cholesterol
VLDL	very low-density lipoprotein

INTRODUCTION

Tissue-vascular interfaces constitute frontier zones with intricate mechanisms of exchange and a delicate balance of supply and demand. Even slight disturbances in either may lead to severe disease. Within the retina, frontier zones are twofold, an inner, the retinal vasculature and an outer, towards the choroidal circulation. The macula constitutes a special area with high oxygen consumption, high choroidal capillary flow and asymmetrical metabolic supply at the centre. Within the foveal avascular zone, photoreceptors are especially heavily dependent on the choroidal circulation. This is also the region with the highest photoreceptor density and the retinal area responsible for clear sharp central vision, essential for most basic activities of daily life, its loss devastates quality of life on a very fundamental level. Interposed between the metabolically highly active photoreceptors and retinal pigment epithelium (RPE) and their major source of nutrition, the choriocapillaris is Bruch's Membrane (BrM). In addition to acting as a support element and an attachment site for the RPE, BrM also provides a semi-permeable filtration barrier through which metabolic exchange takes place. Nutrients pass from the choriocapillaris to the RPE and photoreceptors and cellular metabolic end-products pass in the opposite direction. Abnormalities of this outer vascular interface of the retina are at the core of many macular and peripheral, inherited and acquired disease states including Age-Related Macular Degeneration (AMD), the leading cause of severe irreversible central visual loss among the elderly in western industrialized countries [1]. Its prevalence is estimated to increase substantially in the coming decades [2]. The aetiology and pathogenesis of AMD are poorly understood. Although novel and promising anti-angiogenic therapies have recently emerged, their long-term efficacy and economic viability remains to be conclusively proven. With an increasing mean life expectancy within the global population, AMD remains a significant socio-economic burden and thus warrants investigations not just into immediate and profitable therapeutic options but also into the basic underlying mechanisms and etiological factors, in search of a definitive solution. In this PhD thesis I would like to present clinical and experimental investigations into the role of pathological changes within the outer vascular interface of the retina with a focus on Age-Related Macular Degeneration.

1. Functional aspects of drusen regression in AMD.

1.1. AMD - Aetiology and pathogenesis.

The aetiology and pathogenesis of AMD are poorly understood. AMD is currently considered a heterogenous, multifactorial disease, in which the interactions of genetic and environmental factors are necessary for the development of the disease [3-6]. Risk factors identified by epidemiologic studies include age, some genetic variants, smoking and the presence of macular soft drusen with high-risk characteristics [1, 7-12]. AMD affects primarily the RPE, Bruch's Membrane (BrM) and choriocapillaris (the RPE/BrM complex). Early AMD is characterized by the accumulation of lipid-rich deposits under the retinal pigment epithelium (RPE) and within Bruch's membrane (BrM) [13, 14]. Sub-RPE deposits may be diffuse (Basal Deposits, Laminar or Linear) or focal (Drusen) [15]. Basal Laminar Deposits (BlamD) are currently defined as a layer of amorphous, granular material of intermediate electron density, with wide-spaced collagen, located between the RPE plasma membrane and basement membrane and are not considered to be specific for AMD [16, 17]. Basal linear deposits (BlinD) are composed of densely packed, electron-dense, membrane-bounded and non membrane-bounded vesicles located along with Drusen (and in late, exudative AMD, type 1 choroidal neovascular membranes) between the RPE basement membrane and the inner collagenous layer of Bruch's Membrane [17-19].

The origin and mechanism of debris deposition are little known. All three types of deposits are associated with aging as well as AMD and their causative factors, pathogenesis and relative significance remain unclear. A consequential reduction in hydraulic conductivity may impede transport through BrM and thus contribute to the pathogenesis of lesions seen in late disease, along with the accumulation and deposition of lipofuscin, progressive oxidative damage, and the involvement of immune-mediated pathways [3, 4].

1.2. Clinical manifestations of AMD

Clinically, early AMD is characterized by abnormalities of the retinal pigment epithelium (hyper- and hypopigmentation), soft drusen and mild visual symptoms, predominantly under dark-adapted conditions [20, 21]. Late AMD is dominated by

either an atrophy of the RPE and photoreceptors, Geographic Atrophy (GA) or neovascularisation (NV), from the choroid (choroidal neovascularisation, CNV) or the retina (Retinal Angiomatous Proliferation, RAP) characterised by exudation, haemorrhage, or subretinal fluid and a detachment of the neurosensory retina, inevitably with severe central function loss [20, 22]. CNV may also be presaged or accompanied by a detachment of the RPE (Pigment Epithelial Detachment, PED). Large and highly elevated PEDs can induce tangential stress and lead to a rupture (RPE tear) thereby directly leading to visual loss [23].

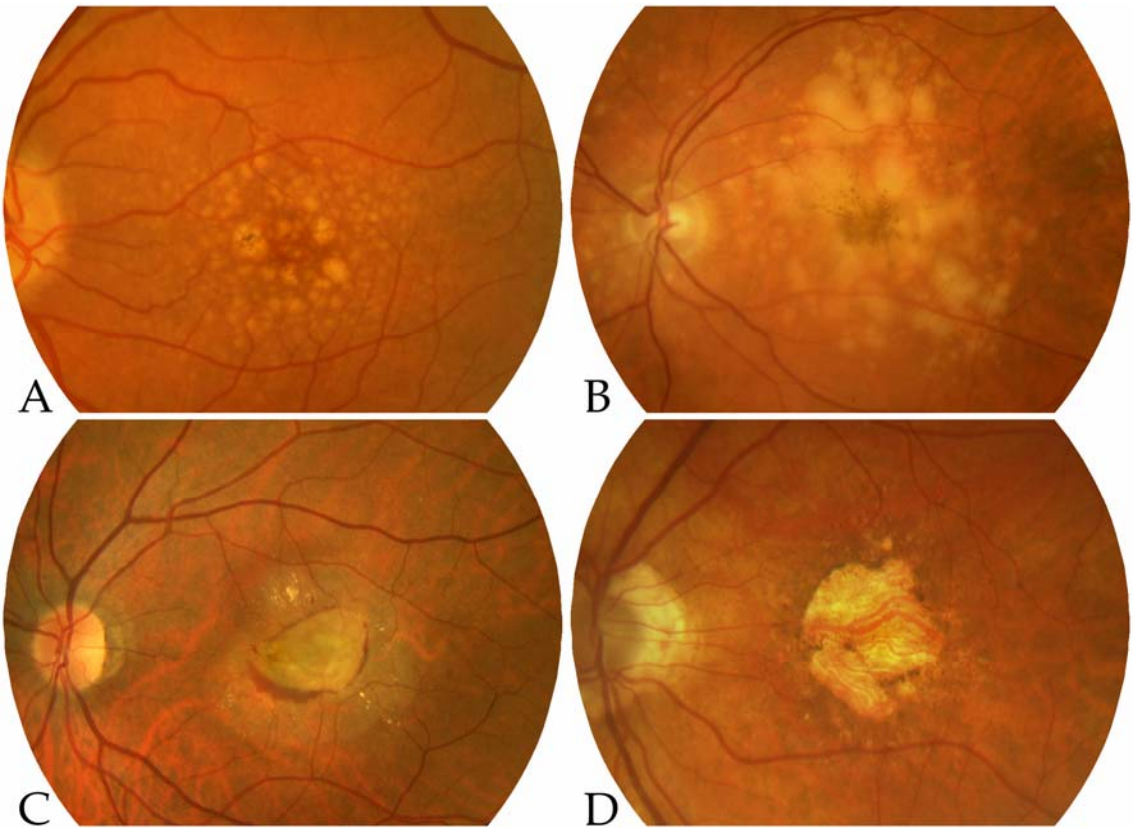

Figure 1. Major AMD phenotypes. A: Predominantly distinct large soft macular drusen with pigmentary changes in early AMD. B: Large confluent soft drusen with RPE hyperpigmentation. C: Choroidal neovascular membrane with subretinal exudtate and haemorrhage. D: An extensive area of Geographic Atrophy.

1.3. Drusen

Of the sub-RPE deposits, drusen alone are currently readily detectable clinically (in vivo), using widely available imaging techniques (Figure 1. A and C). Drusen are clinical hallmarks of AMD. In the earliest stage, they may be visible ophthalmoscopically as semi-translucent punctate dots in retroillumination. As the

overlying RPE thins, drusen are more obvious as yellow-white deposits. Clinically, drusen are classified morphologically either as hard or soft. Hard drusen are pinpoint yellow-white lesions, less than 63μm in diameter that appear as window defects on fluorescein angiography. In small numbers, they are not considered risk factors for the development of AMD [24], but numerous hard drusen are an independent risk factor for visual loss from AMD [25]. Soft drusen are larger (>125μm) and have indistinct edges with a tendency to become confluent. Typically drusen are clustered in the central macula. Sarks et al. presented a refined classification of drusen incorporating not only clinical characteristics, but also temporal evolution, histopathology, and angiographic findings [26].

A prospective study of patients with drusen in the fellow eyes of unilateral exudative AMD suggests that the risk of developing choroidal neovascularization in the second eye peaks at 4 years, with an increasing incidence of geographic atrophy thereafter [27]. The annual incidence of CNV ranges from 5–14%. Greater size, number and confluence of drusen were associated with higher rates of CNV [25]. The risk of legal blindness in the fellow eye of patients with unilateral visual loss from CNV is approximately 12% over 5 years [25]. In patients with bilateral drusen and good vision in both eyes, the annual incidence of exudative or atrophic lesions is approximately 8% over 3 years [28]. These patients have a cumulative risk of 14.5% of developing CNV over 4 years [29]. In this group, confluence of drusen, focal hyperpigmentation or atrophy, and delayed choroidal filling were strong risk factors. Four independent risk factors for the development of CNV in fellow eyes have been established from multivariate analyses in the Macular Photocoagulation Study (MPS) [9, 25]. The presence of five or more drusen seems to be the strongest predictor, with a relative risk of 2.1. Focal RPE hyperpigmentation has a relative risk of 2.0, followed by systemic hypertension (RR =1.7) and the finding of one or more large drusen (RR =1.5). Extramacular drusen also are a risk factor for the development of AMD [30].

Although the presence of macular soft drusen has been clearly and consistently identified by epidemiologic studies as a risk factor of late AMD and vision loss, their immediate significance in relation to photoreceptor health and function, and their predictive value for the outcome of the disease are still unclear [7-9, 12, 25, 28, 29, 31-33].

The natural history of soft drusen may involve an increase in size, area and confluence with subsequent neovascularisation, calcification (crystalline drusen) or fading and disappearance which is believed to be associated with atrophy of the overlying RPE and photoreceptors [8]. Interestingly, spontaneous resolution of large confluent drusen, hyperpigmentation, or nongeographic RPE atrophy was observed in a significant proportion of patients in a 5-year follow up of the Maryland Waterman study [34]. The functional and prognostic implications of true drusen regression, however, have not been demonstrated.

1.4. Functional characteristics of the retina in aging and AMD

Psychophysical studies of retinal sensitivity in aging and AMD indicate that rods may be at increased risk for degeneration. Older adults with no detectable fundus abnormalities, have reduced rod-mediated light sensitivity with a near uniform magnitude throughout the parafoveal region [35, 36]. In 80% of older adults evaluated, scotopic loss was not only greater than photopic impairment but also declined faster throughout adulthood than photopic sensitivity [36]. In early AMD patients, mean scotopic sensitivity within 18° of fixation was significantly lower than in age-matched controls without AMD [37]. The topography of sensitivity loss in the central 36° of the visual field varied considerably among individual patients with early AMD. Of the AMD patients with reduced light sensitivity in this region, 59% showed reduced scotopic sensitivity, 27% showed both reduced scotopic and photopic sensitivity, and only 14% had reduced photopic sensitivity in an isolated fasion. In 87% of these patients, the magnitude of mean scotopic sensitivity loss exceeded the magnitude of mean photopic sensitivity loss. The AMD-related deficit in scotopic sensitivity was most severe within 9° of fixation, corresponding to the parafovea and suggesting that the emergence of regional sensitivity impairments within this region may be an early sign of AMD [37].

Histopathologic studies have identified clear morphological correlates to these psychophysical findings. In young adults, rods outnumber cones 9:1 within the macula and 20:1 in the entire eye, so the macula can be considered cone-enriched but not cone-dominated. In the maculae of older adults without visible hallmarks of AMD (drusen and pigmentary changes) the number of cones in the cone-enriched part of the macula is

stable at approximately 32000/mm^2 throughout six decades [38]. In contrast, the number of macular rods in the same eyes decreases by 30%, with the greatest loss occurring within the parafovea (3.5–10° from fixation). In AMD eyes with large drusen and thick basal deposits the foveal cone mosaic appears similar to that of age-matched controls, and the total number of foveal cones is normal, while in the parafovea, cones appear enlarged and misshapen, and few rods remain [39]. In eyes with late ARM, nearly all surviving photoreceptors in the macula are cones, a reversal of the normal rod predominance. Preferential loss of rods over cones was found in 3 of 4 of early and late AMD eyes examined [40].

In addition to the reduced sensitivity of the rod system, the kinetics of rod function also change with aging and AMD [21, 41, 42]. The dark adaptation function describes the recovery of sensitivity after a bright flash of light and consists of an early portion exclusively mediated by cones, a transition to rod function (rod-cone break), and a later portion exclusively mediated by rods. In elderly adults with normal fundus appearance, the rod-mediated portion of dark adaptation is significantly slower than in younger adults [41]. In early AMD patients, rod-mediated dark adaptation is much slower (mean=13 minutes) than in normal age-matched controls and delays in rod-mediated dark adaptation are greater than those for cone-mediated dark adaptation. This however is not correlated with scotopic sensitivity in these patients, indicating that the mechanisms underlying these two aspects of rod function are not identical [36].

Taken together, these studies indicate that photoreceptor degeneration and loss occurs well before disease progresses to late AMD and the loss in aging, early AMD, and late AMD is greater for rods than for cones.

1.5. Fundus Autofluorescence

Abnormal fundus autofluorescence may also be considered a signature of RPE and photoreceptor injury [43]. Autofluorescent imaging of the ocular fundus relies on the stimulated emission of light from molecules in the retinal pigment epithelium, chiefly lipofuscin [44-46]. Lipofuscin (LF) is a diverse group of molecular species, yellow to brown in colour that accumulates in all postmitotic cells, especially in the RPE [47, 48]. Lipofuscin's complex mixture results from the oxidative breakdown of a number of different molecules, including polyunsaturated fatty acids, retinoids, and proteins.

Whereas the lipofuscin that is amassed by most non-proliferating cells is derived from autophagy [49], lipofuscin fluorophores of the retinal pigment epithelium originate, in large part, from incompletely digested photoreceptor outer segment discs [50-52], with 90% of the fluorescent material being generated from conjugates formed by retinoids of the visual cycle [53, 54]. In human RPE cells, lipofuscin accumulates with age within the lysosomal compartment and may occupy 20% to 33% of the free cytoplasmic space of the RPE cell at ages 70 years and above [55]. Excessive accumulation of LF also represents a common pathogenetic pathway in various monogenetic (including Best disease and Stargardt disease) as well as complex retinal diseases including AMD and is believed to precede photoreceptor degeneration [56-58].

Accumulating LF may exert toxic effects. Components of lipofuscin inhibit lysosomal protein degradation [59], are photoreactive [60, 61], are capable of producing a variety of reactive oxygen intermediates and other radicals [62] and lipofuscin may even induce apoptosis of the RPE [63].

RPE lipofuscin fluorophores that have been characterized so far are the bisretinoid fluorophore A2E and its isomers (13-(Z)-double-bond isomer iso-A2E, and other minor Z-isomers) [52, 64-67]. Spectrophotometric studies of RPE lipofuscin have however generally reported excitation spectra that are broader than that of A2E, with the excitation maximum of A2E occurring at slightly shorter wavelengths [68]. Consequently, the lipofuscin of RPE cells is likely to consist of a mixture of fluorophores, only some of which have been identified so far [69]. A2E has been shown, because of its amphiphilic properties, to exert detergent-like effects on cell membranes [63, 70-72] and exert inhibitory effects on the lysosomal proton pump, with a subsequent increase in lysosomal pH, inhibition of lysosomal enzymes, and impaired degradation of phagocytosed material [61, 73-76]. Lipofuscin is considered to be responsible for the sensitivity of the cell to blue-light damage and this effect may also be attributable to A2E [74, 77].

Photoreceptor function is dependent on normal RPE cell function for its contribution to the visual cycle and in particular for the constant phagocytosis of shed distal outer segment stacks, a process that maintains photoreceptor cell renewal. If LF inhibits degradative metabolism, the rate of phagocytosis of photoreceptor outer segment (POS) discs may be impaired. A negative-feedback mechanism had been

proposed, where in cells with LF-loaded secondary lysosomes would phagocytose less shed POS [75]. If these RPE cells were incapable of clearing obsolete tips of POS to a sufficient degree, it would be assumed that abnormal photoreceptor function would result. These may be the mechanisms or account for the association of increased LF in RPE and impaired photoreceptor function.

1.6. Fundus autofluorescence imaging and its limitations

Imaging the spatial distribution of autofluorescence in the fundus (fundus autofluorescence, FAF) represents an additional tool for evaluating RPE health. [54] The intensity of fundus autofluorescence parallels the amount and distribution of lipofuscin. Thus the amount of autofluorescence, is a signature of previous, and possible future oxidative injury [43, 58].

Visualised by a confocal Scanning Laser Ophthalmoscope (cSLO), using an argon laser blue line (λ=488nm) for excitation and a broad band-pass filter with a short wavelength cut off at 521nm for recording autofluorescence has a number of advantages [54]. Media opacities and, above all, lens opacification may result in FAF images that cannot be analyzed adequately. Yellowish discolouration of the lens in cataract formation is associated with the absorption of the wavelength range used for excitation (i.e., 488nm). Confocal scanning laser ophthalmoscopic imaging has the advantage over conventional fundus cameras that it helps reject the competing autofluorescence of the crystalline lens, because the plane of the detection system is conjugate to the fundus, and light from alternate planes is rejected [53].

Individual SLO images are inherently noisy because of the light source used and the resultant autofluorescent signal is weak. To compensate for this, the computerized image capture system has the facility to overlay and average a number of individual scans thus amplifying the signal and reducing random noise. Absolute quantification of the FAF signal however is difficult but not necessary for analyzing variations in the topographic distribution of FAF changes.

Alternative fluorophores to RPE lipofuscin are present in various anatomic layers of the posterior pole. Bruch's membrane has been shown to possess autofluorescent properties [46, 51, 78], (Figure 2), however, the excitation and emission spectra are

different, although with slight overlap, from those of lipofuscin in RPE cells (compare Figures 2 and 3).

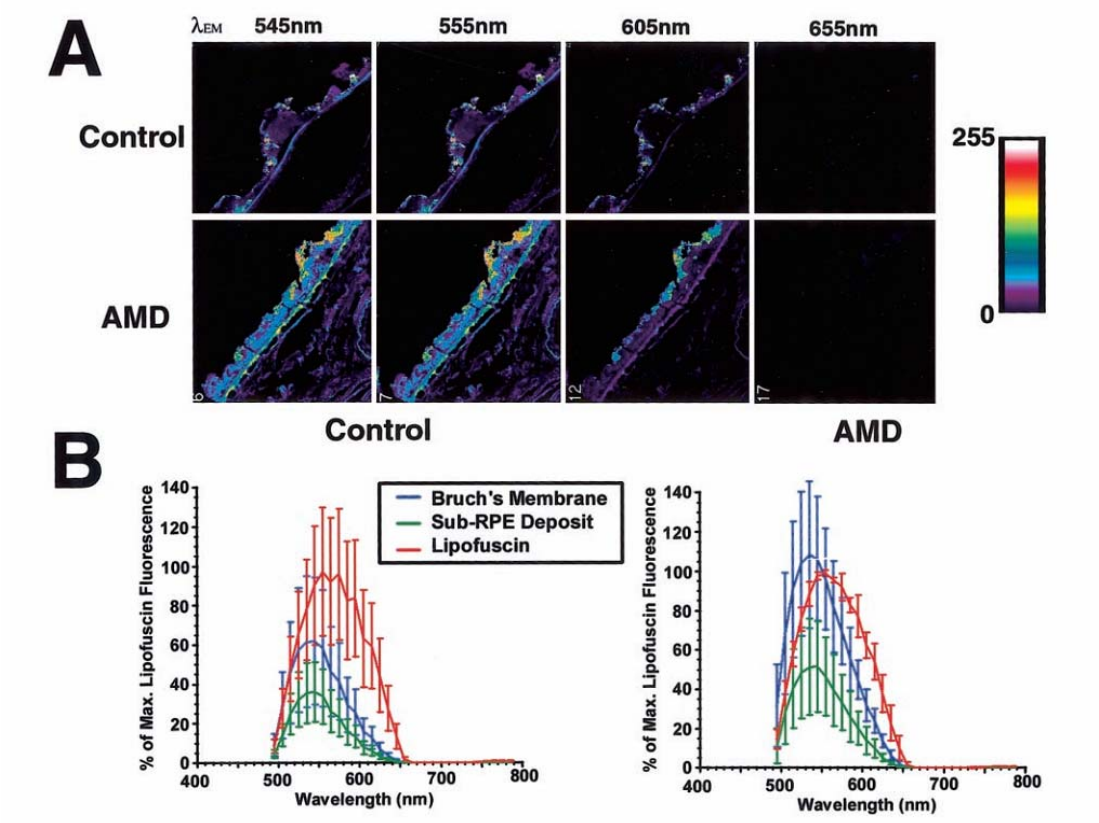

Figure 2. Spectrum of Bruch's membrane, sub-RPE deposits and lipofuscin using λ_{ex} of 488nm. (A) Pseudocolour representation from control and AMD spectral data sets. Each panel derives from a select 10nm window centered on the indicated λ. The pseudocolour scale is shown on the right. (B) Sample spectra from representative donor eyes. Data are the mean ± SD from the three fields examined in each eye. Note the increase in Bruch's membrane's intensity in the AMD-affected eye relative to lipofuscin. Source: Marmorstein et al. [79]

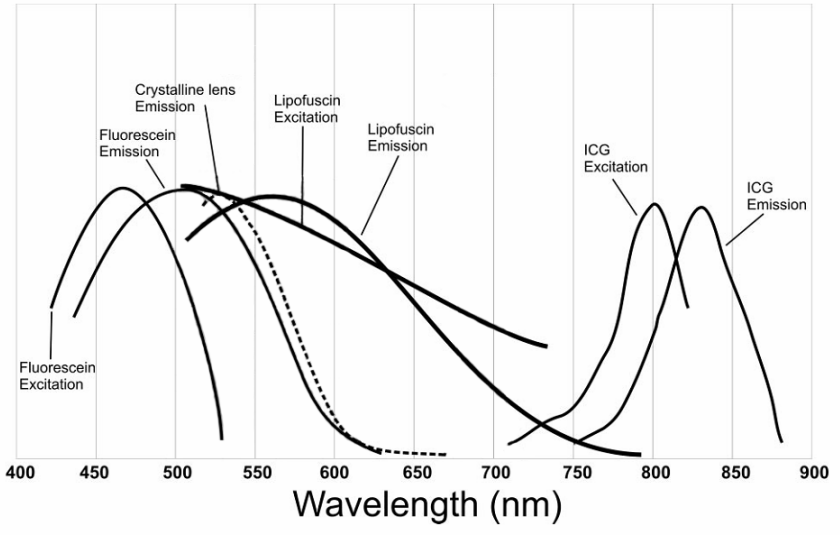

Figure 3. Absorption and emission spectra involved in fundus autofluorescence. Source: Spaide [80]

The same is the case for choroidal components and the sclera. It must also be taken into account, that sub-RPE fluid in the presence of pigment epithelial detachments or longstanding subretinal hemorrhages may also contain fluorophores that induce an increased FAF signal in the relevant wavelength ranges [81]. Also, this method cannot distinguish between melanolipofuscin or RPE cells that have migrated into the neurosensory retina and lipofuscin at the normal RPE cell layer.

1.7. Fundus autofluorescence anomalies associated with AMD

A normal FAF pattern is characterized by a homogeneous background autofluorescence with a gradual decrease in the inner macula toward the foveola due to the masking effect of yellow macular pigment (Figure 4). Many previous studies have been made on correlations of change in AF distribution with pathologic features in AMD [54, 82-84]. FAF changes do not necessarily correlate topographically with visible fundus changes in patients with early AMD [85].

The distribution of drusen and abnormal FAF correlate poorly. The autofluorescence signal may be normal, decreased, or increased in corresponding drusen areas [83, 84], presumably related to the nature of RPE change overlying them. Von Ruckmann et al. and Lois et al. reported drusen having normal or near normal autofluorescence (which would make them invisible by autofluorescence imaging), but they and other investigators also reported decreased autofluorescence over drusen and increased autofluorescence in large soft foveal drusen [54, 84, 86]. A detailed study of small drusen by Delori and coworkers found that there is a central core of decreased autofluorescence, surrounded by a ring of autofluorescence. They postulated that the decreased central autofluorescence in drusen may be related to the RPE being stretched over the drusen, with a thinner layer of lipofuscin granules over the drusen and with overall conservation of the amount of lipofuscin.

Increased autofluorescence may correspond to hyperpigmentation (melano-lipofuscin) or may precede the development of GA or the enlargement of pre-existing GA [82, 87, 88]. Markedly decreased autofluorescence, especially over larger areas, is characteristic of Geographic Atrophy and crystalline drusen [89]. Serous PED shows diffusely increased autofluorescence corresponding to the area of the detachment, in some cases with a surrounding ring of decreased FAF. Autofluorescence in areas with

drusenoid PED may show levels of autofluorescence ranging from decreased to increased, influenced significantly by concurrent pigmentary changes [90].

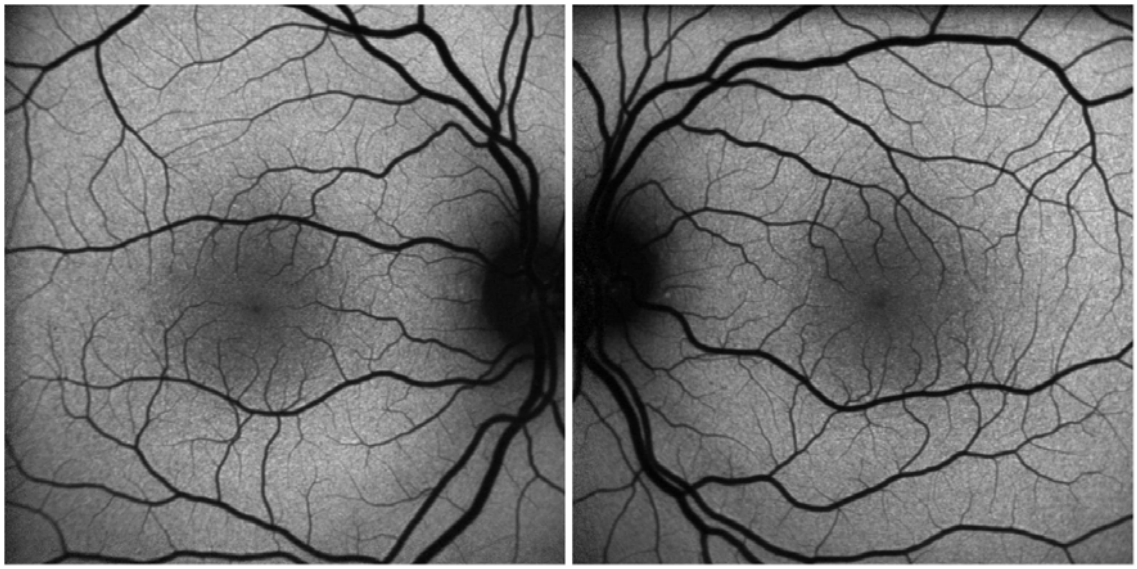

Figure 4. Fundus autofluorescence imaging of a normal individual shows diffuse fundus fluorescence with decreasing intensity at the fovea due to increasing luteal pigment density. Blood vessels and optic disc show as negative shadows.

1.8. Functional correlates of pathological fundus features and FAF patterns associated with AMD

Scholl et al. [91] investigated the functional correlates of various fundus features in AMD using Fine Matrix Mapping (FMM), a high-resolution microperimetric method. CNV showed a central area with decreased FAF, surrounded by focal areas with both decreased and increased FAF. Photopic sensitivity loss associated with active CNV was relatively uneven over the lesion, ranging from moderate to nondetectable thresholds. Scotopic FMM revealed severely reduced sensitivity over the lesion with decreased FAF. In the case of Geographic Atrophy, FAF imaging showed a central area of decreased FAF surrounded by a ring of increased FAF. Photopic FMM revealed mildly to moderately reduced sensitivity over the area of decreased FAF, normal sensitivity over the area of increased FAF and also eccentric to the area of increased FAF. Scotopic FMM showed a complete loss of sensitivity over both the central area of decreased FAF and the surrounding ring of increased FAF. Eccentric to the area of increased FAF, the scotopic sensitivity was moderately reduced. FAF imaging revealed increased FAF

corresponding to large, soft foveal drusen. Moreover, the area covered by the large, soft druse showed mildly reduced photopic and considerably reduced scotopic sensitivity.

The distribution of smaller soft drusen and FAF correlated poorly and no association between drusen and photoreceptor dysfunction was demonstrable. Thus both increased and decreased abnormal FAF seems to be associated with significantly reduced scotopic sensitivity. Elevation in photopic thresholds in the same areas varies and may or may not be detectable. Increased FAF in AMD has a functional correlate in a preferential dysfunction of the rod system. This was corroborated by Schmitz-Valkenberg et al. who found variable degrees of functional impairment of the neurosensory retina associated with elevated FAF in the junctional zone of areas with Geographic Atrophy [92].

In summary, since the RPE/BrM complex is essential for photoreceptor survival, psychophysical assessment of photoreceptor function may yield information about the significance of clinically observable retinal changes that may not be provided by other methods until later or at all [40]. Psychophysical testing and Fundus Autofluorescence are two sensitive and complementary techniques for detecting early retinal abnormalities.

2. Characterisation of Bruch's membrane ultrastructure in apoB-100 and biglycan transgenic mice.

2.1. The histopathology of the RPE-choriocapillaris interface

The outer vascular interface of the retina, towards the choroid, is formed by the retinal pigment epithelium, Bruch's membrane and the choriocapillary endothelium (Figures 5 and 6).

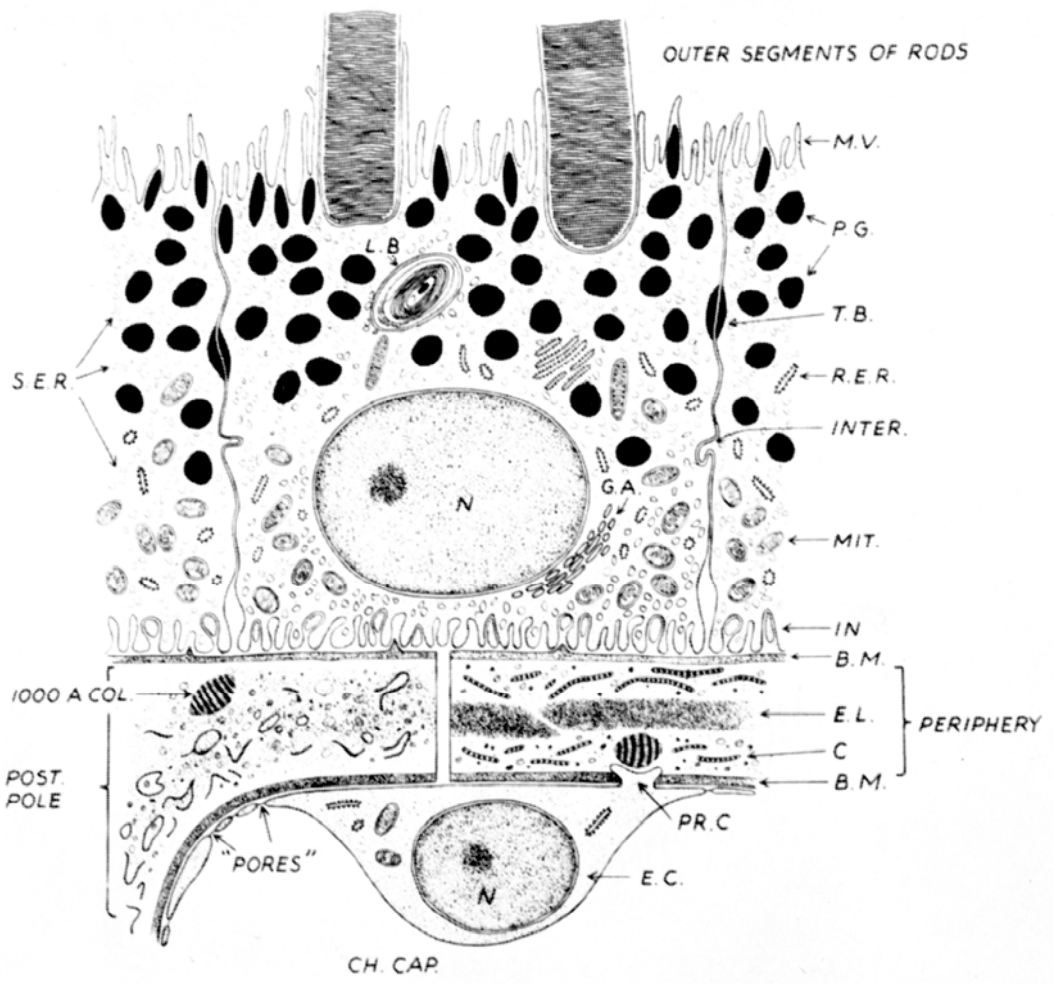

Figure 5. Schematic representation of Bruch's membrane and its neighbouring structures. Bruch's membrane is shown in two parts: at the left as it appears around the posterior pole and at the right as it is found in the region of the equator. MV, microvilli; PG, pigment granules; TB, terminal bar; SER, smooth endoplasmic reticulum; RER, rough endoplasmic reticulum; LB, shed photoreceptor discs; GA, Golgi apparatus; N., nucleus with nucleolus; INTER, interdigitation of plasma membranes; MIT, mitochondria; IN, RPE basal membrane infoldings; BM, basement membrane; EL, elastic layer. PRC, endothelial cytoplasm prolapsed through the BM; EC, choriocapillary endothelium showing fenestrations; 1000Å COL, collagen-like banded material with 100µm periodicity; CHCAP, choriocapillaris. Source: Garron [93]

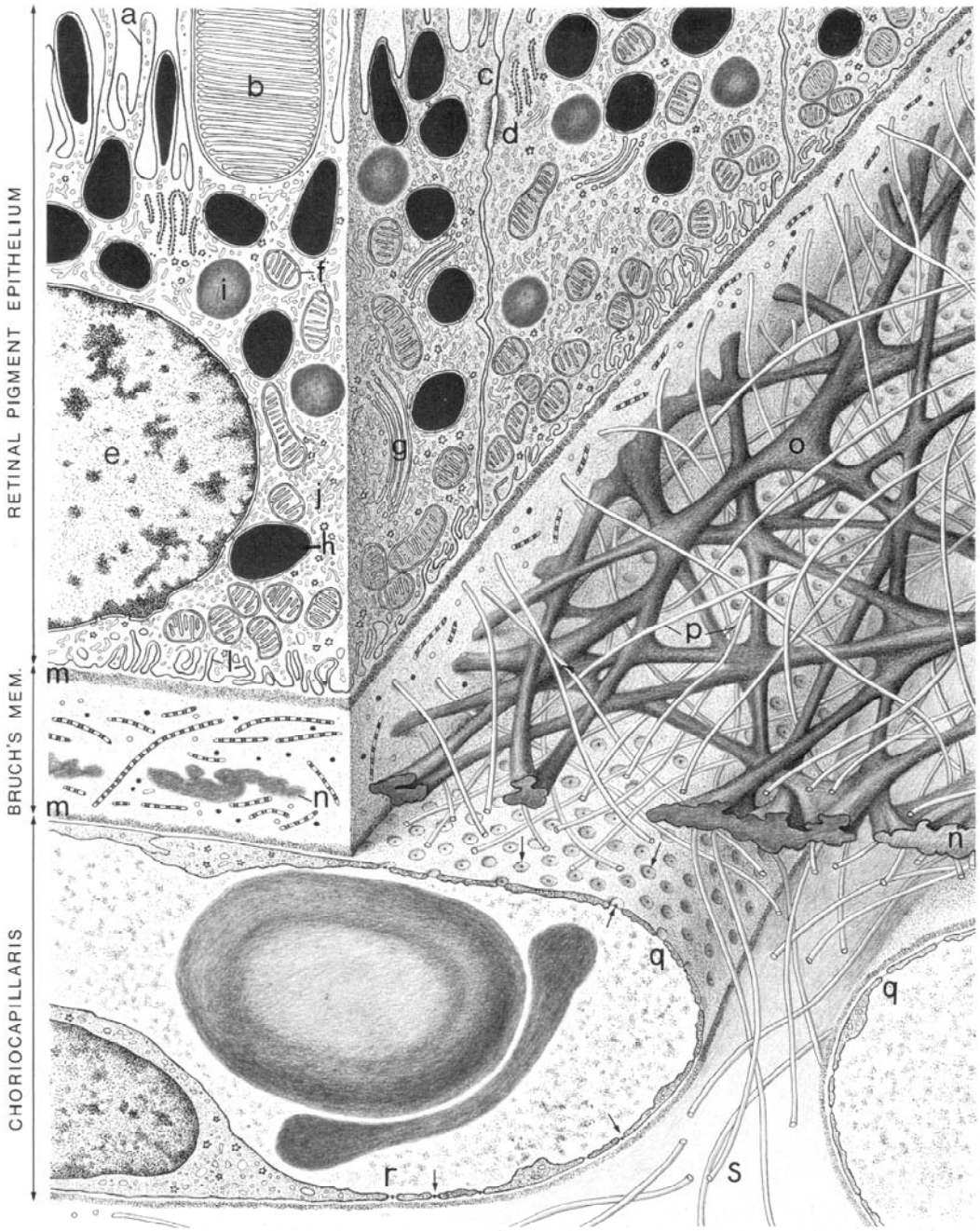

Figure 6. Three-dimensional drawing of the inner choroid and retinal pigment epithelium. The apical villi of the RPE (a) extend to enclose the photoreceptor outer segments (b). The intercellular junctions are characterized by a zonula occludens (c) and a desmosome (d). The cytoplasm of the RPE cells contains a nucleus (e). mitochondria (f), a Golgi apparatus (g), pigment granules (h), phagosomes (i), and it is characterized by a large amount of smooth-surfaced endoplasmic reticulum (j). The basal cell membrane shows complex infoldings (I) and a basement membrane (m). Bruch's membrane shows an apparently interrupted elastic zone (n) in meridional section, but the elastica is layered and continuous in flat section (o). Collagen fibrils (p) that form the inner and outer collagenous layers have a random orientation around the elastic layer. The choriocapillaris (q) shows a fenestrated endothelium towards BrM, laterally and to a lesser extent externally (r). The intercapillary zone shows considerable collagen (s). The lumen of the capillary, contains two red blood cells. Source: Hogan & Alvarado [94]

The RPE is a monolayer of regular hexagonal cells that separate the outer surface of the neural retina from the choriocapillaris. RPE cells within the macular region contain more pigment than in the periphery and are about 10-14µm tall and 14µm in diameter. At the ora serrata they become flatter, wider and less regular, measuring up to 60µm in diameter. The nucleus is located in the basal portion of the RPE cell and measures 5-12µm. Many of the cells are multinucleated. Mitoses have not been observed in RPE cells and it is generally believed that cell loss is not followed by replacement, rather adjacent cells slide laterally to fill the space left by a dead cell. The RPE cell membrane is a typical unit membrane, at the base of the cell facing BrM, it shows dense complex infoldings which extend 1µm or more into the cytoplasm. External to the cell membrane is a space of low electron density (ED) separating the cell membrane from the adjacent fibrillar basement membrane. The lateral cell membranes are only slightly interdigitated, cells are separated by a normal space of varying width, sealed off from the apical lumen by zonulae occludentes and zonulae adherentes which are regularly found external to these. Desmosomes are found only inconstantly along the lateral cell membranes. By light microscopy, these junctional complexes along the lateral cell membranes produce the effect of a continuous membrane (Verhoeff's membrane). As the underlying choriocapillaris is fenestrated and leaky, the functional site of the outer blood-retinal barrier is at the level of the RPE tight junctions. The apical membrane of the RPE cells facing the photoreceptor outer segments shows numerous microvilli, surrounded by the interphotoreceptor matrix. Junctional complexes do not unite the POS to the RPE [94].

Five layers are readily discernible within Bruch's Membrane, the basement membrane (BM) of the RPE, an inner collagenous layer, an elastic layer, an outer collagenous layer and the BM of the choriocapillary endothelium (Figure 7). The basement membrane of the retinal pigment epithelium is composed of very fine filaments, which extend from the inner and outer surfaces to join the cell membrane of the RPE and adjacent collagen [93]. Its thickness is about 0.3µm and it is separated from the cell membrane by a space measuring approximately 100nm. The inner collagenous layer is about 1.5µm thick and is composed of clearly interwoven but loosely arranged collagen filaments oriented in all directions but generally parallel to the outer retina. The fine filaments of the RPE basement membrane merge with the

Figure 7.

Schematic representation of Bruch's membrane.

1. Basement membrane of the RPE
2. inner collagenous layer
3. interrupted elastic tissue layer
4. outer collagenous layer
5. basement membrane of choriocapillary endothelium

(ENDO = endothelium) Note the basal infoldings of the plasma membrane of the pigment epithelial cells and the fenestrations in the choriocapillary endothelium. Source: Nakaizumi [95]

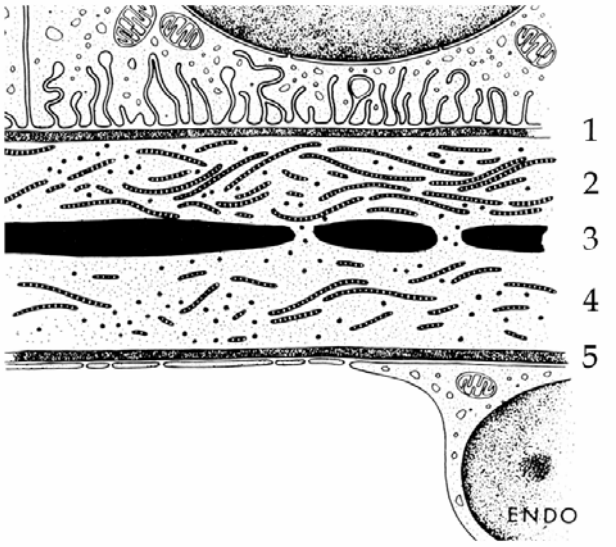

collagen providing a strong bond between the RPE and the choroid. The elastic layer is the backbone of BrM and lies closer to the choriocapillaris than the RPE. This layer is continuous from the optic disc to the pars plana and has a fairly regular structure and is formed of long, thin, straight fibres, forming a meshwork, two to four fibres thick with irregular spaces. The elastic layer is three to six times thinner and two to five times more porous in the macular region than it is in the periphery [96]. Collagen fibres pass randomly back and forth through the openings in the elastic layer. The outer collagenous layer is thinner than the inner, measuring about 0.7µm in thickness. It has the same structure as the inner collagenous layer except in the inter-capillary pillars where it becomes continuous with the stroma of the choroid and subcapillary connective tissue. The basement membrane of the choriocapillary endothelium is at 0.14µm thinner than the RPE basement membrane.

The inter-fibre matrix of Bruch's membrane is comprised largely of heparan sulfate and chondroitin/dermatan sulfate proteoglycans, and it has been suggested that the chondroitin sulfate side chains provide an electrolytic barrier to diffusion. Heparan sulfate appears to be concentrated in the basement membrane portion adjacent to the RPE and chondroitin/dermatan sulfate is located predominantly within the collagenous layers and along the basal laminar of the choriocapillaris [97].

BrM extends from the margin of the optic disc to the ora serrata. It becomes modified beyond the ora serrata in the ciliary body. The RPE basement membrane continues as the basement membrane of the ciliary pigment epithelium, the elastic and collagenous layers become further separated from the basement membrane by layers of

collagen and finally disappear in the stroma of the ciliary body, near the posterior part of the pars plicata. In the young human eye BrM is about 2-4µm thick near the disc and gradually thins to 1-2µm in the periphery. BrM thickness increases with advancing age [94].

In the posterior pole, the choriocapillary bed is sinusoidal, consisting of a mesh of flat and wide capillaries interspersed with intercapillary connective tissue pillars in a lobular pattern (Figures 8 and 9). External to the BrM elastic layer the inter-capillary collagen becomes more dense and is oriented circularly around the capillary wall, with less ground substance. Choriocapillary endothelial cells have numerous circular fenestrations measuring approximately 80nm in diameter, with a covering diaphragm and a central density. The endothelial cells are joined by sloping, somewhat folded borders, the intercellular space measuring 10nm. An occluding junction is seen between the cells near the lumen and marginal folds are common. The sub-capillary connective tissue is dense with marked imbrication of the fibrils [94, 95, 98,].

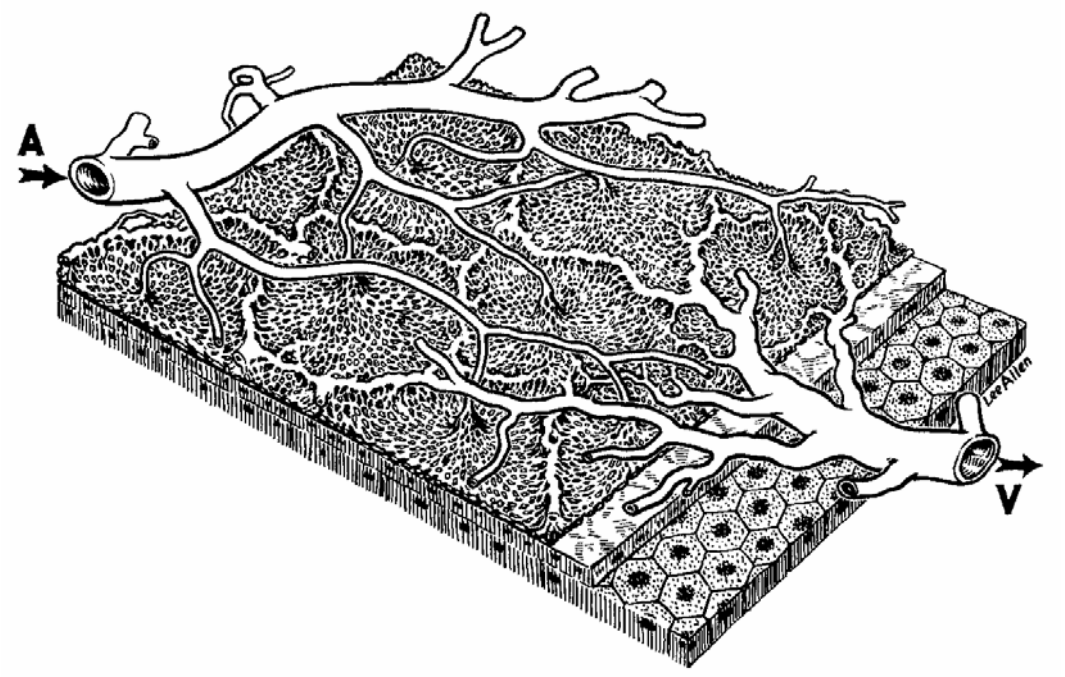

Figure 8. A three dimensional schematic representation of the lobular choriocapillary pattern, Bruch's membrane and the hexagonal monolayer of the RPE. A: choroidal arteriole, B: Choroidal vein. Source: Hayreh et al. [99]

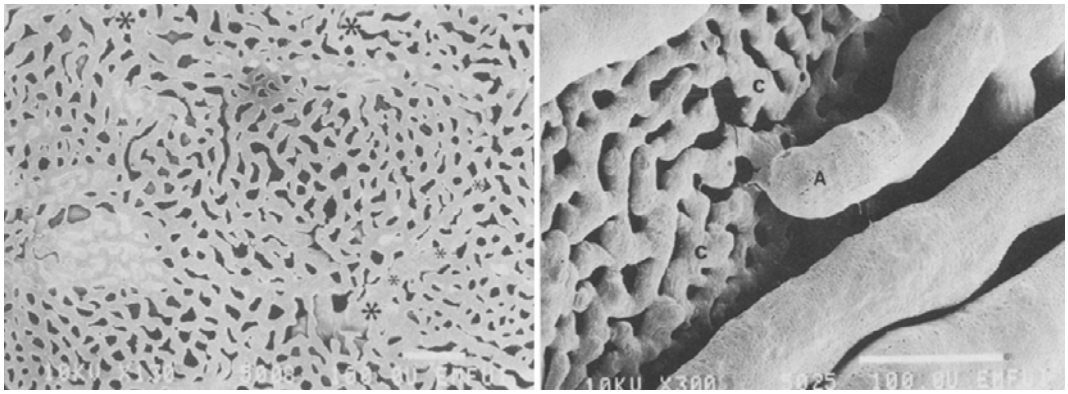

Figure 9. Left: Anterior view of a corrosion cast of the choriocapillaris in the posterior pole of a human eye. Note the lobular structure and the intercapillary pillars. Wide collector venules (asterisks) entervene between two neighboring lobules (x130). Right: Scleral view of the corrosion cast. An arteriole (A) joins the choriocapillaris (C) at a right angle. A sharp constriction is present just before the arteriole joins the choriocapillaris (x300). Source: Yoneya et al. [100]

2.2. Histopathologic features associated with aging and early age-related macular degeneration (AMD)

Aging changes within the RPE are characterised by the accumulation of residual bodies containing lipofuscin. These are similar to the 'age pigment' found in other organs, including the brain [101]. After the seventh decade, the RPE basement membrane becomes thickened and the number and complexity of basal infoldings become less [19, 102, 103].

With advancing age there is a reduction in cross-sectional area of choriocapillaris, and a trend for the normal sinusoidal capillaries to be replaced by a tubular system [104, 105]. In normal maculae, from the first decade to the tenth decade, choriocapillaris density (the ratio of the sum of the lengths of the lumina of the capillaries to the length of the zone in which measurements are made) decreases in a linear fashion from 0.75 to 0.41 (45%), although with increasing age, the variability is also increased. The choriocapillaris diameter decreased from 9.8μm in the first decade of life to 6.5μm in the tenth decade (34%). The choroidal thickness decreased linearly from 193.5μm to 84μm. In the macula, the age-related decline in choriocapillaris density is also accompanied by a widening of the inter-capillary pillars from 25% in young subjects (21 to 50 years) to 60% in old subjects (80 to 97 years) [105-108].

Bruch's Membrane undergoes an overall thickening as well as a structural reorganisation with progressing age. Ramrattan et al. demonstrated an age-related overall increase in Bruch's Membrane thickness [105]. In normal maculae this increased

by 135% from 2.0µm in the first decade to 4.7µm in the tenth decade and a skewed distribution toward higher values with increasing age was observed. Collagen content and cross-linking increases with the accumulation of so-called wide-spacing material and a structural disorganization of the collagen fibres [109]. There is an increased number of striated collagen fibres present in both the inner and outer collagenous layers with increasing age. This 64nm banded material is assumed to be the fibrillar type I collagen [110]. This is accompanied by the deposition of short segments of a banded material whith a periodicity of 100-120nm which is assumed to be collagen type VI Bundles of this material may appear amorphous rather than showing the characteristic banding when cut in cross section [111].

There is a highly significant decline in the solubility of Bruch's membrane collagen with age, from near 100% in the first decade of life to 40-50% in the ninth decade at both macular and peripheral sites, due to an increase in crosslinking [112]. Glycosaminoglycans in the inter-fiber matrix of Bruch's membrane increase in size, which may reflect an inability of cells to process the core protein normally [97]. Heparan sulfate becomes a more predominant proteoglycan, and changes in the negatively charged field may impede the passage of negatively charged macromolecules thus affecting normal filtration [97, 113-115]. Laminin, a major structural basement membrane glycoprotein involved in many biological functions of basement membranes is deposited in the inner collagenous layer and between the outer collagenous layer and the basal lamina of the choriocapillaris [116, 117].

With age, the fibre number increases in the elastic layer and the immature elastic elements (oxytalan) mature from an anterior to posterior direction [118]. Calcification can also occur which renders Bruch's membrane brittle [119]. In early AMD, the integrity of the elastic layer is significantly reduced and as the disease progresses an overall thickness of the elastic layer is also seen [96, 120, 121].

2.3. Accumulation of sub-RPE debris

The initial age related change in Bruch's membrane, as seen by electron and light microscopy, is the accumulation of lipid- and protein-rich debris under the retinal pigment epithelium and within BrM [111, 122]. Sub-RPE debris has previously been characterized in different ways by various studies according to the particular method

used. Killingsworth et al. using standard TEM techniques described coated membrane-bound bodies (CMBB) 400-2500nm in size, surrounded by a limiting membrane coated often on both sides of the membrane bilayer. CMB bodies contained fine granular material, electron-lucent droplets, occasional dense particles and 70nm coated vesicle-like (CVL) bodies. The breakdown of CMB bodies appeared to be the main source of debris within the ICL/OCL (Figure 10). Larger (110nm) CVL bodies not found within CMB bodies were also present slightly more frequently in the ICL than the OCL. They contained pale amorphous material and displayed an irregular or "spiked" membrane coat. The limiting membranes of these bodies were poorly defined, seldom appearing as bilayers. Fibrous banded material (FBM), also a component of age-related deposits, displayed a regular periodicity between 120-133nm [123].

Sarks and coworkers found in patients after the fifth decade, that the thickening of BrM with age was due mainly to the accumulation of coated membrane-bound bodies. These typically ruptured to release their content of vesicular and granular material as well as fragments of the coated membrane. Membranous debris was composed of coiled membrane fragments (in LM sections giving it a vacuolated appearance), and small membrane-bound vesicles. Early basal laminar deposit appeared on LM as pale-staining layer with faint vertical striations, on EM a homogenous basement membrane material that can also appear fibrillar and later banded [18].

Curcio and Millican used a conventional TEM technique and found fibrous long-spacing collagen and an amorphous basement membrane-like material between the RPE plasma and basement membranes. Within BrM, the two most common features were membranous debris and non-membrane-bounded electron-lucent droplets. Closed membranous profiles with empty interiors were large, irregular and variable in size (33-267nm). Electron-lucent droplets were smaller, rounder and more uniform in size (33-117nm) scattered throughout both collagenous layers, lacked a distinct membrane, but were occasionally surrounded by a single thin electron-dense line (Figure 11), [17].

Ruberti et al examined macular Bruch's membrane of normal human eyes by quick-freeze/deep-etch (QFDE) electron microscopy, a method that provides a quasi-three-dimensional view of connective tissue ultrastructure and lipid particles in great detail. This method minimizes the loss of the extracellular matrix and lipids that often accompanies dehydration through graded alcohol, providing a clearer view of these

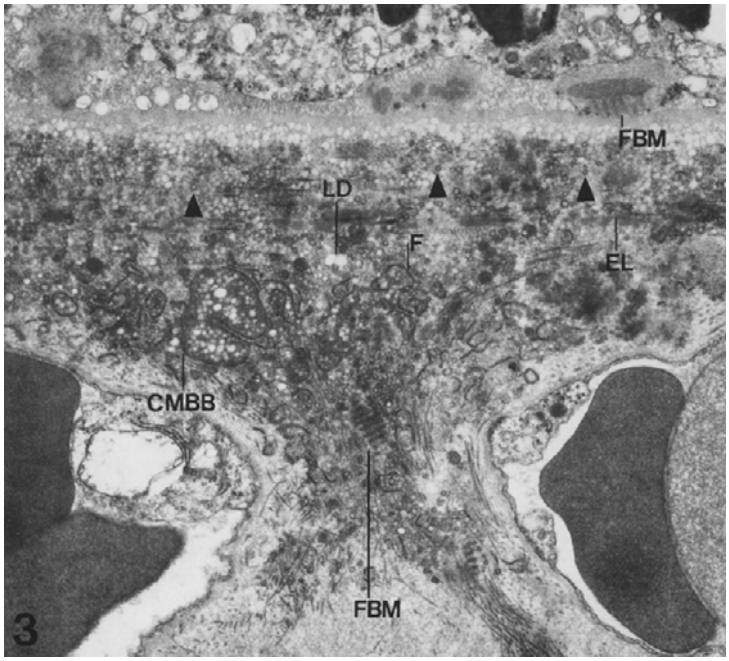

Figure 10. Bruch's membrane from a 69-year-old patient showing age-related material extending into the intercapillary zone. 110nm CVL bodies (arrowheads), electron-lucent droplets (LD) and dark amorphous material may be seen in both the inner and outer collagenous layers. CMB bodies (CMBB), coated membrane fragments (F) and fibrous banded material (FBM) are contained within the OCL. Coated membrane fragments and electron-lucent droplets appear to be derived from ruptured CMB bodies (x10740) Source:Killingsworth et al. [123]

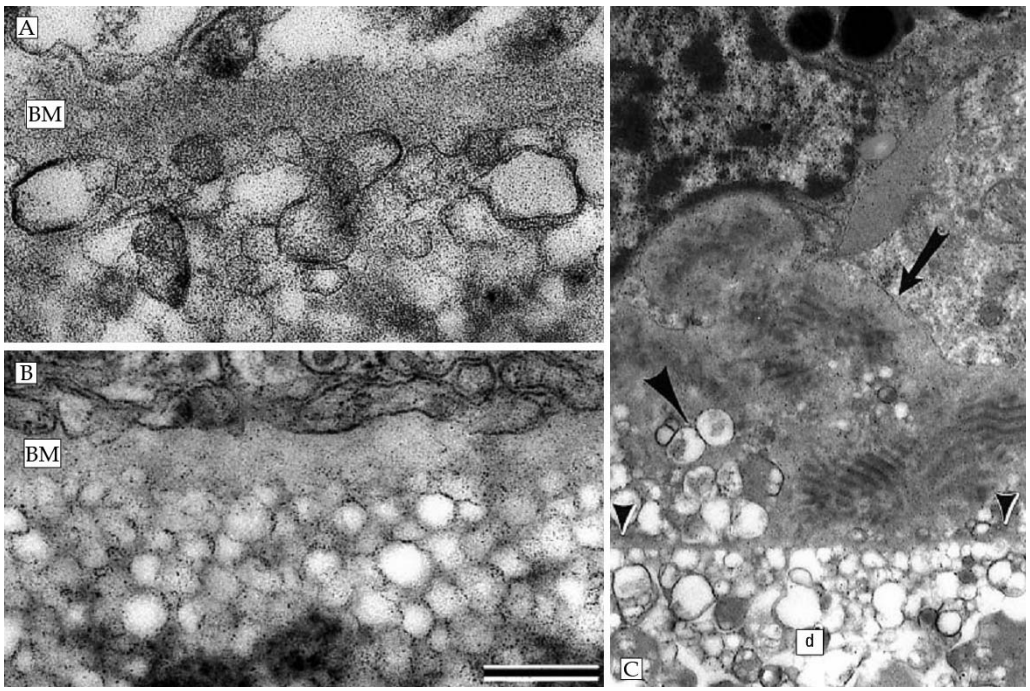

Figure 11. Ultrastructure of BlamD, membranous debris and electron-lucent droplets. A: diffusely distributed membranous debris. B: non-membrane-boudned droplets. Scale bar: 250nm. C: long arrowhead and (d) indicate membranous debris, black arrow BlamD with banded material, short arrowheads the RPE basement membrane (BM). Source: Curcio & Millican [17]

structures than traditional methods of preparation for TEM (Figure 12). The most prominent features of older eyes were the disorganization or disappearance of the RPE basal infoldings, increased electron density of the ICL, a paucity of collagen fibrils immediately adjacent to the RPE basal lamina and the presence of numerous spherical and elliptical electron-lucent profiles 80.8±20.7nm (mean±SD) in diameter distributed along fibrils in the ICL and in a band between the ICL and the RPE basal lamina. An exterior shell was apparent on many lipid-rich particles [124].

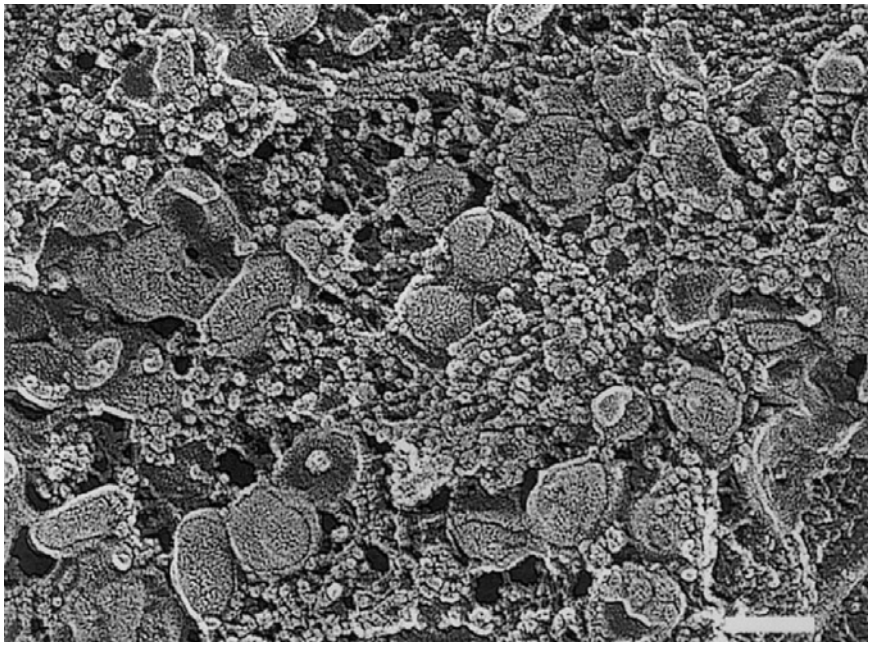

Figure 12. QFDE image of lipids in a region adjacent to RPE basal lamina of 78-year-old eye showing ultrastructural detail of lipid-extracellular matrix interaction. The lipid-rich particles (80nm in diameter) appear intimately involved with matrix molecules. Scale bar. 100nm.ads the RPE BM. Source: Ruberti et al. [124]

These profiles were previously identified as cholesterol-containing particles, because they are solid when viewed with lipid-preserving ultrastructural techniques, they are extractable with lipid solvents and they become more numerous with age along with histochemically detectable and directly assayed esterified and unesterified cholesterol [125].

Li et al used negative staining electron microscopy to characterize ultrastructure and electrospray ionization mass spectrometry to determine lipid composition of electron-lucent particles resembling lipoprotein particles (lipoprotein-like particles, LLPs) in normal aged human Bruch's membrane/choroid. Particles detected included one group with heterogeneous size and morphology, containing predominantly

phospholipid and unesterified cholesterol. A second group were solid, round lucent particles in the 100nm diameter range as well as larger and more irregular assemblies with an electron-lucent surface and moderately electron-dense core were enriched with esterified cholesterol. Coated membrane-bounded bodies (CMBBs) were also present [126].

Huang and coworkers found, using a QFDE technique, three basic types of inclusions: lipoprotein-like particles (LLPs), small granules (SGs), and the membrane-like structures that formed coated membrane-bound bodies (CMBBs) when combined with LLPs and SGs. The size of the LLPs varied from 60 to 100nm but sometimes could be as large as 300nm. LLPs were frequently seen in contact with fine filaments, presumably proteoglycans that extended among collagen and elastic fibrils. SGs appeared as round particles of approximately 10nm in diameter with no other obvious morphological characteristics, present in the middle layers of BrM sometimes in tightly packed clusters. Similar to the LLPs, the SGs also were attached to the fine filaments. Sometimes a complex composed by a single LLP and one or more layers of surrounding SGs was seen (Figures 13 and 14). The CMBB was composed of LLPs and SGs surrounded by a membrane-like structure about 15nm wide and sometimes double-layered, showing a granular appearance and forming either a closed or opened loop [127].

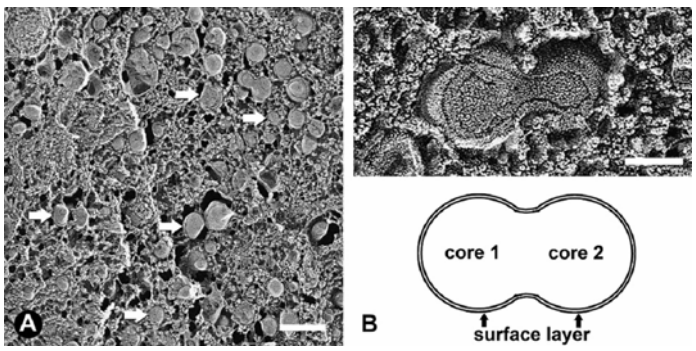

Figure 13. (A) LLPs (arrows) were the major inclusions seen in BrM of a 45-year-old eye. The particle was usually 60-100nm in diameter and comprised of a core surrounded by a thin surface layer Scale bar 200nm. (B) Two LLPs fused to form a dumbbell-shaped particle in a 78-year-old eye. Scale bar 50nm. Source: Huang et al. [127]

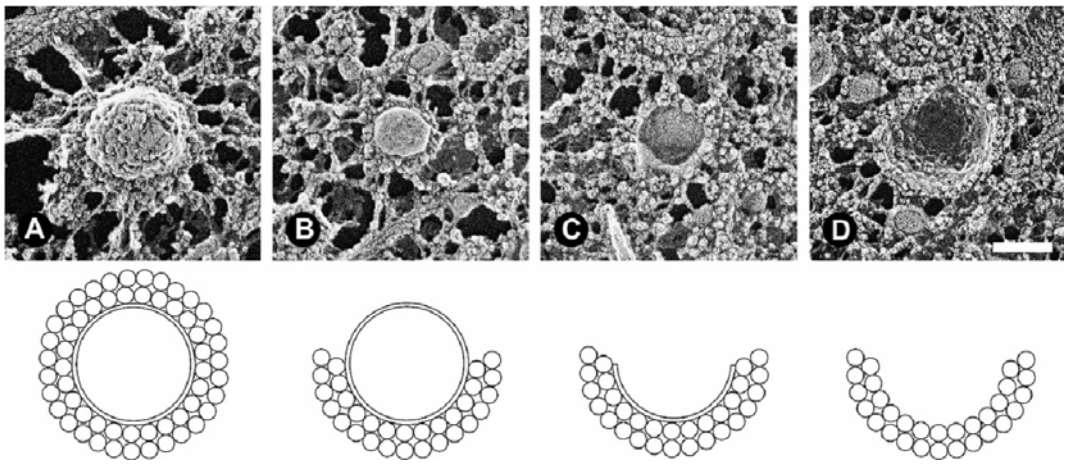

Figure 14. The ultrastructure of the LLP-SGs complex as revealed by fracturing of four LLPs (34-year-old eye). Under each image is a sketch depicting the observed LLP—SGs complex. (A) A complete complex. Short struts were seen radiating from the complex and associating with other extracellular matrix components. (B) A complex with the upper half of SGs surrounding layers removed. (C) A complex with both the upper SGs and the core of LLP removed. (D) A complex with only the lower half SGs surrounding layers remained. All four conformations of the complex were often observed. Scale bar 100nm. Source: Huang et al. [127]

Curcio and coworkers used standard TEM methodology as well as the lipid-preserving osmium-tannic acid-paraphenylenediamine (OTAP) method to examine aged normal and AMD eyes. Particles seen included membranous debris and solid 100nm diameter esterified cholesterol-rich particles as well as complex coated membrane-bound bodies. Viewed by conventional TEM, individual profiles in a sub-RPE aggregation of membranous debris had an electron-dense exterior, a more lucent and an apparently extracted interior. An OTAP preparation of the same eye showed that individual profiles in a similar sub-RPE aggregate were in fact solid spheres with highly electron-dense surfaces (Figure 15). Profiles in the OTAP images were generally smaller (87–348nm) than those in standard TEM images (87–871nm), and the overall aggregate in the OTAP section was distorted and condensed relative to that in the osmium treated one. Solid particles in AMD lesions were variable in size, electron-density, and morphology. There appeared to be at least two types: small, uniformly dense, and spherical versus large and distorted with a prominent electron-dense exterior, similar to those found by Huang et al [128].

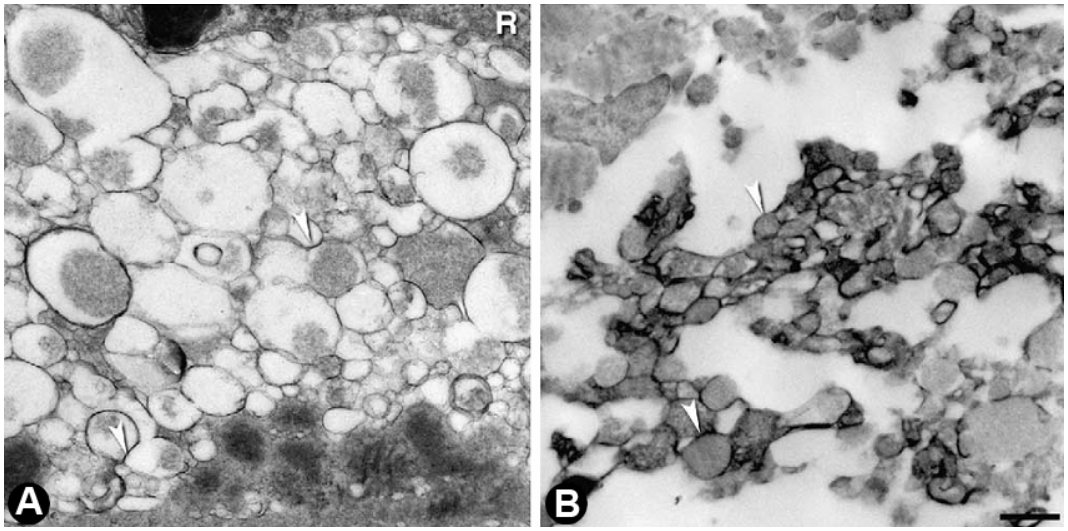

Figure 15. (A) Individual profiles in a sub-RPE aggregate of membranous debris (arrowheads) are enlarged and partially extracted by processing; glutaraldehyde/paraformaldehyde, 2% osmium. (B) Individual profiles in a similar sub-RPE aggregate of the same eye as (D) are solid and surrounded by an electron-dense band; glutaraldehyde/paraformaldehyde, OTAP. Source: Curcio et al. [128]

Combinations of these particles may contribute to the formation of Sub-RPE deposits found in AMD [102, 129]. Sub-RPE deposits are classified as focal (drusen) or diffuse (Basal Deposits, Laminar or Linear) [15]. Basal Laminar Deposits (BlamD) are characterized as a layer of amorphous or granular material of intermediate electron density, with wide-spaced collagen, located between the RPE plasma membrane and basement membrane. BlamD occur in numerous unrelated disease states are thus not considered to be specific for AMD [16, 17, 119]. Basal linear deposits (BlinD) are composed of typically densely packed, electron-dense, membrane-bounded and non membrane-bounded vesicles located (as well as drusen and in neovascular AMD, Type 1 CNV membranes) between the RPE basement membrane and the inner collagenous layer of BrM [17-19]. These deposits are all associated with aging as well as AMD and their origin, pathogenesis and relative significance remain unclear.

2.4. The lipid-barrier hypothesis

According to the lipid-barrier hypothesis, the accumulation of lipids and possibly proteoglycans within BrM may lead to a critical decrease in the hydraulic conductivity of BrM, thereby impeding transport of fluids and hydrophilic substances. Since photoreceptors depend on the RPE and the choriocapillary circulation for nutrients (including essential retinoid derivatives), as well as for the clearance of metabolic end-products, impairment of transport across BrM could contribute to abnormalities associated with late AMD.

Fisher, using a relatively low number of specimens (n=6), recorded a linear age-related decrease in hydraulic conductivity (flow per unit pressure) with extremely low values of hydraulic conductivity in his youngest sample (22 years of age) [130].

Using a modified Ussing chamber, Moore et al measured the pressure-induced flow of physiological buffer through isolated human Bruch's membrane-choroid complexes. Hydraulic conductivity for individual complexes, was calculated from individual flow values. The hydraulic conductivity of the complex exhibited an exponential decrease with increasing age of donor, the most rapid decline occurring during the first four decades of life. The age-related change was most pronounced in the macula, where hydraulic conductivity halved every 9.5 years, compared to 19 years in the periphery [14].

Starita et al using a similar method found that hydraulic conductivity of isolated, macular regions of BrM/choroid complexes undergoes an age-related exponential decline with a half-life of 15 years [131]. The data presented showed good correlation with that of Moore et al. with the exception of the half-life of the exponential. The greatest decrease in conductivity occurred in the first four decades of life. The mechanisms underlying these changes in early life are not known. Histochemical and biochemical studies have shown that the accumulation of neutral fats or phospholipids begins to rise steeply in the fifth decade [13, 132, 133]. This coincides with a time period in which the greatest resistance to flow was measured. Given a loss of 90% of hydraulic conductivity by the age of 50 any further minor changes in the barrier properties of the membrane could have profound implications, lipid accumulation in Bruch's membrane may sufficiently disturb the homeostasis of the outer retina to lead to death of overlying cells and may further promote the deposition and stabilization of

lipid soluble substances by increasing transit times for the passage of molecules through the membrane, leading to a secondary deposition of lipids, which would act synergistically to suppress hydraulic conductivity even further.

Table 1. Comparative age profile of hydraulic conductivity of human Bruch's and BrM-choroid preparation obtained by three different methods

	Fisher (1987)	Moore et al. (1995)	Starita et al. (1996)
Experimental method	membrane relaxation	dynamic method (continuous pressure changes)	static method (fixed pressure)
Tissue preparation	isolated Bruch's membrane	Bruch's-choroid complex	Bruch's-choroid complex
Number of eyes	6	13	23
Age range (years)	22-71	16-90	1-91
Tissue diameter	2.5 mm	4 mm	3.5 mm
Pressure	up to 2700 Pa	486.65-3406 Pa	583.98-2336 Pa
Hydraulic conductivity m $sec^{-1}Pa^{-1}$ x 10^{-10}	2.8-1.52	110.54-2.45	130.6-0.52
Age profile	linear	exponential $t_{1/2}$ = 9.5 years	exponential $t_{1/2}$ = 15 years

After: Starita & Hussein [131].

Starita et al. also examined the relationship between levels of lipid deposition and loss of hydraulic conductivity of BrM and found a non-linear relationship between the level of lipid deposits and the resistance of the membrane to fluid transport. Low level accumulation of lipid (up to 50 mg/m^2) did not appear to influence resistance to any appreciable extent - such levels would be present during the first four decades of life. In later life however lipid accumulation leads to significant alterations in the resistance of the membrane [131].

All studies used a comparable range of pressure and had a similar age-bias with proportionally more samples in the aged group. These results support the original hypothesis that lipid deposition in the ageing macula would be expected to impart hydrophobic properties to Bruch's membrane and thus interfere with local fluid dynamics (Table 1) [5, 134].

2.5. Lipid deposition – pathways in atherosclerosis and AMD

The deposition of lipid- and proteoglycan-rich extracellular material is a feature common to both atherosclerosis and AMD [121, 125, 135]. According to current theories of atherosclerosis, inflammatory pathways may play a central role in atherogenesis, with the retention of atherogenic lipoproteins in the arterial wall being a key pathological event (Response-to-retention hypothesis) [135-139]. In humans, serum lipids are transported from hepatic to peripheral tissues mainly in the form of LDL particles consisting of neutral lipids (triglycerides and esterified cholesterol, EC) surrounded by a monolayer surface membrane of phospholipid and unesterified cholesterol (UC) with embedded apolipoproteins.

ApoB-100, a large protein with globular and helical amphipathic domains and beta-sheets [140] is considered to play a central role in the retention of LDL in atherogenesis. In humans, the full-length apoB-100 (4536 residues, 550 kDa) is synthetized and assembled into very low density lipoproteins (VLDL) in the liver [141]. Submerged in the LDL phospholipid surface membrane, apoB-100 contains the LDL receptor-binding domain and is (along with ApoE) a ligand of the LDL (B, E) receptors that facilitate the uptake and internalization of plasma LDL in peripheral tissues. A truncated form, apoB-48 (2152 residues) is produced in the human small intestine as an essential component of dietary chylomicrons [142, 143]. ApoB-100 and apoB-48 are products of a single gene, with apoB-48 resulting from post-transcriptional editing of apo B-100 mRNA [144]. High plasma concentrations of LDL cholesterol (exceeding 2 mmol/L (80 mg/dL), are one of the principal risk factors for atherosclerosis [136, 145].

Several lines of evidence suggest that intramural retention of atherogenic lipoproteins involves extracellular matrix (ECM) components, primarily proteoglycans (PGs) [137, 139, 146-152] and lipolytic enzymes, including lipoprotein lipase (LpL) and sphingomyelinase (SMase) [137]. Proteoglycans are macromolecules composed of a protein core to which one or more glycosaminoglycan (GAG) side chains are covalently bound [153]. The GAGs are sulfated polysaccharides that contribute to many of the properties of PGs, especially to the high density of negative charge characteristic of these molecules [154]. Of the several proteoglycans found in human atherosclerotic plaques (biglycan, decorin, perlecan), biglycan appears to be a prime candidate for a significant role in the trapping and retention of lipoproteins [155-157].

Biglycan, a small, leucine-rich PG, has a core protein of 331 amino acids, (45 kDa) with 2 GAG chains (C6S, or C4S type dermatan sulfate) attached to its N-terminal region [130, 154]. Biglycan is secreted in the ECM of many tissues including vascular endothelial and smooth muscle cells (SMCs) [158, 159]. Its core protein binds TGF-β with high affinity, and since its synthesis is in turn controlled by this growth factor, it is thought to form a negative feedback loop regulating TGF-β activity [160-162]. Biglycan interacts with ECM components, including collagen types I and V and fibronectin and can bind to phospholipase A2, which may act on arterial wall LDL, thus contributing to the migration of endothelial cells [154, 163-165]. Biglycan was found to co-localize with apoB (and apoE) in human atherosclerotic plaques [150, 166-168], and in vitro studies have demonstrated that biglycan can bind apoB- (and apoE-) containing particles [166]. The interaction between LDL and Biglycan involves the interaction of negatively charged sulfate and carboxylic groups on their glycosaminoglycan side chains with positively charged residues on apolipoproteins B and E [137, 150, 152, 169-171]. Kinetic analyses suggest that LDL trapping is due to selective retention by proteoglycans rather than increased influx [137, 172, 173].

Retained LDL undergoes several modifications, including oxidation, lipase modification, glycation, aggregation and incorporation into immune complexes [136]. Oxidation has been proposed to be central to atherogenesis [135, 136, 174, 175]. Oxidized LDL (lipid peroxide) has a number of biological effects that can initiate and contribute to the progression of an immune response. It is chemoattractive via the induction of endothelial and smooth muscle cells [176] or at higher degrees of oxidation directly [177] to monocytes, SMCs, [178] and (CD4 & CD8) T-lymphocytes [179]. It stimulates the multiplication of macrophages (by up-regulating the expression of genes for macrophage colony-stimulating factor) [180-182].

Monocyte-derived macrophages in the activated state produce chemokines, cytokines, growth factors and proteolytic enzymes (particularly metalloproteinases), eventually leading to focal necrosis [183]. Modified LDL is avidly taken up by macrophages, leading to foam cell formation [184, 185], which further stimulates the release of LpL [186] and other atherogenic factors [187] and has also been shown to alter proteoglycan metabolism, thus further facilitating the accumulation of cholesterol esters [180, 181]. Another function of macrophages is to present antigens (via

expression of class II histocompatibility antigens such as HLA-DR) to T lymphocytes [188], one possible antigen being oxidized LDL itself [189]. Modified LDL is taken up by SMCs as well [190], which also can present antigens to T-cells [191].

Retained altered lipoproteins together with macrophages can stimulate chemotaxis and transformation of SMCs to the proliferative state, causing increased synthesis of proteoglycans [161, 178, 192, 193] and possibly LpL [194, 195], leading to expansion of the lesion and remodeling of the arterial wall [196]. CD4 and CD8 T-lymphocytes are present in the atherosclerotic lesion at all stages [197]. T-cell activation results in the secretion of cytokines (including interferon-g and tumor necrosis factors α and β,) that amplify the inflammatory response [191]. Certain mediators of inflammation (tumor necrosis factor (TNF-α, interleukin-1, and macrophage colony-stimulating factor) increase binding of LDL to endothelium and smooth muscle and also increase [198] the transcription of the LDL-receptor gene. Thus, a vicious circle of lipoprotein retention, modification, and inflammation leads to the progression of the atheromatous lesion [135, 136].

Some observations suggest that atherosclerosis and AMD may share certain common pathogenetic pathways [199]. BlinD material is structurally similar to extracellular material in atheromatous plaques [200, 201]. The presence of several factors known to play a role in atherogenesis including neutral fats [125, 132, 202], esterified cholesterol (EC) [125, 203], unsaturated fatty acids, phospholipids [132, 204, 205], and peroxidized lipids [206], apoB-100 [207] and proteoglycans [97, 208-211] have been demonstrated in Bruch's membrane and/or sub-RPE deposits in AMD eyes.

There is also growing evidence for the involvement of immune-mediated processes in AMD [3, 4, 212-214]. Protein components of virtually all clinically defined phenotypes of hard and soft drusen include immunoglobulin and components of the complement pathway associated with immune complex deposition (C5, C5b-9 terminal complex), molecules involved in the acute-phase response to inflammation (e.g. amyloid P component and α_1-antitrypsin), proteins that modulate the immune response (e.g. vitronectin, clusterin, apoE, membrane cofactor protein, and complement receptor 1), major histocompatibility complex class II antigens, and HLA-DR and cluster differentiation antigens [215-218].

Cellular components of drusen include RPE blebs, lipofuscin, and melanin, as well

as [123, 219, 220] central ‘core’ domains which are comprised largely of glycoproteins with O-glycosidically-linked carbohydrate moieties. Cell-associated molecules, including HLA-DR and specific CD antigens, are associated with the core domains. Characterization of these cores indicate that they sometimes include bulbous cell processes that breach Bruch’s membrane, and terminate as bulbous, vesicle-filled sacs, ‘cores’ within the centers of drusen. These processes can be traced back to cell bodies on the choroidal side of BrM. These cells immunoreact with a characteristic subset of CD antigens and MHC class II antibodies, indicating that they are of monocytic origin. Specific markers include CD1a, CD83, and CD86 antibodies, providing strong evidence that they are dendritic cells that belong to the DC1 lineage. DC1 cells are powerful antigen-presenting cells that are believed to participate in the induction of immunity. These cores are observed in all drusen phenotypes [221], and are present in both macular and extramacular drusen. Approximately 40% of drusen contain dendritic cell-associated cores.

Hageman et al. proposed that - similar to the process in atherosclerosis - choroidal dendritic cells may be activated and recruited by injured RPE (eg, via monocyte chemotactic protein) and oxidized proteins and lipids in Bruch’s membrane. Activation of choroidal dendritic cells may also initiate an autoimmune response to RPE and/or retinal antigens or to new antigens created within BrM. Anti-retinal and anti-RPE antibodies have been detected in the serum of patients with AMD [4]. Johnson and coworkers pointed out that the cytoplasmic accumulation of vitronectin, apoE and other drusen-associated molecules suggests that the cells are subjected to a chronic sublethal complement attack. Complement activation and associated inflammatory events occur in other diseases exhibiting cellular degeneration and accumulation of abnormal tissue deposits, including atherosclerosis and Alzheimer disease. In these diseases, damaged cells, highly insoluble protein deposits and extracellular debris activate complement pathways, resulting in chronic cellular damage with attendant cell surface blebbing, endocytosis, and upregulation of defense proteins [3]. Poorly degradable RPE debris and Bruch’s membrane components (eg, wide-spaced collagen) might maintain chronic inflammation [119, 222, 223]. Macrophages and foreign body giant cells near Bruch’s membrane become more common when basal linear deposit is present [224]. Activated macrophages and other inflammatory cells secrete enzymes that can damage cells and

degrade Bruch's membrane and by releasing cytokines, might foster CNV growth into the sub-RPE space [225]. In the later stages of AMD, accumulations of giant multinucleated cells [226, 227] and other leukocytes [223] in the choroid of donors and in excised CNVs have been noted and HLA-DR immunoreactivity of retinal microglia is also increases in AMD [228].

2.6. Murine models of lipid retention.

Modelling lipid entrapment and retention in mice poses a number of problems, due to the inherent disparities between murine and human lipid transport. ApoB contained within murine LDL is predominantly a truncated form, apoB-48, which contains proteoglycan-binding sites different from those in apoB-100 [229]. Unlike apoB-100, lipoprotein containing apoB-48 can be cleared from the plasma by receptors other than LDL-R [230]. Inserting the human apoB-100 gene into the C57BL/6 genome has been shown to render its lipoprotein profile similar to the human, including a sharp increase in plasma LDL following ingestion of a high-fat diet [231]. These animals are also more prone to develop atherosclerosis [232]. Introducing the human biglycan gene into apoB-100 transgenic mice may further improve this model. Considering the apoB-100-binding ability of biglycan, an overexpression of the human biglycan protein in apoB-100 overexpressing mice may be expected to provide an improved animal model of atherosclerosis and related conditions and AMD.

AIMS

1. The aim of the clinical part of our investigations was to probe the functional implications of macular soft drusen regression in AMD eyes, with the following questions in mind:
    1.1. Is the regression of macular soft drusen accompanied by signs of progression of the underlying AMD process, detectable in colour fundus images?
    1.2. Is the regression of macular soft drusen associated with consequent abnormal fundus autofluorescence?
    1.3. Is the regression of macular soft drusen associated with subsequent function loss?

2. In the experimental morphological part of our investigations, we aimed to characterize ultrastructural changes in Bruch's Membrane with respect to serum lipid characteristics of transgenic mice overexpressing the human apoB-100, biglycan or both genes in combination with a high-cholesterol diet, with a view to the following questions:
    2.1. Does a high-cholesterol diet and/or the overexpression of the apoB-100 or biglycan proteins affect serum lipid levels?
    2.2. How does BrM thickness correlate with the above factors?
    2.3. How is the ultrastructure of BrM affected by the above factors?
    2.4. Can morphological indications of consequences for photoreceptor cells be detected?
    2.5. Are there indications for an ApoB100-biglycan interaction as a triggering event for lipid entrapment within BrM?

METHODS

1. Functional aspects of drusen regression in AMD.

1.1. Patients

Patients were selected from a large ongoing collection of clinical data at the Reading Centre of Moorfields Eye Hospital. Inclusion criteria were: a clinical diagnosis of AMD, both manifest and resolved soft macular drusen, a level of fixation and general fitness sufficient to perform the full test sequence. Patients with exudative late-stage AMD in the eye studied were excluded.

Sequential colour fundus and FAF images of 960 patients were screened for disappearing drusen. Soft drusen regression was detected in 34 cases (25 spontaneous, 9 following prophylactic laser treatment). 19 patients met all inclusion criteria, 14 (10 female, 4 male) agreed to participate in the study, ranging in age from 52 to 84 years (median age was 72 years). The baseline of the study was defined as the earliest date when both clinical data and fundus SCI were available, and the endpoint as the date the patient was last seen clinically. The mean follow-up period was 5.9 years (ranging from 2.8 to 14.4 years). In ten cases the drusen regressed spontaneously, four patients received prophylactic laser treatment (one 100µm argon laser spot each clock hour 1000µm from the fovea) prior to drusen regression.

1.2. Imaging

1.2.1. Colour fundus imaging

ETDRS Standard 30º stereo Field 2 colour images (SCI) of the fundus were recorded digitally using a fundus camera [233]. Field 2 images, defined as centred on the macula (see 2 in Figure 16), were taken using the following procedure: the macula is centred near the intersection of the cross hairs in the ocular. To keep the central gray artefact created by some cameras from obscuring the center of the macula, the intersection of the cross hairs should be placed about 1/8 - 1/4 DD above the center of the macula. A suitable position can often be obtained by rotating the camera temporally from the Field 1 position, without vertical adjustment. A comprehensive protocol of the "Modified 7-Standard Field Color Fundus Photography and Fluorescein Angiography

Procedure" can be found at the University of Wisconsin website at http://eyephoto.ophth.wisc.edu/Photographers.html With respect to Field 2 images, this protocol is essentially identical to the one used in our study.

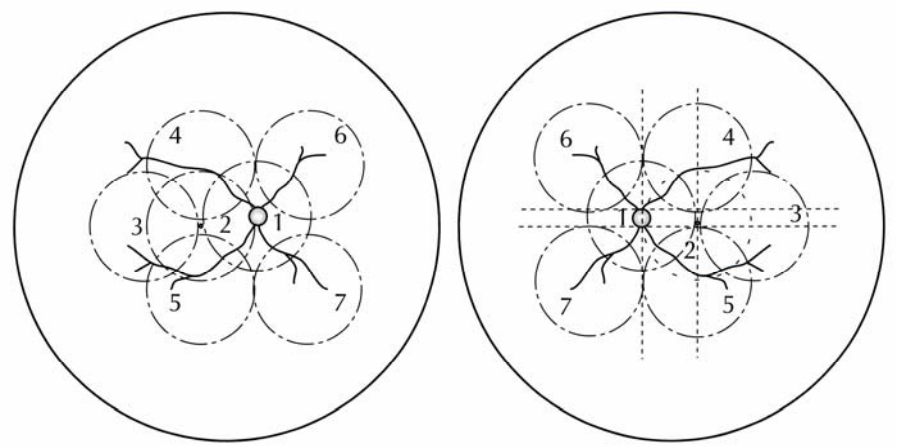

Figure 16. The 7-standard fields for color photography specified by the ETDRS protocol. Source: [233] In our study, Field 2 images (2) were used.

1.2.2. Fundus Autofluorescence Imaging

FAF imaging was performed using a cSLO (Heidelberg Retina Angiograph 2, Heidelberg Engineering GmbH, Dossenheim, Germany). A cSLO system was selected for FAF imaging due to the inherent advantage of these devices over conventional fundus cameras that the plane of the detection system is conjugate to the fundus, and light from alternate planes is rejected, thus the competing autofluorescence of the crystalline lens is minimised [53]. The fundus was illuminated using a solid-state laser (488nm), induced fluorescence was recorded through a long-pass filter with a short-wavelength cut-off at 500nm. The image of a 30°x30° retinal area centred on the fovea was recorded digitally at 1536x1536 pixel (5µm/pixel) resolution on a 256-level grey-scale. To reduce random noise, a master image was produced by averaging 16 individually recorded images for each eye in the study. Lens opacities, where present, were in all cases diffuse and permitted adequate imaging of FAF.

1.3. Phenotyping

Stereoscopic image pairs were displayed on an Eizo FlexScan L997 monitor (Eizo Nanao Co, Hakusan, Ishikawa, Japan) utilising a 21" Hitachi S-IPS TFT panel

(TX54D11VC0CAC), calibrated for colour accuracy using a Datacolor Spyder 2 colorimeter (Datacolor Inc., Lawrenceville, NJ, USA). Stereo image pairs were viewed using Screen-Vu^{TM} Stereoscopes (PS Manufacturing, Portland, Oregon, USA).

Detailed phenotyping was performed by grading based on digital Field 2 colour and FAF images, according to the system defined in the International Classification for ARM and AMD [20]. The grading process uses a standard grid template adapted from the International ARM Epidemiological Study Group, see Figure 17. Images were graded for image quality and features of AMD as specified in the coding manuals (The complete coding manual can be found in the Appendix). Definitions have been established for the grading terms 'absent', 'questionable', 'present', and 'cannot grade' (obscuring lesion or photo quality). 'Absent' means that the abnormality under consideration is not present or the grader is less than 50% certain that the abnormality is present in the area under consideration. 'Questionable' means that the grader is at least 50% but less than 90% certain that the abnormality is present in the area under consideration. 'Present' means that the grader is at least 90% certain that the abnormality is present in the area being graded. 'Cannot grade' means that either an obscuring lesion or poor photographic quality prevents assessment of any abnormality in the area under consideration. The definitions of hard drusen, the abnormalities of early AMD (soft drusen, areas of increased pigment or hyperpigmentation, areas of depigmentation or hypopigmentation) and late AMD (GA and CNV) were used as previously established by the International ARM Epidemiological Study Group [20]. Other lesions that are not considered characteristic of AMD were identified and recorded.

Data were collected using grading forms and entered into a database once all the grading was completed. Grading was performed independently by two certified graders masked to the identity of the patients and the main aim of the study. These gradings were compared for inter- and intra-observer reliability as well as for reliability over time [234, 235]. A final copy was created by adjudication and changes over time in the final copy were analysed. In cases where the simultaneous presence of AMD, disappearance of drusen and absence of exudative disease were confirmed, the patient was invited for functional testing.

1.4. Psychophysical testing

For psychophysical testing Fine Matrix Mapping (FMM) was selected due to its superior spatial resolution and its ability to measure wide ranges of sensitivity changes. The full test sequence included a visual acuity test, a standard visual field examination using the 30-2 program of the Humphrey Field Analyzer (HFA, Carl Zeiss Ltd., Welwyn Garden City, UK), a photopic FMM test, pupil dilatation with 1.0% tropicamide and 2.5% phenylephrine, dark adaptation for 45 minutes, a scotopic 30-2 visual field test, scotopic FMM and finally the determination of the location and stability of fixation.

1.4.1. Fine-Matrix Mapping

FMM was performed using a modified HFA. Test flashes were positioned over the retinal area of interest, including both drusen and areas where the resolution of drusen was confirmed by grading. The coordinates of four interlaced 5x5 grids (25 locations with 2° intervals) were entered in the "Custom Grid" feature of the perimeter. Each grid was offset relative to the other grids by 1° on either the *x, y,* or both axes. Data thus obtained were merged into a single 9° x 9° matrix of 100 test locations with 1° intervals (Figure 17). A standard (Goldmann) size 3 stimulus was used. Photopic testing was done using a white stimulus with a background illuminance of 31.5 apostilbs, scotopic measurements were done using a blue stimulus with no background illumination. Fixation stability was monitored through an infrared camera. Detection threshold sensitivity was expressed in decibels and thresholds as log units. The maximum stimulus illuminance of 10,000 apostilbs was interpreted as 0dB (Figure 18).

1.4.2. FMM Data processing

FMM thresholds were processed by (3x3) Gaussian filtering to improve repeatability [236]. The attenuation of the original signal and loss of detail inherent in all smoothing methods was in our case insignificant and outweighed by the benefits with respect to noise reduction (repeatability) [237]. Reference data from age-matched normal individuals was obtained by point-by-point averaging of the sensitivity thresholds of individuals from the correct age group previously tested for the matching retinal area, under identical conditions, using the same equipment as for the test subjects (n=8).

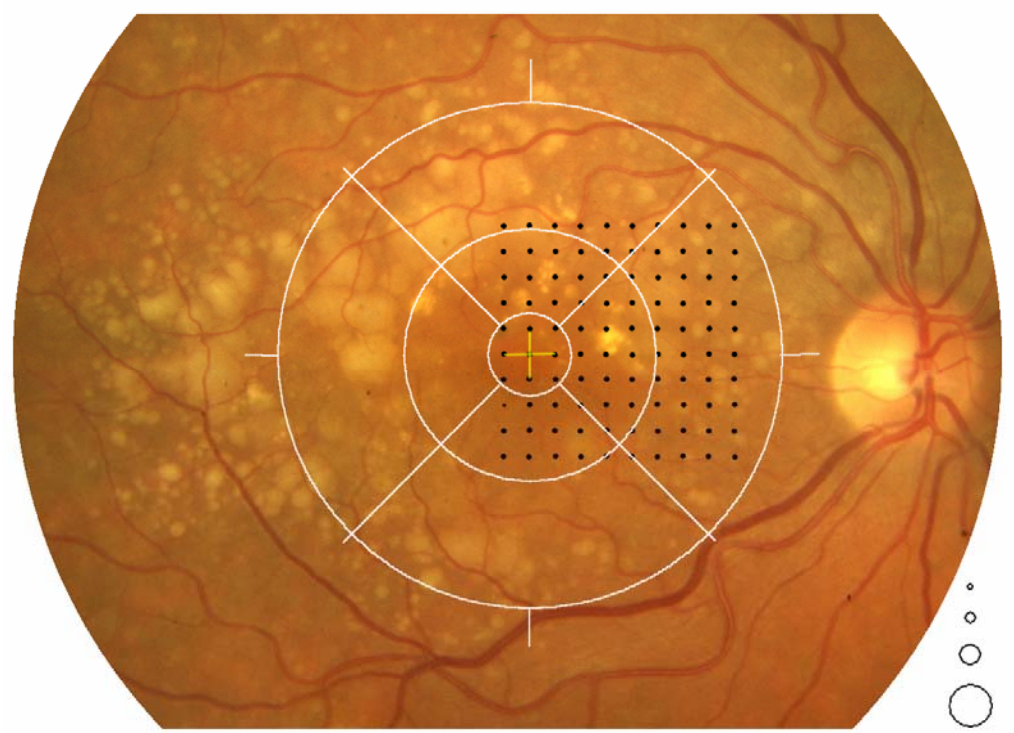

Figure 17. Fundus image of patient 3 together with the standard grid used for grading abnormalities of age-related macular degeneration and the 9°x 9° FMM matrix of 100 test locations. The grid consists of 3 circles defining 3 zones of the fundus photograph. The diameter of the central (zone 1), middle (zone 2), and outer (zone 3) circle is, respectively 1000, 3000, and 6000µm. Spokes on the grid help in centering the grid on the macula. A set of graduated circles (displayed on the right) is used to estimate the size of drusen, pigment abnormality or geographic atrophy. The approximate diameter of the 4 standard circles corresponds to 63µm, 125µm, 250µm, and 500µm, respectively. The FMM matrix in this case is offset nasally relative to the point of fixation to capture thresholds within the retinal area of interest.

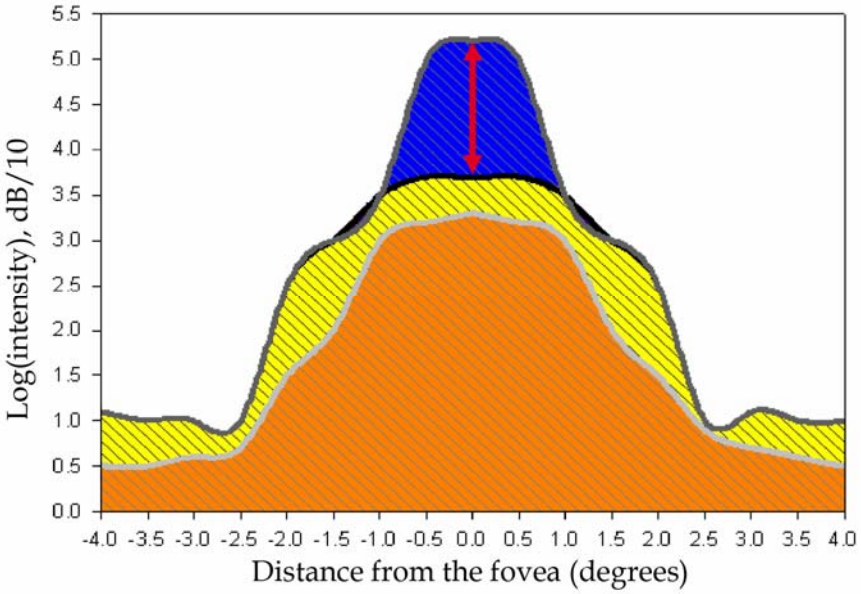

Figure 18. Scotopic retinal sensitivity threshold graph indicating a limitation of FMM. The maximum attainable stimulus intensity is 10000 apobstilbs, retinal thresholds above this intensity level are not detectable using this method. This is a limitation inherent in all testing systems at various levels. Orange area: thresholds of a normal patient, yellow area: thresholds of an AMD patient, Blue area/red arrow: thresholds not detectable using this method. Source: Mr Vy Luong.

Some of these reference data have been used previously in other publications [91, 238-240]. Figure 19 shows the standard plots of a normal individual.

For each patient, sensitivity data were analyzed intra-individually as well as compared with age-matched normal data through point-by-point subtraction of averaged normal values at corresponding coordinates within the FMM matrix. Filtered data were used to calculate the mean and the maximum threshold elevation from baseline as well as elevation relative to averaged threshold levels of the normal control group. Interpolated threshold values at 0.25° intervals were used to generate a contour plot showing luminance sensitivity gradients across the matrix. Three-dimensional threshold profiles were also generated.

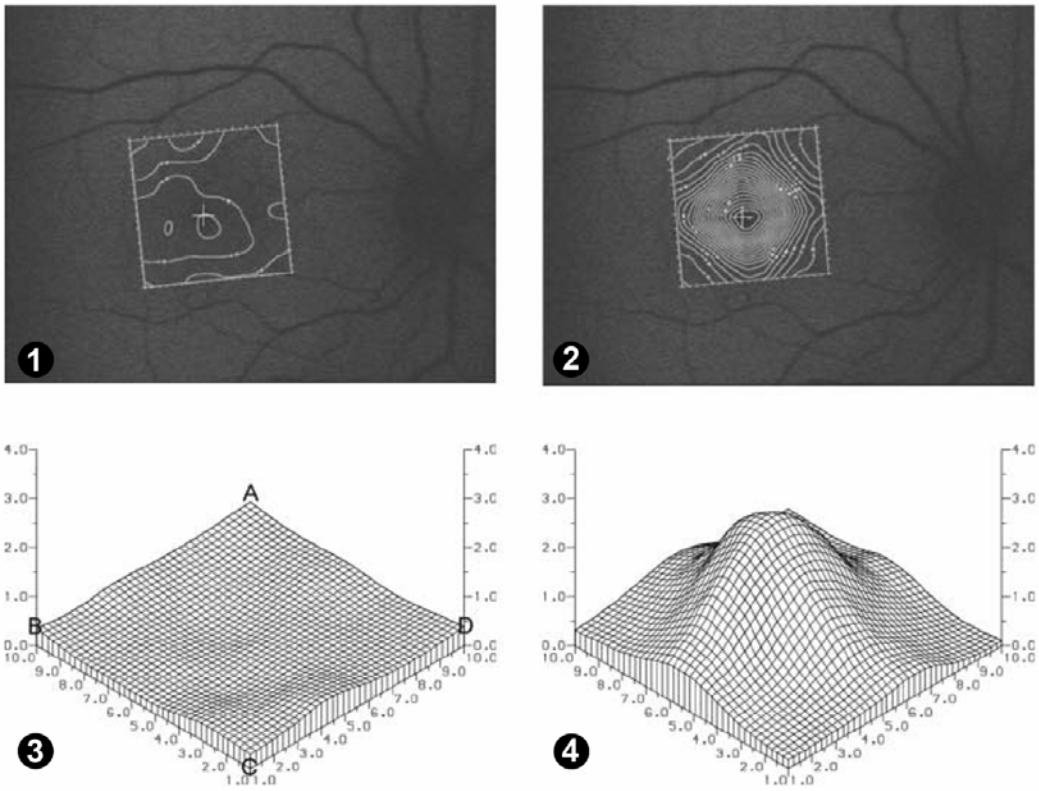

Figure 19. Photopic (images 1 & 3) and scotopic (images 2 & 4) in a normal subject. The FMM testing grid was centred on the fovea. 1 and 2 show contour plots placed in the correct position in FAF images, 3 & 4 show three dimensional surface plots of the threshold data. In all FAF contour maps shown, A corresponds to the bottom right corner, B to the bottom left corner, C to the top left corner, and D to the top right corner, respectively. Source: [91]

1.5. Fixation stability

A major factor influencing FMM test reliability is the stability of fixation. For the measurement of fixation stability, a customized cSLO was used in a way similar to a technique described previously [241]. A fixation stimulus in the shape of a cross with

positive contrast was provided by a helium-neon laser (633nm) that is modulated through an acousto-optic modulator. An infrared (830nm) diode laser allowed high-contrast imaging of the subject's fundus. The subject was asked to fixate the stimulus for 30 seconds. Following an initial 10-second delay, the image of the patient's fundus was acquired throughout a period of 20 seconds as a standard (PAL) allowed high-contrast imaging of the subject's fundus. The subject was asked to fixate full-motion video sequence, recorded on an SVHS video tape. From this sequence 250 consecutive images were digitized at 25 frames per second. The digitized images were reviewed and images of low quality were discarded, resulting in an approximately 10-second sample. One image of this sequence was selected as the master to which all the other images were aligned digitally by custom software. The alignment procedure provided the magnitude of image mismatch on both the x- and y-axes. These values reflect eye movements and are used to calculate the bivariate contour ellipse area (BCEA), which is the area of an ellipse on the retinal surface within which the centre of the target was imaged 68% of the time [242]. BCEA is a standardized measure which provides a means for quantification and comparison of fixation stability. Smaller BCEA values correspond to more precise fixation.

1.6. Image processing and analysis

For each patient, colour fundus images taken at base line and at subsequent visits as well as FAF images were imported into individual layers within a multi-layered composite image in Adobe PhotoShop. The colour fundus image taken at FMM testing was considered the master and layer geometry for all other layers was adjusted to obtain exact correspondence between fundus features within individual layers and to eliminate distortions of images taken at different points in time and in many cases using different fundus cameras. Original colour profiles were preserved. Retinal sensitivity threshold contour plots obtained through Fine Matrix Mapping were superimposed over the fundus images. Anatomic and perimetric landmarks (choroidal pattern, retinal vasculature, centre of the optic disc and the blind spot, centre of fixation and the fovea) were used for correct alignment.

Composite images were analysed for correlations at identical retinal locations between fundus appearance at different points in time, autofluorescence, and retinal

sensitivity. By switching from one layer to the next and back, even minute differences in fundus appearance were detectable at specific and identical fundus locations, a significant advantage of this overlay method compared to previous sequential or side-by-side analysis methods.

Total area covered by drusen within the macula at baseline and at FMM testing was marked in a semi-automated fashion using custom software in individual area markup layers. For each zone within the IC grading grid (Figure 17), areas were measured with a single-pixel precision. Changes in drusen area were identified through binary logical operations between markup layers (using the operands AND and NOT): areas with disappearing drusen were defined as pixels present at baseline NOT at FMM testing, persistent drusen as pixels present at baseline AND at FMM testing, new drusen as pixels present at FMM testing NOT at baseline. Areas with disappearing drusen, persistent drusen and drusen-free areas were identified delineated and associated levels of sensitivity loss were compared.

Software used include: Adobe Photoshop versions 7, CS and CS2 (Adobe Systems Inc., San Jose CA, USA) with the 'FoveaPro' plug-in (Reindeer Graphics Inc., Asheville, NC, USA), ImageJ analysis package v1.38x (US National Institutes of Health, Bethesda, Maryland, USA), Microsoft Excel 2002 (Microsoft Co., Redmond, WA, USA) and SPSS v11 (SPSS Inc. Chicago, IL, USA)

1.7. Legal issues

The study protocol adhered to the tenets of the Declaration of Helsinki and was approved by the local ethics committee. Before inclusion, written, informed consent was obtained from each participating patient after explanation of the nature of the study. Maximum retinal irradiance of lasers used was well below the limits established by the American National Standards Institute (ANSI Z136.1; 1993) and other international standards.

2. Characterisation of Bruch's membrane ultrastructure in apoB-100 and biglycan transgenic mice.

2.1. Mice

Transgenic mice were produced at the Biological Research Center of the Hungarian Academy of Sciences in Szeged, Hungary. ApoB-100 mice were produced as described previously [243]. Briefly, fertilized oocytes from wild-type female mice (C57BL/6 x CBA F1) were collected and injected with purified P1-phagemid DNA containing the entire 43 kb human apoB-100 gene, the 19 kb of the 5' and the 14 kb of the 3' flanking genomic sequences [244] (kind bequest of Professor Edward M Rubin, Life Sciences Division, Lawrence Berkeley Laboratory, University of California, Berkeley, CA, USA) in a concentration of 1 ng/ml, according to a standard technique [245]. The $apoB^{+/+}$ transgenic mice were homozygous for the human apoB transgene. Both the wild-type F1 and the Tg F1 generation mice lines were backcrossed twice with the C57BL/6 strain in order to approach closer to the susceptible genetic background. The wild-type animals were not littermates of apoB transgenic mice. The tail DNA of 10-day-old pups was purified [246], and integrated transgenes were detected by PCR, using primers from the 5' promoter region of the human apoB-100 gene [244]. The best-expressing line was selected for further studies.

Biglycan transgenic mice were generated as described by Bjelik et al [247]. A GeneStorm® Expression-Ready clone expressing the human biglycan gene construct (Invitrogen, Carlsbad, CA) involves human biglycan cDNA fused to a CMV promoter, a V5 epitope and a 6X His Tag sequence at the 3' end of the cDNA. A 3440bp fragment including the transcription unit was separated from the vector backbone, and the purified DNA was microinjected at 2ng/ml into the fertilized oocytes of female C57BL/6XCBA F1 mice, using the standard pronucleus microinjection technique. Microinjected eggs were implanted into the oviduct of pseudopregnant Swiss female mice. Transgenic founders were identified by using PCR analysis and dot blot hybridization on tail DNA samples. For PCR analysis, the following primers were used: forward primer: 5'-GGA CTC TGT CAC ACC CAC CT-3', and reverse primer: 5'-AGC TCG GAG ATG TCG TTG TT-3'. For dot-blot hybridization, a 824 bp, *Nru*I–*Hind*III fragment was radiolabeled with [α-^{32}P]dCTP using the Ready-to-Go Kit and

hybridized to 5μg of genomic DNA. Integrated transgenes were also confirmed by quantitative RT-PCR (QRT-PCR) in their offspring. The clone expressing the human biglycan mRNA at the highest level, was selected for further study. Homozygous apoB-100 (apoB-$100^{+/+}$, group 3) and biglycan (biglycan$^{+/+}$, group 5) transgenic mice were crossed to produce hemizygous double transgenic (apoB-$100^{+/-}$ x biglycan$^{+/-}$, group 7) littermates. Increased gene expression levels were confirmed by QRT-PCR. Wild-type C57BL/6 mice were used as controls (group 1).

2.2. Diet and environment

All animals (n=5 per group) were initially raised on a standard diet (CRLT/N, EU registration code HU13100039). Experimental groups (groups 2, 4, 6, 8, see Tables 5 and 6) were switched to a diet supplemented with 2% cholesterol at 6 weeks of age, for 17 weeks. All mice had free access to food and water and were maintained on 12-hour light-dark cycles with standard day ambient light maintained at 500 lux. Cages were kept on middle shelves of the cage rack and were not exposed to direct sunlight. All experiments were conducted according to the Declaration of Helsinki and Guiding Principles in the Care and Use of Animals and in compliance with the Association for Research in Vision and Ophthalmology statement for the use of animals in ophthalmic and vision research. The experimental protocol was approved by the local animal care ethical committee.

2.3. Determination of serum cholesterol levels

Serum lipid levels were measured by the Cardiovascular Research Group, at the Department of Biochemistry of the University of Szeged, Hungary. Blood samples were obtained by cardiac puncture, following anaesthesia. Total and LDL cholesterol levels were measured in triplicate, using commercially available colorimetric assays adapted to 96-well plates (Diagnosticum Ltd., Budapest, Hungary) [248]. The accuracy of the assays was monitored by using Standard Lipid Controls (Multiparametric HDL/LDL Calibrator, Sentinel Diagnostics SpA, Milano, Italy).

2.4. Tissue preparation

Animals were sacrificed through anesthesia by ether and the eyes were removed.

Specimens for microscopy were promptly fixed, for light microscopy by immersion in 10% formaldehyde and for transmission electron microscopy in a solution of 1% glutaraldehyde and 1.5% paraformaldehyde in 0.1 M PBS at pH 7.2. The external ocular muscles, optic nerve, and anterior segment were removed. Specimens were post-fixed with 1% osmium tetroxide in 0.1 M PBS for 50 minutes, dehydrated and embedded in Araldite. For electron microscopy, ultra-thin sections were cut and washed in 1% uranyl acetate and Reynolds' lead citrate. Semi-thin sections for light microscopy were also cut and stained with Toulidine blue. For the analysis of semithin sections, the MIRAX Image Viewer was used (Carl Zeiss MicroImaging Inc. Thornwood, NY, USA)

2.5. TEM measurements

Electron microscopy was performed using a JEOL JEM-1010 Transmission Electron Microscope (Japan Electron Optics Laboratory Co. Ltd, Tokyo, Japan). Images were collected using a Gatan Orius CCD camera (Gatan Inc., Pleasanton, CA, USA) and converted from the proprietary Digital Micrograph DM3 format to 8 bit TIFFs for analysis, at 4008x2762 pixels resolution. Following an initial qualitative assessment of randomly selected sections from each group, measurements of Bruch's membrane thickness were performed on sections where the optic nerve head was clearly identified, the choriocapillary lumen was open and lined by a single layer of endothelium. Inter-capillary pillars and regions far peripheral to the optic nerve head were avoided (Figure 20). Measurements were taken at progressive and wherever possible, equal intervals. Three eyes per group were processed and at least 10 images per eye were taken for measurement. In each image, the boundaries of Bruch's membrane were marked manually and BrM thickness was measured in a semi-automated fashion with single-pixel resolution. A mean thickness value per image was calculated. Focal sub-RPE nodule severity was estimated according to the system devised by Sarks and van der Schaft [19, 106], (Table 2).

Measurements and analysis of Bruch's membrane ultrastructure were performed at x10,000 magnification. Morphometric analysis was performed using Adobe Photoshop CS (Adobe Systems Inc., San Jose CA, USA) with the Fovea Pro v4.0 plug-in (Reindeer Graphics Inc., Asheville, NC, USA) and the ImageJ analysis package v1.8 (US National Institutes of Health, Bethesda, Maryland, USA).

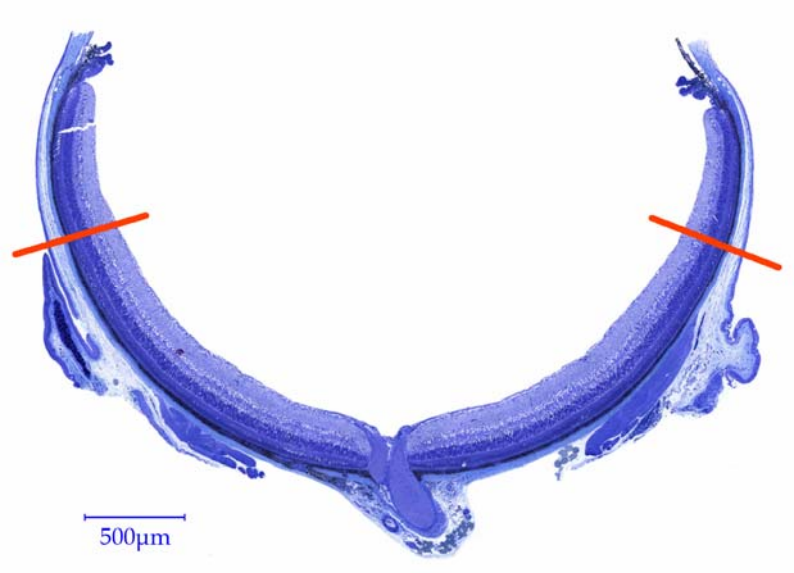

Figure 20. Semi-thin section of an eye of an apoB-100 x biglycan double transgenic mouse (Toluidine blue stain). For electron microscopic morphological and morphometric analysis, in order to avoid peripheral retinal parts, only sections were used where the optic nerve was fully present and measurements were made only in the posterior approximately two-thirds along the c-shaped section on either side of the ONH (boundaries indicated by red lines).

Table 2. Classification of BlamD according to Sarks & van der Schaft.

Class	Characteristics
0	No basal laminar deposit
1	Small solitary patches on the basal side of the RPE
2	Thin continuous layer, less than half the height of the RPE
3	Thick layer, greater than or equal to half the height of the RPE

2.6. Statistical analysis

Bruch's membrane thickness and serum lipid values of the groups were compared by one-way analysis of variance (ANOVA). Correlations were determined by calculating the Pearson Correlation Coefficients. Results were considered to be significantly different at a probability level of $p<0.05$. Software packages used included SPSS version 14 (SPSS Inc. Chicago, IL, USA) and GraphPad Prism 4 (GraphPad Software Inc., La Jolla, CA, USA)

RESULTS

1. Functional aspects of drusen regression in AMD.

1.1. Phenotype

The predominant phenotype in the study eye at baseline was "soft drusen" in all cases. Disappearance of drusen was followed by CNV in one, GA in 3 cases, while in 10 cases no indications of end-stage disease were seen in the colour fundus images. In most cases, parallel to fading drusen, new drusen in other locations appeared and grew in size and confluence (Table 3). New drusen tended to form at increasingly peripheral locations relative to the fovea. Repeated appearance of drusen in the same retinal location was not seen. Representative images are shown in Figure 1.

Table 3. Change in area covered by drusen.

patient	Zone 1		Zone 2		Zone 3	
	A	B	A	B	A	B
1	-90%	-31%	-50%	-5%	-13%	0%
2	-100%	-62%	-98%	-59%	-61%	8%
3	-98%	-97%	-69%	-23%	-41%	1%
4	-100%	-5%	-60%	-3%	-48%	1%
5	-5%	19%	-47%	0%	-46%	1%
6	-62%	-2%	-38%	14%	-61%	5%
7	-40%	-4%	-38%	-3%	-64%	-3%
8	-51%	8%	-72%	-16%	-72%	-7%
9	-100%	-46%	-89%	-8%	-48%	3%
10	-100%	-61%	-97%	-40%	-67%	0%
11	-100%	-11%	-66%	-1%	-49%	6%
12	-97%	-90%	-92%	-35%	-61%	-5%
13	-100%	-14%	-84%	-9%	-66%	5%
14	-11%	28%	-10%	23%	-16%	5%

Columns: (A) Reduction in area of soft drusen present at baseline in respective zone of the IC grading grid. (B) Overall change in area covered by drusen, including drusen appearing after baseline. Negative numbers indicate net decrease from baseline.

1.2. Autofluorescence

FAF associated with drusen varied from decreased to increased, no good correspondence was detectable. FAF corresponding to areas with disappearing drusen in the absence of pigmentary changes was normal in 7 cases. In two patients increased FAF was seen, in one case in an area adjacent to the junctional zone of a GA, in the other adjacent to a large crystalline druse. One other patient showed widely varying levels of FAF in connection with regressed drusen (Figure 21, row 3). GA was associated with decreased FAF centrally and increased FAF along the boundaries. Crystalline drusen showed decreased, granular hyperpigmentation and increased FAF.

1.3. Functional characteristics

Best corrected visual acuities in the study eye assessed at the time of FMM testing ranged from 6/12 to 6/5 (median=6/6). All patients had less than two lines loss in BCVA compared to the baseline value. Fixation Stability was good in all cases (Table 4). Two patients (2 and 4), both with end-stage disease, showed significant (more than 2 lines) deterioration in BCVA at the endpoint as compared to the baseline value. Fine Matrix Mapping showed generalised threshold elevation relative to normal controls both under photopic and scotopic conditions (Table 4). Scotopic sensitivity loss exceeded photopic loss in all cases (Figure 22). Scotopic loss over areas with drusen or regressed drusen did not differ significantly from that over non-drusen areas ($p=0.289$ and $p=0.989$ respectively, ANOVA, Figure 23). Elevated scotopic thresholds were seen associated with GA, crystalline drusen and coarse granular hyperpigmentation, all in connection with abnormal FAF. Photopic thresholds showed little topographic variation except in areas with GA.

Table 4. Functional characteristics.

Patient	FMM Photopic loss		FMM Scotopic loss		Fixation stability (BCEA, arc min^2)	BCVA (study eye)
	Background (mean)	Discrete (max)	Background (mean)	Discrete (max)		
1	0.34	0.91	1.04	1.62	74.41	6/6+1
2	0.77	3.22	1.15	2.32	16.60	6/12
3	0.75	1.01	0.78	1.27	88.20	6/6-1
4	0.87	1.25	1.48	1.81	26.50	6/12-1
5	0.53	0.70	0.69	1.06	46.51	6/6-4
6	0.58	0.87	1.26	2.13	42.08	6/6-2
7	1.00	1.40	1.11	1.83	50.90	6/6-1
8	0.69	1.02	1.03	1.93	116.15	6/5
9	0.26	0.44	1.11	1.55	133.10	6/6
10	0.82	1.93	1.38	2.19	63.22	6/6+2
11	0.64	0.75	0.90	1.50	90.83	6/12-2
12	0.52	0.75	1.60	2.36	80.99	6/12
13	0.52	1.08	1.69	2.40	42.59	6/5
14	0.63	1.00	1.45	2.13	50.55	6/9

FMM Global estimates of sensitivity loss are based on Gaussian filtered data and are expressed in log units.

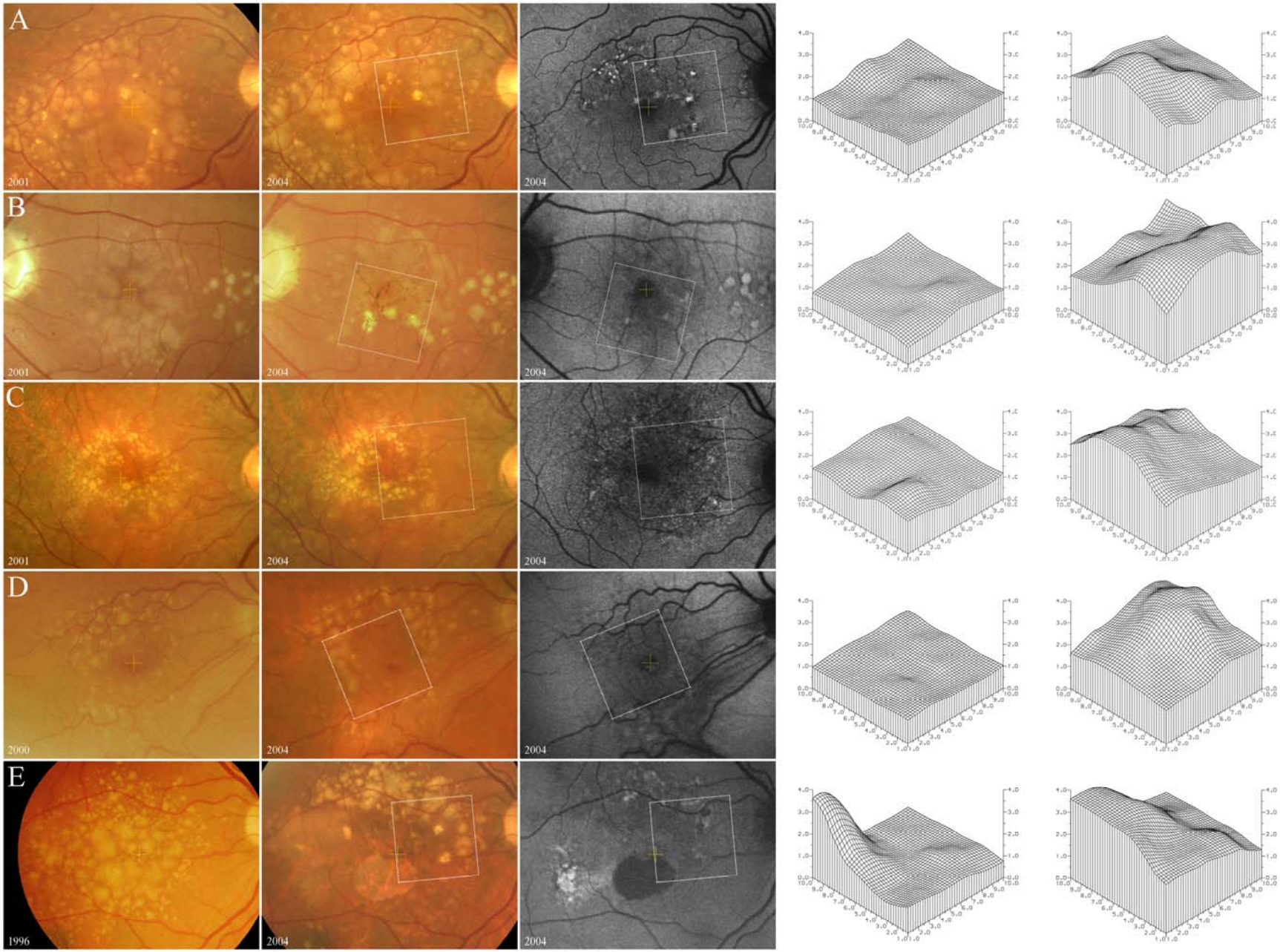

Figure 21. (see next page)

Figure 21. (previous page)
Representative images from selected cases. The first column shows the fundus at baseline, the second and third columns colour and FAF images taken at FMM testing, white rectangles mark the placement of respective FMM test grid, fourth and fifth columns show surface plots of photopic and scotopic FMM thresholds. Rows A, B and D (patients 3, 6 and 11) illustrate the typical picture seen in the majority of patients. Row C shows a case (patient 7) where areas with regressed drusen appear normal in the colour fundus image but show a speckled variation in FAF. Row E shows a case where progression to atrophy was noted (patient 2).

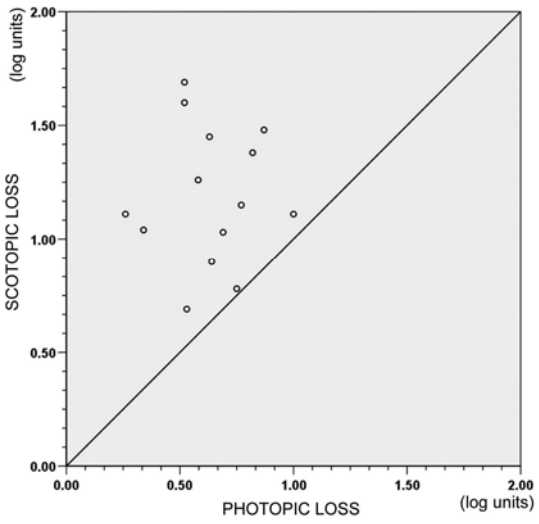

Figure 22. Photopic versus scotopic sensitivity loss of the 14 patients in the study.

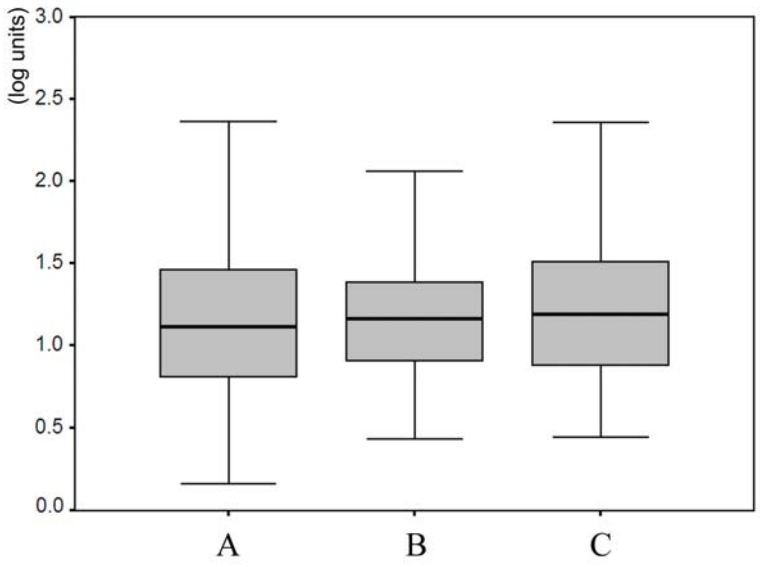

Figure 23. Regional differences in scotopic sensitivity loss at retinal locations with (C) drusen, (B) regressed drusen and (A) areas with normal appearance.

2. Characterisation of Bruch's membrane changes in apoB-100 and biglycan mice.

2.1. Serum Lipid Levels

In cholesterol-fed apoB transgenic (group 4) and apoB$^{+/-}$ x biglycan$^{+/-}$ double transgenic mice (group 8), serum total cholesterol levels were significantly elevated. Similarly, LDL-cholesterol was significantly increased in group 4, while a tendency of increase was observed in group 8 reaching statistical significance relative to biglycan transgenic mice on normal diet (group 5) (Table 5).

2.2. Bruch's Membrane Thickness

TEM measurements of BrM thickness showed a statistically significant increase in groups 4, 5, 6 and 8 compared to group 1. Groups 4 and 8 showed significant cholesterol-dependent increase in BrM thickness compared to non-cholesterol treated groups 3 and 7 respectively. The thickening of BrM in groups 5 and 6 was present irrespective of the diet. When group 5 and 6 are excluded, there is a strong correlation between BrM thickness and cholesterol levels in the remaining samples ($r=0.98$, $p<0.006$). (Table 6)

2.3. Bruch's Membrane Ultrastructure

Ultrastructural features of groups 1-8 are shown in Figure 24.

2.3.1. *Electron-lucent profiles*

Two distinct types of electron-lucent profiles were observed. One type was circular, 30-50nm in diameter with indistinct margins and appeared mostly in clusters that were often confluent. These were seen in all animals in groups 3-8, most densely in groups 4 and 8, but only in 3/6 animals in group 2 and 2/6 animals in group 1. Profiles of the second type were larger and more variable in size (100-350nm in diameter), usually oval in shape, with sharply demarcated outlines, delimited by a double-layered electron-dense membrane and were mostly as solitary or in small clusters, often surrounded by large numbers of the smaller, slightly more electron-lucent vacuoles. This type was

Table 5. Serum cholesterol levels (mmol/l).

Group		n	Total cholesterol		LDL cholesterol	
			mean	SEM	mean	SEM
1	C57BL/6 mice on normal diet	5	3.1	0.2	1.2	0.1
2	C57BL/6 mice on high-cholesterol diet	5	3.1	0.2	1.3	0.1
3	ApoB-100 transgenic mice on normal diet	5	3.4	0.4	1.4	0.1
4	ApoB-100 transgenic mice on high-cholesterol diet	5	5.0[(1)]	0.4	2.7[(1)]	0.5
5	Biglycan transgenic mice on normal diet	5	2.5	0.2	1.0	0.1
6	Biglycan transgenic mice on high-cholesterol diet	5	2.6	0.3	1.6	0.2
7	ApoB-100 x Biglycan double transgenic mice on normal diet	5	3.1	0.2	1.2	0.1
8	ApoB-100 x Biglycan double transgenic mice on high-cholesterol diet	5	4.9[(2)]	0.5	2.1[(3)]	0.2

Statistically significant differences ($p<0.05$): [(1)] relative to groups 1, 2, 3, 5, 6 and 7, [(2)] relative to groups 1, 2, 5, 6 and 7, [(3)] $p=0.015$ relative to group 5. (one-way ANOVA with the Sidak probe for pair-wise comparisons).

Table 6. Bruch's Membrane thickness.

Group		n	Bruch's membrane thickness (nm)			
			mean	SD	min	max
1	C57BL/6 mice on normal diet	6	345	47	246	434
2	C57BL/6 mice on high-cholesterol diet	6	348	57	249	515
3	ApoB-100 transgenic mice on normal diet	3	369	63	261	536
4	ApoB-100 transgenic mice on high-cholesterol diet	3	475$^{(1)(2)}$	116	291	795
5	Biglycan transgenic mice on normal diet	3	519$^{(1)}$	120	327	806
6	Biglycan transgenic mice on high-cholesterol diet	3	545$^{(1)}$	195	306	1567
7	ApoB-100 x Biglycan double transgenic mice on normal diet	3	381	52	282	489
8	ApoB-100 x Biglycan double transgenic mice on high-cholesterol diet	3	476$^{(1)(3)}$	138	293	998

Statistically significant difference, $p<0.05$ $^{(1)}$relative to group 1, $^{(2)}$relative to group 3, $^{(3)}$relative to group 7, (one-way ANOVA)

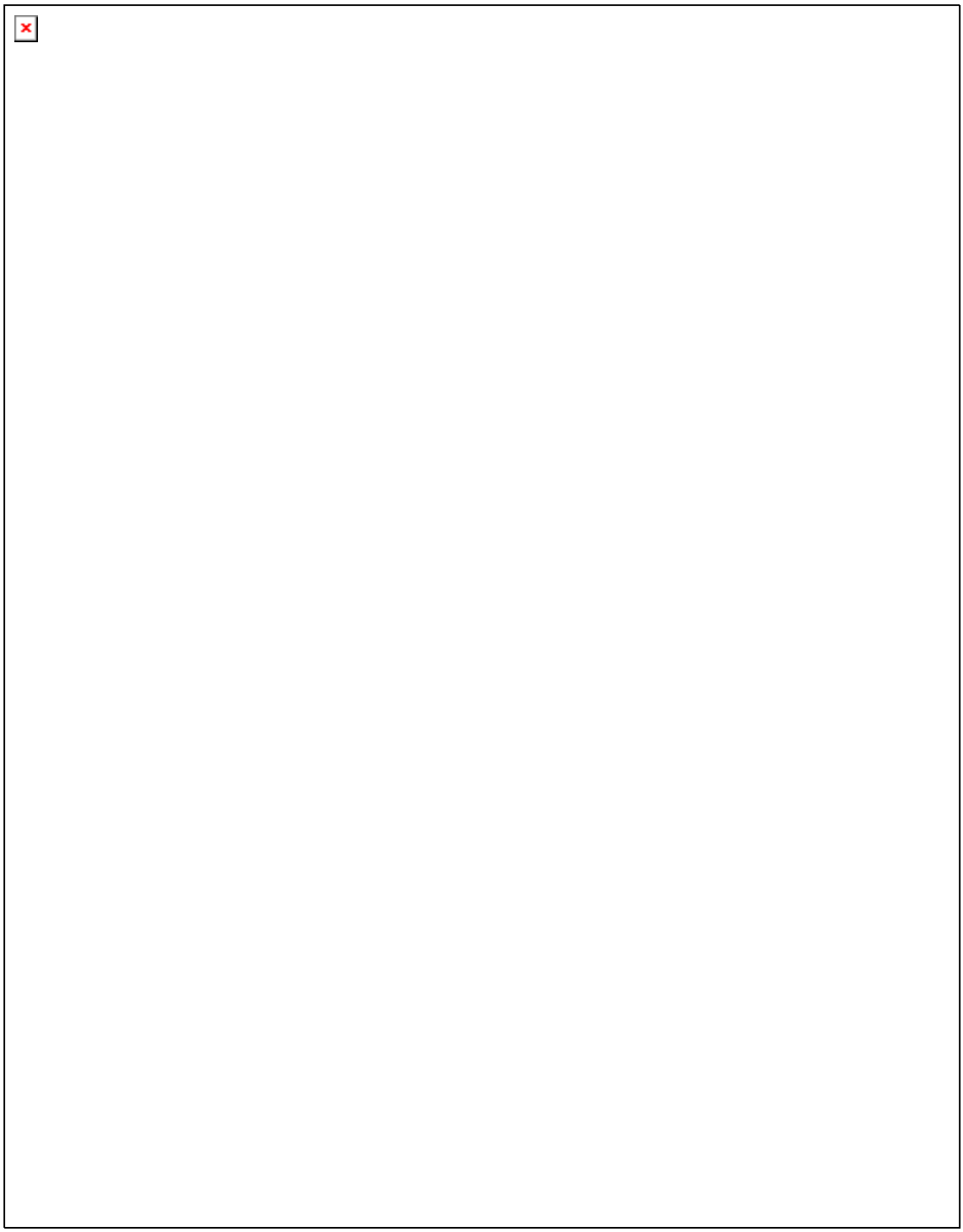

Figure 24. Representative TEM images from all 8 groups studied. Left column (A, C, E, G): animals on normal diet, right column (B, D, F, H): animals on a high-cholesterol diet. (A-B): wild-type mice; (C-D): ApoB-100 transgenic mice; (E-F): Biglycan transgenic mice; (G-H): ApoB-100xBiglycan double transgenic mice. (Scale bars 500nm). Bruch's membrane (BM) is aligned horizontally between the pigment epithelium (RPE) on top and the choriocapillaris (Ch) at the bottom. Arrowheads indicate the boundaries of BM. The asterisk in image H indicates the accumulation of material between the RPE basal processes, showing a banding pattern.

present in all transgenic groups, most frequently in group 4, but only occasionally in 3/6 animals of group 2 and were not seen in group 1. A summary of these results can be seen in the supplementary information provided (table 4). Both types of electron-lucent profiles occurred scattered throughout the inner and outer collagenous layers of BrM, the smaller type occurring with higher density in and near the inter-capillary pillars (Figure 25).

2.3.2. *Focal sub-RPE nodules*

In transgenic animals, focal nodules of an amorphous material of intermediate-electron density were present between the plasma and basement membranes of the RPE, amid misaligned and disorganised or atrophied RPE basal processes (Figure 25, G-H). These nodules were most frequent and extensive in group 4. The estimated severity scores according to the system devised by Sarks and van der Schaft et al. [19, 106]. were class 2 (thin continuous) in 2/3 animals of group 4, class 1 (focal) in 1/3 of group 4 and all other transgenics, and class 0 (not present) in wild-type animals.

2.3.3. *Focal thickening of BrM*

In groups 5 and 6, a significant thickening of BrM was noted. This was in all cases associated with a continuous layer of varying thickness of a basement membrane-like material in outer BrM. Frequently, this layer became focally massive, resulting in an up to fourfold thickening of BrM (Figure 26). This phenomenon was also present with similar frequency but more attenuated amplitude in groups 7 and 8 animals and was not seen in animals not carrying the human biglycan gene. Measurement of the thickness of this layer was not possible with reasonable precision due to a lack of a clear boundary towards the inner layers of BrM.

2.3.4. *Fragmentation of the elastic lamina*

Longer continuous segments of the elastic lamina were only visible in wild-type and biglycan transgenic animals. In all other groups, only fragments were apparent (Figure 25). No differences in the degree of fragmentation could be determined.

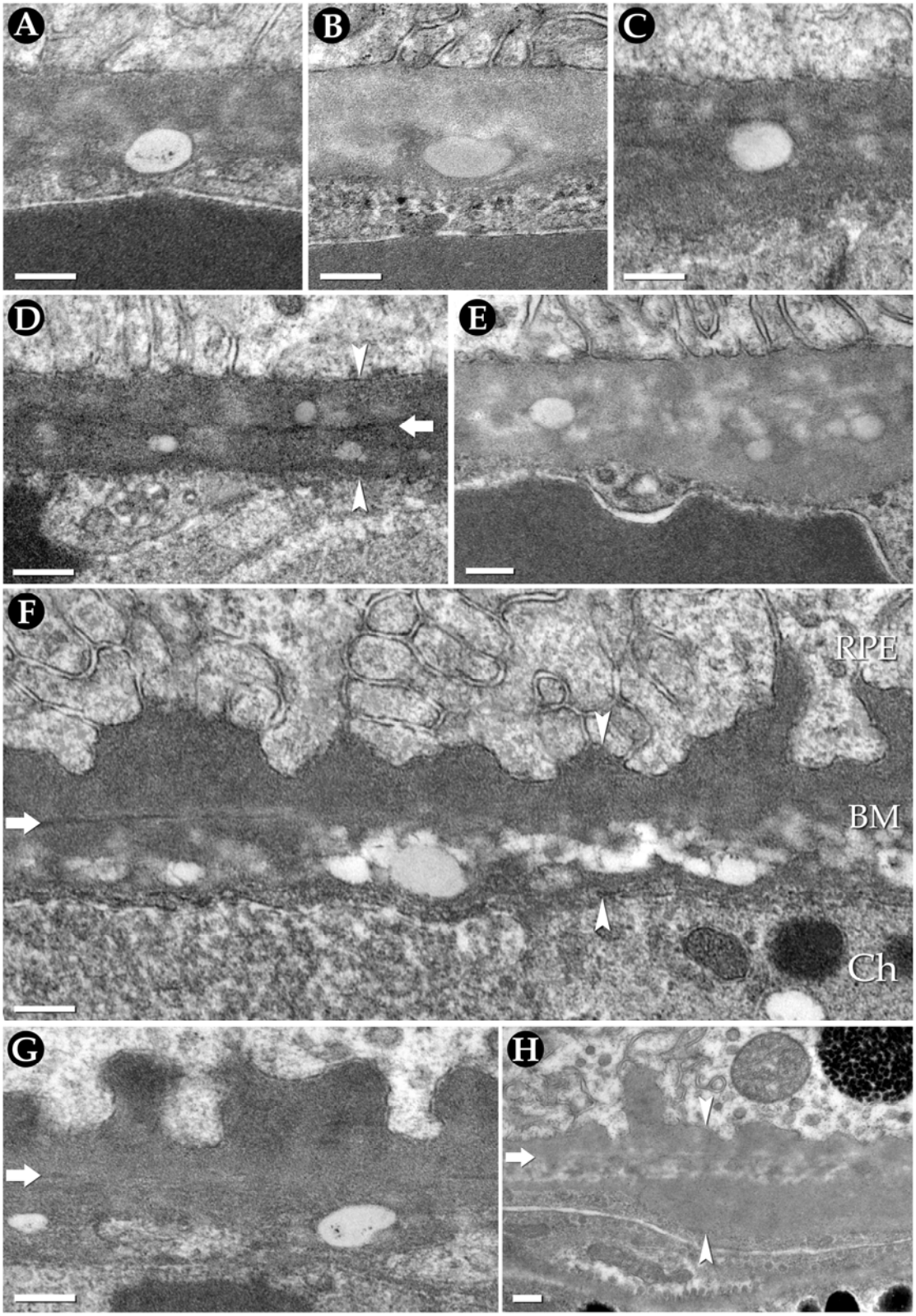

Figure 25. A-G: Sharply defined electron lucencies in Bruch's Membrane. E-F: Amorphous electron lucencies were present in great numbers adjacent to the sharply defined particles. G-H: Focal deposition of an amorphous material between the RPE plasma membrane and basement membrane. Images A and E: group 4, B-D and F-H: group 8, scale bars A-G 200nm, H 500nm. Bruch's membrane (BM) is aligned horizontally between the pigment epithelium (RPE) on top and the choriocapillaris (Ch) at the bottom. Arrowheads indicate the boundaries of BrM and arrows indicate fragments of the elastic lamina.

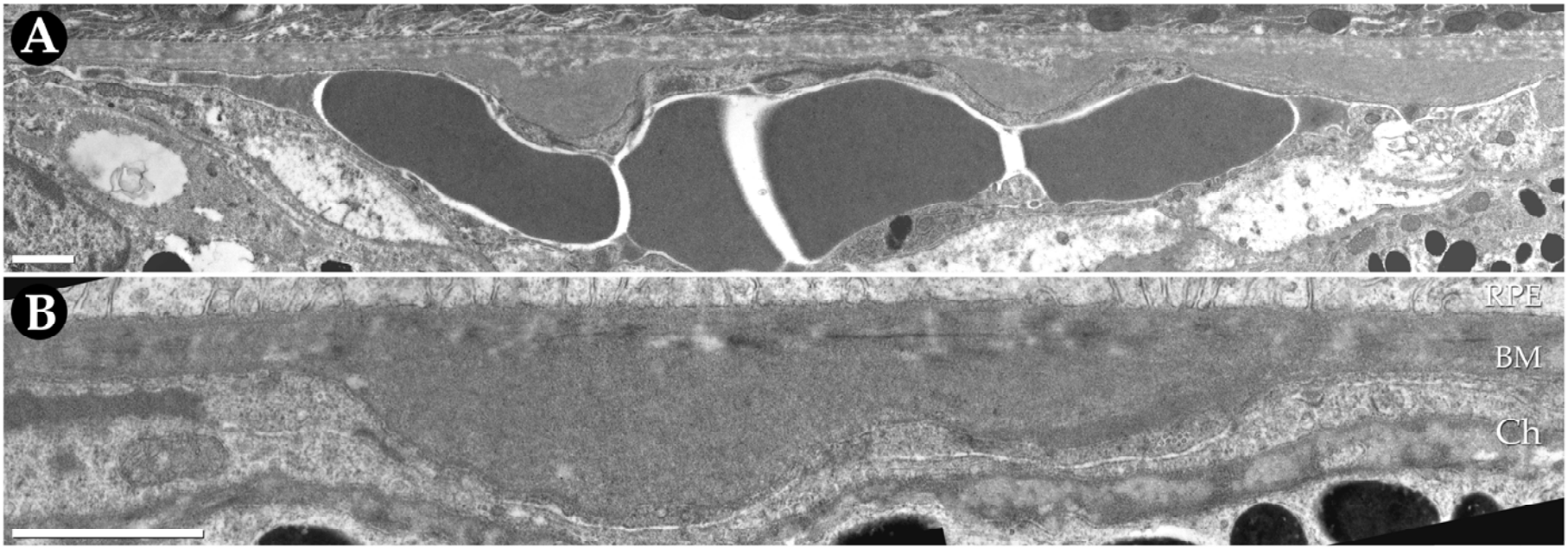

Figure 26. Thickening of BrM as a consequence of a layer of amorphous or fragmented fibrillar material, most likely from the basement membrane of the choriocapillaris, in animals overexpressing the biglycan gene (A: group 6, B: group 8, both scale bars: 1000nm). Bruch's membrane (BM) is aligned horizontally between the pigment epithelium (RPE) on top and the choriocapillaris (Ch) at the bottom. A: The dark objects in the typically wide and flat choriocapillary lumen are red blood cells. B: The choriocapillary lumen in this image is collapsed and only seen as a virtual gap. Fragments of the elastic layer are detectable in BrM.

2.4. Photoreceptor Outer Segments, RPE and Choriocapillaris

Classical signs of photoreceptor damage or atrophy were not evident (Figure 27). Some photoreceptor outer segments showed a cytoplasmic cap at the apex (Figure 28, left). The RPE cytoplasm contained occasional electron-lucent vacuoles of a size and structure similar to those found within BrM. Endothelial fenestrae of the choriocapillaris were of uniform size (50-70nm) and density, no differences between groups were detectable (Figure 28, right).

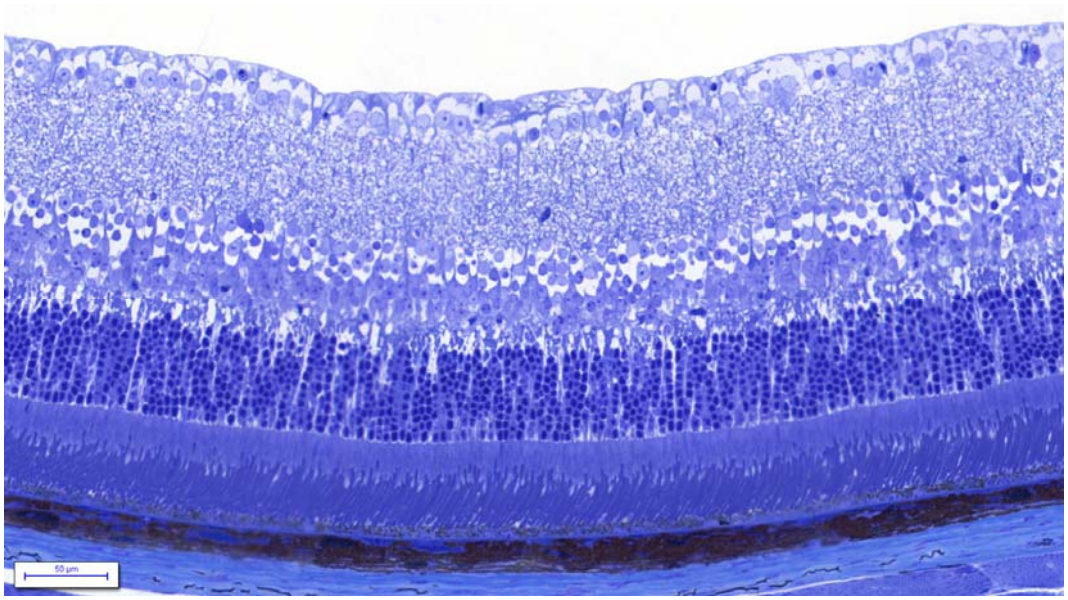

Figure 27. Light microscopic image of the retina of an apoB-100 transgenic mouse on normal diet. Signs of photoreceptor damage are not detectable. Differences between groups in the thickness of the outer nuclear layer and in photoreceptor density were not significant (Toulidine blue staining, scale bar: 50µm).

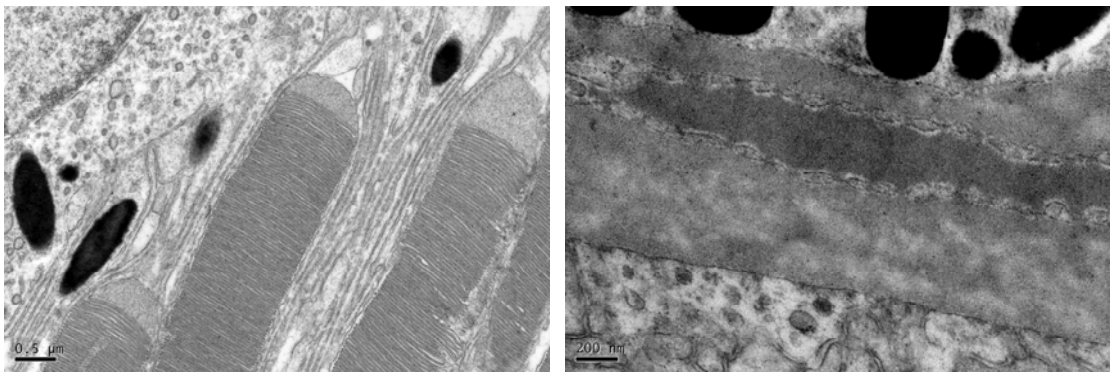

Figure 28. Left: unusual photoreceptor outer segment morphology with a cytoplasmic cap at the apex. (scale bar: 500nm) Right: Endothelial fenestrations lining BrM were of regular size and density (scale bar: 200nm)

DISCUSSION

1. Functional aspects of drusen regression in AMD.

Regression of macular soft drusen has been described in clinical [7, 10, 34], as well as in histopathological studies [8, 18]. Gass noted that drusen may fade and disappear, leaving only an irregular mottling of the RPE, while visual acuity may not be affected. Gass also observed that most cases of GA follow the fading of drusen or the collapse of a serous detachment of the RPE [8].

Bonnet et al. noted that spontaneous gradual absorption of macular colloid bodies (i.e. drusen) can be seen in some patients. In some cases the colloid bodies become confluent before resorbing. Confluence of drusen may lead to a large hyalin detachment of the RPE which should be differentiated from serous detachment. In some other cases small drusen spontaneously disappear without prior confluence. The absorption of a small druse can lead to a ring shape transitory stage. Usually the natural course eventually leads to a GA [249].

Sarks and coworkers interpreted drusen regression as a failure of the overlying RPE. In their experience, drusen usually shrink slowly, developing irregular margins and foci of calcification before disappearing to leave local patch of atrophy. Most cases of geographic atrophy of the RPE evolve in relation to regressing drusen. It was also noted that occasionally soft drusen fade with little trace other than a patch of attentualed RPE [26]. Drusen disappearance is thus generally considered to be associated with subsequent degeneration and atrophy of the RPE and photoreceptors.

It was however noted in large population-based studies that in some patients, drusen may also regress without residual signs. In the Melton Mowbray study, 20% of soft drusen regressed over a 7-year period [10], while in the Chesapeake Bay Waterman Study, after a 5–year follow-up, the disappearance of large drusen, focal hyperpigmentation, and AMD-3 (defined as one or more of the following within 1500μm of the foveal center: large or confluent drusen, focal hyperpigmentation of the RPE, or nongeographic atrophy of the RPE) was noted in 16 (34%) of 47 participants, 11 (58%) of 19 participants, and 17 (28%) of 61 participants, respectively, who initially had these findings in 1985 [34]. In the Beaver Dam Eye Study, drusen disappearance

rate was 34.5% for soft indistinct drusen and approximately 72.5% of the disappearance of soft indistinct drusen was not accompanied by the appearance of more severe lesions. Masked side-by-side comparisons of the photographs from examinations minimized the effect of media opacity, photographic artifacts, and grader error as a cause of disappearance of these lesions [7].

The prognostic implications of true drusen regression are unknown. From the clinical aspect, it raises the possibility that arrested progression or even regression of the disease process may exist naturally. In this study, ten out of 14 patients showed no ophthalmoscopic indications of manifest or incipient end-stage disease in the fundus following drusen regression. However, in nine, parallel to regression, new drusen in other locations appeared and grew in size and confluence, signifying the continued activity of the disease, with a tendency toward the periphery.

In diseases, where the RPE is primarily affected, the presence of abnormal FAF may be an early sign of progression. Diffusely increased autofluorescence at the posterior pole associated with GA may reflect a large area of incipient atrophy. Holz and coworkers found that the development of new and enlargement of preexisting atrophy is invariably confined to areas with abnormally high levels of fundus autofluorescence at baseline in eyes with geographic atrophy associated with AMD [87]. Decreased FAF over the drusen overall may also reflect incipient atrophy [89]. In eyes with soft drusen but without apparent GA, if focal decreased FAF is present, patches with increased FAF in areas adjacent to rather than corresponding to drusen may be markers for progression to atrophy [88].

In this study, autofluorescence of retinal areas with normal appearance in the colour image following drusen regression was in most cases normal and none of the above FAF patterns associated with impending atrophy was detectable.

In our study, mean retinal sensitivity relative to normal controls was reduced in all patients tested, both in the light and dark adapted states, with significantly higher loss under scotopic conditions. This observation confirms that in AMD, rods are at increased risk for degeneration and function loss occurs before progression to the late clinical stage [40]. Earlier psychophysical studies found that rod-mediated sensitivity declines

faster with age than photopic sensitivity [36] and patients with early AMD have significantly lower mean central scotopic sensitivity than age-matched controls. Also, in most AMD patients, mean scotopic sensitivity loss exceeded mean photopic sensitivity loss and the peak deficit in scotopic sensitivity was within 9° of fixation, corresponding to the parafovea [37].

Histopathologic studies show direct correlates to these findings. In early AMD, a preferential loss of macular rod photoreceptors was demonstrated, with the greatest loss occurring in the parafovea. In late AMD this leads to a reversal of the macular (9:1) rod predominance seen in the young [40]. Our data are in perfect accord with these observations.

The retinoid deficiency hypothesis proposed by Curcio and coworkers provides one possible explanation for this preferential vulnerability of rod photoreceptors [40]. Early defects in rod sensitivity and delayed rod-mediated dark adaptation may be signs of a local depletion of certain essential nutrients. Several lines of evidence suggest that the nutrient reduced in aging and in AMD eyes is a retinoid derivative. Slowed rod-mediated recovery implies limited availability of 11-cis-retinal to the rods, resulting in the accumulation of intermediates that actively desensitize the retina [250]. Delayed dark adaptation is a hallmark of systemic vitamin A deficiency and genetic disorders affecting visual cycle components or the retinoid transport system [251-253]. The visual cycle comprises biochemical reactions in the RPE and photoreceptors that produce the vitamin A derivative 11-cis-retinal from all-trans precursors delivered across Bruch's membrane by plasma proteins [253]. 11-cis retinal is essential for the regeneration of photoreceptor pigment after bleaching by light as well as for photoreceptor survival. RPE cells are responsible for the transport of nutrients from the choriocapillary circulation to the photoreceptors, as well as for the recycling of the end-products of photoreceptor outer segment disc degradation.

In AMD, diffuse sub-RPE deposits may act as a diffusion barrier between the choriocapillaris and the RPE [3], thereby disrupting transport across BrM and leading to a local scarcity of 11-cis-retinal. Not only is 11-cis retinal required to regenerate the photoreceptor pigment after bleaching by light, but retinoids are also required for photoreceptor survival. Vitamin A deprivation leads to outer segment degeneration and photoreceptor death in vivo [254-256] and accelerated degeneration of photoreceptors

with mutant rhodopsins in vitro [257].

Mice lacking a key visual cycle component (the RPE65 gene product) have a normal cone electroretinogram but no measurable rod sensitivity [258], suggesting that cones have an additional retinoid delivery pathway. This probably involves Müller cells and possibly the neurosensory retina rendering cones less vulnerable to reduced transport across Bruch's membrane [40, 259]. Lack of vitamin A affects primarily rods but does eventually impact cones as well [260]. One consequence of these findings is that tests of visual acuity, currently the standard clinical functional assessment for the elderly and AMD patients, may underestimate the degree of visual dysfunction by using high contrast stimuli presented in bright light to foveal cones and tests of rod function, particularly those that probe dynamic properties, would permit detection of AMD at earlier stages than tests of cone function.

Although generalised sensitivity loss was measured in all our patients, topographic variation in scotopic and photopic sensitivity loss over drusen relative to areas with normal appearance was not significant. This confirms earlier observations that the presence of macular soft drusen seems to have little effect on the local sensitivity of affected retinal areas.

Sunness et al. used a modified 30° fundus camera (Zeiss Inc., Thornwood. NY, USA), with fundus illumination reduced to scotopic levels by a deep red cutoff filter. An achromatic stimulus transmitted by a single optical fiber, subtending a visual angle of 30 minutes of arc was positioned in a plane conjugate to the retina. Large drusen were tested directly, when smaller drusen were present, a grid of points covering the drusen-bearing areas was tested and compared with findings in drusen-free areas equidistant from the center of the fovea. Approximate drusen sizes were measured. Drusen sizes ranged from 23 to 70 minutes of arc (115-350um), with a mean of 40 minutes (200um). No significant differences between scotopic retinal sensitivity measured over drusen and nondrusen areas were found [261].

Scholl and coworkers used photopic and scotopic fine matrix mapping to correlate retinal sensitivity with patterns of fundus autofluorescence and fundus features characteristic of AMD. The distribution of drusen and FAF correlated poorly and photoreceptor dysfunction deficits followed the distribution of both increased and decreased FAF but did not follow the distribution of drusen, with the exception of large,

soft foveal drusen. These may be regarded as small RPE detachments and showed mildly reduced photopic and considerably reduced scotopic sensitivity as well as increased FAF [91].

Similarly reduced scotopic sensitivity has been found in patients with central serous retinopathy [262]. It appears reasonable, that the impact of focal barriers such as drusen on RPE metabolism and photoreceptor function may be more limited than that of diffuse deposits.

One previous interventional pilot study investigated retinal sensitivity following disapperance of drusen. 12 patients with drusen demonstrating high-risk characteristics received prophylactic argon laser retinal treatment. Scotopic fine matrix mapping was performed prior to as well as following the laser treatment. Retinal threshold measurements showed no indication of geographic atrophy one year after treatment [239].

In this study, we examined 14 patients. In ten cases drusen disappeared spontaneously, the remaining four received prophylactic laser treatment. Because of the predominance of cases with spontaneous drusen resolution in our sample, functional testing prior to disappearance of the drusen was not feasible. The follow-up period ranged from 2.8 to 14.4 years (mean = 5.9 years). In nine cases no sign of end-stage disease was detectable at the end-point. Photopic and scotopic sensitivity over areas with regressed drusen was not substantially different from that over unaffected retinal areas equidistant from the fovea. Thus, we did not find functional evidence for manifest or incipient photoreceptor atrophy and although the generalised disease persists, retinal sensitivity and fundus autofluorescence, two direct, sensitive and complementary measures of retinal health do not indicate that disappearance of drusen is necessarily followed by local function loss and atrophy.

2. Characterisation of Bruch's membrane changes in apoB-100 and biglycan transgenic mice.

Modelling pathological events associated with AMD is essential for understanding disease progression and testing treatment strategies. Transgenic mouse strains are widely used for these purposes. In our study mice over-expressing the human apoB-100 gene alone or in combination with the human biglycan gene were significantly more susceptible to elevated lipid levels, a thickening of Bruch's membrane and formation of sub-RPE electron-lucent (EL) particles when fed a cholesterol-enriched diet. Expression of the human biglycan gene alone was associated with an intriguing, diet-independent increase in BrM thickness.

Several previous studies using murine models have reported degenerative changes in BrM in association with elevated serum lipid levels in C57BL/6 wild-type mice [263-266] as well as in mice with genetically-determined hyperlipidemia [267-271]. Diet-induced hyperlipidemia in combination with advanced age and a blue-light-induced damage was associated with basal laminar deposit (BlamD) formation in C57BL/6 mice [264-266]. Deposits were more severe in female animals [266]. In C57BL/6 wild-type mice but without laser treatment, deposit morphology was similar to basal linear deposit (BlinD) [263, 264].

Mice expressing modified variants of the apoE gene show varying degrees of basal deposits [267, 268, 270]. ApoE knockout mice exhibit increased serum cholesterol levels even on a normal diet, accumulation of EL particles at an earlier age and have more membrane-bounded material in BrM than wild-type mice [267]. Transgenic mice expressing the apo*E3-Leiden gene, a dysfunctional form of the human apoE3, associated with hyperlipoproteinaemia and early-onset atherosclerosis, showed basal laminar deposit formation when fed a high fat/cholesterol (HFC) diet [268]. Eyes of aged, targeted-replacement mice expressing human apoE2, apoE3, or apoE4, maintained on a HFC diet showed apoE isoform-dependent pathologies of differential severity. Particularly, the apoE4 isoform was associated with diffuse sub-RPE deposits, drusenoid deposits, thickened BrM as well as atrophy, hypo- and hyperpigmentation of the RPE [270]. LDL receptor (LDL-R) knockout mice are not able to incorporate plasma cholesterol into peripheral tissues sufficiently and respond to a high-fat diet with

severe hypercholesterolemia and massive BlinD formation [271]. ApoB-100 transgenic mice on high-lipid diet have also been demonstrated to develop moderate BlamD formation at an early age, following exposure to blue-green light [269].

The cause and significance of variation in deposit type among models is not clear. Notably, all studies using blue-green light irradiation as a model of oxidative damage found predominantly BlamD [264-266, 269], while most studies that restricted variables to age and hyperlipidemia found electron lucent deposits, similar to those in BlinD [263, 267, 271]. The relative influence of oxidative damage is difficult to assess from available data, as this was not attempted in these studies. It is also pertinent to keep in mind the known inherent propensity of C57BL/6 wild-type mice to hyperlipidemia with advancing age [265, 272].

In our animal model, the factors age and light damage were eliminated through the exclusive use of untreated mice of a single age-group. Transgenics were bred from the same C57BL/6 stock as controls. Also, the apoB-100 transgenic mouse model has a significant inherent advantage. The proteoglycan-binding sequence of apoB-100 in LDL is different in apoB-48 [232], and apoB-48-containing lipoprotein can also be cleared from the plasma by receptors other than LDL-R [230]. Mice expressing the human apoB-100 gene have a lipoprotein profile similar to humans and show a sharp increase in plasma LDL following ingestion of a high-fat diet [231]. Nonetheless, significant differences between our model and human lipid metabolism remain, including that in mice the main vehicle of lipid transport to peripheral tissues is HDL. BrM deposits seen in our animals were of two main types. Located between the RPE plasma and basement membranes, we found focal deposits of an amorphous material similar to early-type nodular BlamD [16, 273].

A more pronounced feature in these animals was the presence of sharply defined (membranous) and more amorphous (non-membrane bounded) electron-lucent particles with morphological features similar to membranous debris and small electron-lucent droplets described previously in basal linear deposits [17]. While the small electron lucent droplets were abundant, membranous debris occurred predominantly solitarily or in small clusters scattered throughout the inner and outer collagenous zones of BrM, only occasionally forming a continuous layer.

Depending on the technique used, similar particles have previously also been

described as coated vesicle-like bodies [123], lipoprotein-like particles [127], small membrane-bounded vesicles [13], or simply collectively as "electron-lucent particles" in other animal models as well as in human AMD eyes [17, 18, 123]. Using a quick-freeze deep-etch technique, a characteristic clustering of the smaller particles around the large ones was described, sometimes resulting in a morphology giving the impression of spiked particles when viewed by standard TEM [123, 127]. We also noted this phenomenon which may be a step towards drusen assembly [127].

The mechanism of deposit formation and the source of lipids within the deposits found in AMD remain controversial [274]. Previous studies have demonstrated that circulating LDL is taken up by RPE and to a lesser extent, by Müller cells and is quickly delivered to different compartments within the retina [275]. Thus, serum LDL may be a source of lipids in sub-RPE deposits via a mechanism directly analogous to that established in atherosclerosis. However, size, density profile and lipid composition of lipoprotein-like, apoB and apoA1-containing particles isolated from human BrM/CH differed from that of plasma LDL, which points to possible alternative sources [207].

The mechanisms of lipid transport and metabolism within the retina are little known. ApoB has been shown to colocalize with EC and UC in BrM, drusen and sub-RPE deposits of AMD eyes [207]. In a primate model, apoB has also been demonstrated in the choriocapillaris (including in deposits on the luminal surface), in BrM, in RPE cells, in POSs, within the inter-photoreceptor matrix (IPM), in ganglion cells and - in small amounts - in the outer plexiform layer (OPL) [275]. The majority of apoB found was a 70kDa degradation product and within the RPE, apoB was located in the basolateral aspect of the cells, mostly colocalized with lipofuscin and LDL-R, - all signs of an exogenous origin. Nonetheless, some of the original (540kDa) apoB-100 could also be detected and other authors reported the presence of the full-size apoB-100 as well as apoB mRNA in RPE and ganglion cells [207, 276]. In addition to apoB, the primate retina expresses many other proteins involved in systemic lipid transport, including ABCA1, apoA1, apoE, CD36, SR-BI, SR-BII, CETP and LCAT.

Based on these findings, a model of intraretinal lipid transport has been proposed [277]. In this model endogenous (apoA1/apoB/apoE-containing?) lipoprotein particles may serve as vehicles for transport of lipids taken up from the systemic circulation by RPE and Müller cells into the retina as well as for the removal of oxidized lipids,

especially those arising in the membranes of the POS. Signs of local apoB synthesis along with the presence of apoB in the inter-photoreceptor matrix and outer plexiform layer support the idea of an intraretinal lipid transport process involving locally synthetised apoB-containing (HDL- or LDL-like?) lipoproteins. These liporoteins may also serve as a source of lipids in sub-RPE deposits and local proteoglycans (like biglycan or decorin) may play a role in the entrapment of these during secretion by the RPE into the choriocapillaris.

Biglycan transgenic mice (groups 5 and 6) exhibited a significant increase in BrM thickness, irrespective of the diet, while the severity of EL particles was consistently less than in corresponding apoB-100 or double transgenic animals. This thickening of BrM was to a degree attributable to a layer of varying thickness of an amorphous or disorganized fragmented material in the outermost part of BrM. The most likely source of this layer is the basement membrane of the choriocapillaris. In pathological states, the basal lamina can undergo a variety of alterations. Amorphous or fragmented "laminae" may contain proteins normally found in a basal lamina (laminin, collagen IV) but in a more active state with regard to cell biological processes such as migration, proliferation and differentiation [278, 279]. Biglycan transgenic mice are known to show an upregulation of TGF-β, collagen (types I, III and IV) and a downregulation of decorin, a potent TGF-β inhibitor [280]. TGF-β can induce both fibrosis and angiogenesis and is an important factor in neoplastic transformation, which involves a remodelling of the ECM [281]. Overproduction of TGF-β is a major inducer of tissue fibrosis, as it stimulates deposition of ECM by up-regulating synthesis of ECM components such as collagens, proteoglycans and fibronectin, the inhibitors of matrix-degrading enzymes and down-regulation of the expression of these degradative enzymes. Recent reports have also linked biglycan with ECM remodelling and collagen matrix formation in scarring and fibrosis [282, 283]. Increased expression of biglycan with collagen type III was demonstrated in experimentally induced pulmonary fibrosis [284] and with collagen type I in keloid scarring [285]. Rat pulmonary tissue injected with the biglycan gene via an adenovirus showed a fibroblastic response in the interstitium and a fibrotic thickening of the pleura with evidence of increased collagen but not elastin deposition [286]. These fibrotic responses are believed to be mediated at least partially through TGF-β.

Thus, BrM thickening seen in our mice overexpressing the biglycan gene appears to be attributable mainly to increased production of a material (most likely collagen IV), probably mediated via TGF-β. We found no evidence of other effects associated with TGF-β like macrophage and neutrophil infiltration or angiogenesis. It is also remarkable, that this layer of amorphous material was only seen in BrM and not in other parts of the choriocapillary vascular wall. At the other end of the spectrum, ageing appears to be associated with a decline in biglycan levels [287] as well as a reduction in the mRNA levels for (type I and II) collagens in many tissues [288]. It is tempting to speculate, that a loss of biglycan and collagen with a consequential degradation of the structural integrity of BrM, as well as the thinning and fragmentation of the elastic layer, [96] the overall increase in proteoglycan content with negatively charged glycosaminoglycan chains in BrM and a relative predominance of heparan-sulfate proteoglycans [97, 110] over chondroitin-4-sulfate proteoglycans (like biglycan) seen in AMD may all contribute to changes affecting transport through BrM.

We also investigated a double (apoB-100$^{+/-}$ x biglycan$^{+/-}$) transgenic mouse strain aimed specifically to model lipoprotein entrapment, a key step in the current paradigm of atherogenesis. Relative to wild-type mice, these animals (groups 7 and 8) did show significantly increased serum lipid levels, BrM thickness and severity of EL particles when fed a high-cholesterol diet, but not in the absence of administered high-cholesterol. The degree of BrM abnormalities was however not significantly different from that seen in animals expressing only the apoB-100 gene, the main difference being the presence of a layer of amorphous material in outer BrM of the double transgenic mice. Considering previous in vitro data indicating a likely central role of the apoB-100-biglycan interaction in lipid retention and the overexpression of both factors in these mice, we expected a significantly higher level of abnormalities, especially in the presence of a lipid-rich diet.

One possible explanation for this may be that although biglycan is the proteoglycan that most closely and consistently co-localizes with apoB in humans [166, 289], there are other candidates for lipid entrapment. Decorin has been shown to colocalize with type I collagen in primary atherosclerotic plaques [155], although the colocalization with lipids was much less consistent than that of biglycan [289]. In vitro, decorin has been demonstrated to facilitate binding of LDL to collagen, however this effect was

relatively weak even under optimal conditions [290], which may in turn be due to the absence of essential tissue factors present in vivo, possibly lipoprotein lipase which was shown to enhance the binding of LDL to decorin but not to biglycan or versican [291]. It is also remarkable that on normal diet, biglycan transgenic mice show a significant thickening of BrM while double transgenic animals do not. This may be interpreted as an indication that the apoB-100-biglycan interaction may indeed take place even in the absence of elevated serum LDL levels, however without the expected subsequent increase in lipid deposition, while biglycan is thus no longer available to exert its fibrosis-inducing effect via other pathways.

CONCLUSIONS

In our clinical investigations we aimed to probe the functional implications of macular soft drusen regression in AMD eyes. We demonstrated that:

- Macular soft drusen may disappear without detectable signs in stereoscopic colour fundus images of their earlier existence.
- Drusen regression may occur without subsequent FAF or psychophysical signs of local dysfunction or incipient atrophy.

These phenomena suggest that some normal-appearing eyes at the present time may have had some features of AMD in the past and is thus a potential source of misclassification. This needs to be taken into account in epidemiologic studies investigating the natural history of the disease as well as in clinical trials that evaluate the efficacy of therapies. To what extent focal and diffuse sub-RPE deposits coincide, whether the regression of drusen is accompanied by the regression of diffuse deposits and how the prognosis for cases with true regression of drusen compares to those without will need to be considered in future studies on AMD.

In our experimental morphological investigations we characterized the ultrastructure of Bruch's Membrane of transgenic mice overexpressing the human apoB-100, biglycan or both genes in combination with a high-cholesterol diet. We demonstrated that:

- BrM thickness was significantly increased in apoB-100 transgenic and apoB-100 x Biglycan double transgenic mice on a high-cholesterol diet.
- There was a strong correlation between BrM thickness and serum cholesterol level in apoB-100 transgenic and apoB-100 x Biglycan double transgenic mice.
- apoB-100 and double transgenic animals show electron lucent profiles in BrM as well as an amorphous material of intermediate electron-density between the plasma and basement membranes of the RPE, of a morphology compatible with early basal deposits.
- Biglycan transgenic mice show a marked, diet-independent increase in BrM thickness.
- The increase in BrM thickness in biglycan transgenic mice was associated with the accumulation of a basement-membrane like material in outer BrM

In conclusion, our observations further implicate apoB-100 in the process of sub-RPE

lipid deposition in Age-Related Macular Degeneration. The role of biglycan may more likely be the preservation of the integrity of collagen structures, including basement membranes. These unexpected effects of biglycan are intriguing and further investigations are needed to elucidate the underlying mechanisms.

Summary

The aim of our studies was to investigate the role of the outer vascular interface of the retina in age-related macular degeneration (AMD). In our clinical study we aimed to probe the functional implications of macular soft drusen regression in AMD eyes. Of 960 patients screened, soft drusen regression was detected in 34 cases, 14 agreed to participate in the study, ranging in age from 52 to 84 years (median 72), the follow-up period ranged from 2.8-14.4 years (mean 5.9 years). In subjects with confirmed drusen regression, detailed phenotyping was performed according to the system defined by the International Classification for AMD, Fundus Autofluorescence (FAF) was recorded and high-definition sensitivity testing of the central 9º of the retina was performed using Fine Matrix Mapping (FMM). Phenotype and functional data were analyzed for correlations. FMM showed a generalised threshold elevation relative to normal controls both under photopic and scotopic conditions. Scotopic sensitivity loss exceeded photopic loss in all cases. Sensitivity loss over areas with drusen or regressed drusen did not differ significantly from that over non-drusen areas. We concluded that in AMD there is an early generalized preferential loss of central rod function. Macular soft drusen may fade or disappear without detectable ophthalmoscopic, FAF or psychophysical signs of local dysfunction. This phenomenon is a potential source of misclassification. The prognosis for cases with true regression of drusen compared with those without needs to be considered in future studies on AMD.

In our morphological study we aimed to examine the ultrastructure of BrM in transgenic mice. AMD is characterized by the accumulation of lipid- and protein-rich deposits in Bruch's Membrane (BrM). A consequent decrease in hydraulic conductivity and impairment of transport through BrM may play a central role in the pathogenesis of AMD. The mechanism of deposit formation in AMD had been suggested to show similarities to atherogenesis in which the interactions of extracellular matrix proteoglycans with apoB-100 play an important role. A prime candidate for this interaction is the small leucin-rich proteoglycan biglycan. We aimed to test the effect of the simultaneous overexpression of human apoB-100 and biglycan genes in combination with a high-cholesterol diet on BrM morphology in transgenic mice. 6-weeks-old homozygous apoB-100 or biglycan, hemizygous apoB-100/biglycan

transgenic and wild type C57BL/6 mice were fed either a standard chow or a diet supplemented with 2% cholesterol for 17 weeks. Animals were sacrificed, serum lipid levels were measured and eyes were examined using transmission electron microscopy (TEM). Morphometric analysis of BrM showed that in apoB-100 and double transgenic animals fed a high-cholesterol diet, BrM thickness was significantly increased compared to wild-type animals. Both groups had electron-lucent profiles in clusters, scattered throughout BrM, and focal nodules of an amorphous material of intermediate-electron density between the plasma and basement membranes of the RPE. BrM thickness in these two groups correlated well with elevated cholesterol levels. Unexpectedly, animals overexpressing biglycan alone showed a marked, diet-independent increase in BrM thickness associated with a layer of a basement membrane-like material in outer BrM. The effects of biglycan overexpression are intriguing and further investigations are needed to elucidate the underlying mechanisms.

Az értekezés eredményeinek összefoglalása (Summary in Hungarian)

Kutatásaink célja a retina külső vaszkuláris határzóna szerepének vizsgálata volt, az időskori makuladegeneráció (AMD) létrejöttében. Klinikai tanulmányunk során a puha drusenek regressziójának funkcionális vonatkozásait vizsgáltuk. 960 vizsgált betegből 34 esetben találtunk drusen regressziót, 14 beteg kívánt a tanulmányban részt venni. Koruk 52-84 év (medián 72 év), a követési idő 2,8-14,4 év (átlag 5,9 év) volt. Fundusképek alapján részletes fenotípus elemzést végeztünk az International Classification for AMD módszere szerint, fundus autofluoreszcencia képek (FAF) készültek és magas felbontású centrális (9º) látótérvizsgálatot végeztünk (Fine Matrix Mapping, FMM). A fenotípus és a funkciónális adatok összefüggéseit elemeztük. FMM vizsgálat során az egészséges, azonos korú egyedekhez képest AMD betegekben diffúzan emelkedett küszöbszintet találtunk fény és sötét adaptált állapotban egyaránt. A szkotopiás veszteség minden eseben meghaladta a fotopiás veszteséget. A drusenek illetve regrediált drusenek felett mért küszöbszintek nem tértek el szignifikáns mértékben a normál retina felett mért értékektől. Időskori makuladegenerációban tehát a centrális pálcika fotoreceptor funkció sérül korábban. A drusenek eltűnhetnek fundusfotón, FAF képen vagy pszichofizikai módszerrel regisztrálható nyom nélkül. Ezt a jelenséget a betegek klasszifikációja során figyelembe kell venni. A jelenség prognosztikai jelentőségének vizsgálata további tanulmányok feladata lesz.

Morfológiai tanulmányunk során a Bruch membrán (BrM) struktúráját vizsgáltuk transzgenikus egerekben. Az AMD szövettanára jellemző a lipidben és proteinben dús depozitumok felszaporodása a BrM-ban. A BrM áteresztőképességének következményes csökkenéséből adódó transzport zavaroknak központi szerepet tulajdonítanak az AMD pathogenezisében. A depozitumok keletkezésének mechanizmusát több tanulmány hasonlította az atherogeneziséhez, melyben az extracelluláris mátrix proteoglikánok interakciója az apolipoprotein B-100-al (apoB-100) központi szerepet játszik. Célunk az apoB-100 és biglycan gének szimultán túlexpressziójának a BrM morfológiájára kifejtett hatásának vizsgálata volt transzgenikus egerekben, magas koleszerintartalmú táp bevitele mellett. Hat hetes homozigóta apoB-100, biglycan és heterozigóta apoB-100/biglycan kettős transzgenikus illetve kontroll C57BL/6 egerek 17 hétig normál vagy 2% koleszterinnel dúsított tápot

kaptak. Feldolgozás során a szérum lipid szinteket megmértük és szemek elektronmikroszkópos vizsgálatra kerültek. Morfometriai elemzés során a dúsított tápon tartott apoB-100 és kettős transzgenikus állatokban a BrM szignifikáns megvastagodást mutatott. Mindkét csoportban klaszterekben elektron-lucens profilok voltak láthatók a BrM-ban elszórtan, az RPE plazma- és bazálmembránja között pedig fokális, amorf, közepes elektron-denzitású anyag szaporodott fel. Várakozasainkkal ellentétben a biglycant túlexpresszáló állatokban jelentős, a táp jellegétől függetlenül, a BrM külső rétegében egy bazálmembrán jellegű anyag felszaporodását és BrM megvastagodását találtuk. A biglycan hatása meglepő és váratlan, szerepének feltérképezése további vizsgálatok feladata lesz.

REFERENCES

1. Klein, R, Peto, T, Bird, A, and Vannewkirk, MR, The epidemiology of age-related macular degeneration. *Am J Ophthalmol*, 2004;137(3):486-95.

2. Friedman, DS, O'Colmain, BJ, Munoz, B, Tomany, SC, McCarty, C, de Jong, PT, Nemesure, B, Mitchell, P, and Kempen, J, Prevalence of age-related macular degeneration in the United States. *Arch Ophthalmol*, 2004;122(4):564-72.

3. Zarbin, MA, Current concepts in the pathogenesis of age-related macular degeneration. *Arch Ophthalmol*, 2004;122(4):598-614.

4. Hageman, GS, Luthert, PJ, Victor Chong, NH, Johnson, LV, Anderson, DH, and Mullins, RF, An integrated hypothesis that considers drusen as biomarkers of immune-mediated processes at the RPE-Bruch's membrane interface in aging and age-related macular degeneration. *Prog Retin Eye Res*, 2001;20(6):705-32.

5. Holz, FG, Pauleikhoff, D, Klein, R, and Bird, AC, Pathogenesis of lesions in late age-related macular disease. *Am J Ophthalmol*, 2004;137(3):504-10.

6. Ambati, J, Ambati, BK, Yoo, SH, Ianchulev, S, and Adamis, AP, Age-related macular degeneration: etiology, pathogenesis, and therapeutic strategies. *Surv Ophthalmol*, 2003;48(3):257-93.

7. Klein, R, Klein, BE, Tomany, SC, Meuer, SM, and Huang, GH, Ten-year incidence and progression of age-related maculopathy: The Beaver Dam eye study. *Ophthalmology*, 2002;109(10):1767-79.

8. Gass, JD, Drusen and disciform macular detachment and degeneration. *Arch Ophthalmol*, 1973;90(3):206-17.

9. Bressler, SB, Maguire, MG, Bressler, NM, and Fine, SL, Relationship of drusen and abnormalities of the retinal pigment epithelium to the prognosis of neovascular macular degeneration. The Macular Photocoagulation Study Group. *Arch Ophthalmol*, 1990;108(10):1442-7.

10. Sparrow, JM, Dickinson, AJ, Duke, AM, Thompson, JR, Gibson, JM, and Rosenthal, AR, Seven year follow-up of age-related maculopathy in an elderly British population. *Eye*, 1997;11 (Pt 3):315-24.

11. Mitchell, P, Wang, JJ, Foran, S, and Smith, W, Five-year incidence of age-related maculopathy lesions: the Blue Mountains Eye Study. *Ophthalmology*, 2002;109(6):1092-7.

12. van Leeuwen, R, Klaver, CC, Vingerling, JR, Hofman, A, and de Jong, PT, The risk and natural course of age-related maculopathy: follow-up at 6 1/2 years in the Rotterdam study. *Arch Ophthalmol*, 2003;121(4):519-26.

13. Pauleikhoff, D, Harper, CA, Marshall, J, and Bird, AC, Aging changes in Bruch's membrane. A histochemical and morphologic study. *Ophthalmology*, 1990;97(2):171-8.

14. Moore, DJ, Hussain, AA, and Marshall, J, Age-related variation in the hydraulic conductivity of Bruch's membrane. *Invest Ophthalmol Vis Sci*, 1995;36(7):1290-7.

15. Green, WR, Histopathology of age-related macular degeneration. *Mol Vis*, 1999;5:27.

16. van der Schaft, TL, de Bruijn, WC, Mooy, CM, Ketelaars, DA, and de Jong, PT, Is basal laminar deposit unique for age-related macular degeneration? *Arch Ophthalmol*, 1991;109(3):420-5.

17. Curcio, CA and Millican, CL, Basal linear deposit and large drusen are specific for early age-related maculopathy. *Arch Ophthalmol*, 1999;117(3):329-39.

18. Sarks, JP, Sarks, SH, and Killingsworth, MC, Evolution of geographic atrophy of the retinal pigment epithelium. *Eye*, 1988;2 (Pt 5):552-77.

19. Sarks, SH, Ageing and degeneration in the macular region: a clinico-pathological study. *Br J Ophthalmol*, 1976;60(5):324-41.

20. Bird, AC, Bressler, NM, Bressler, SB, Chisholm, IH, Coscas, G, Davis, MD, de Jong, PT, Klaver, CC, Klein, BE, Klein, R, and et al., An international classification and grading system for age-related maculopathy and age-related macular degeneration. The International ARM Epidemiological Study Group. *Surv Ophthalmol*, 1995;39(5):367-74.

21. Steinmetz, RL, Haimovici, R, Jubb, C, Fitzke, FW, and Bird, AC, Symptomatic abnormalities of dark adaptation in patients with age-related Bruch's membrane change. *Br J Ophthalmol*, 1993;77(9):549-54.

22. AREDS, The Age-Related Eye Disease Study system for classifying age-related macular degeneration from stereoscopic color fundus photographs: the Age-Related Eye Disease Study Report Number 6. *Am J Ophthalmol*, 2001;132(5):668-81.

23. Miller, H, Miller, B, and Ryan, SJ, The role of retinal pigment epithelium in the involution of subretinal neovascularization. *Invest Ophthalmol Vis Sci*, 1986;27(11):1644-52.

24. Sarks, SH, Arnold, JJ, Killingsworth, MC, and Sarks, JP, Early drusen formation in the normal and aging eye and their relation to age related maculopathy: a clinicopathological study. *Br J Ophthalmol*, 1999;83(3):358-68.

25. MPS_Group, Risk factors for choroidal neovascularization in the second eye of patients with juxtafoveal or subfoveal choroidal neovascularization secondary to age-related macular degeneration. Macular Photocoagulation Study Group. *Arch Ophthalmol*, 1997;115(6):741-7.

26. Sarks, JP, Sarks, SH, and Killingsworth, MC, Evolution of soft drusen in age-related macular degeneration. *Eye*, 1994;8 (Pt 3):269-83.

27. Sarraf, D, Gin, T, Yu, F, Brannon, A, Owens, SL, and Bird, AC, Long-term drusen study. *Retina*, 1999;19(6):513-9.

28. Holz, FG, Wolfensberger, TJ, Piguet, B, Gross-Jendroska, M, Wells, JA, Minassian, DC, Chisholm, IH, and Bird, AC, Bilateral macular drusen in age-related macular degeneration. Prognosis and risk factors. *Ophthalmology*, 1994;101(9):1522-8.

29. Smiddy, WE and Fine, SL, Prognosis of patients with bilateral macular drusen. *Ophthalmology*, 1984;91(3):271-7.

30. Lewis, H, Straatsma, BR, and Foos, RY, Chorioretinal juncture. Multiple extramacular drusen. *Ophthalmology*, 1986;93(8):1098-112.

31. Wang, JJ, Foran, S, Smith, W, and Mitchell, P, Risk of age-related macular degeneration in eyes with macular drusen or hyperpigmentation: the Blue Mountains Eye Study cohort. *Arch Ophthalmol*, 2003;121(5):658-63.

32. Klein, R, Klein, BE, Jensen, SC, and Meuer, SM, The five-year incidence and progression of age-related maculopathy: the Beaver Dam Eye Study. *Ophthalmology*, 1997;104(1):7-21.

33. Strahlman, ER, Fine, SL, and Hillis, A, The second eye of patients with senile macular degeneration. *Arch Ophthalmol*, 1983;101(8):1191-3.

34. Bressler, NM, Munoz, B, Maguire, MG, Vitale, SE, Schein, OD, Taylor, HR, and West, SK, Five-year incidence and disappearance of drusen and retinal pigment epithelial abnormalities. Waterman study. *Arch Ophthalmol*, 1995;113(3):301-8.

35. Jackson, GR, Owsley, C, Cordle, EP, and Finley, CD, Aging and scotopic sensitivity. *Vision Res*, 1998;38(22):3655-62.

36. Jackson, GR and Owsley, C, Scotopic sensitivity during adulthood. *Vision Res*, 2000;40(18):2467-73.

37. Owsley, C, Jackson, GR, Cideciyan, AV, Huang, Y, Fine, SL, Ho, AC, Maguire, MG, Lolley, V, and Jacobson, SG, Psychophysical evidence for rod vulnerability in age-related macular degeneration. *Invest Ophthalmol Vis Sci*, 2000;41(1):267-73.

38. Curcio, CA, Millican, CL, Allen, KA, and Kalina, RE, Aging of the human photoreceptor mosaic: evidence for selective vulnerability of rods in central retina. *Invest Ophthalmol Vis Sci*, 1993;34(12):3278-96.

39. Curcio, CA, Medeiros, NE, and Millican, CL, Photoreceptor loss in age-related macular degeneration. *Invest Ophthalmol Vis Sci*, 1996;37(7):1236-49.

40. Curcio, CA, Owsley, C, and Jackson, GR, Spare the rods, save the cones in aging and age-related maculopathy. *Invest Ophthalmol Vis Sci*, 2000;41(8):2015-8.

41. Jackson, GR, Owsley, C, and McGwin, G, Jr., Aging and dark adaptation. *Vision Res*, 1999;39(23):3975-82.

42. Brown, B, Adams, AJ, Coletta, NJ, and Haegerstrom-Portnoy, G, Dark adaptation in age-related maculopathy. *Ophthalmic Physiol Opt*, 1986;6(1):81-4.

43. Spaide, RF, Fundus autofluorescence and age-related macular degeneration. *Ophthalmology*, 2003;110(2):392-9.

44. Kitagawa, K, Nishida, S, and Ogura, Y, In vivo quantitation of autofluorescence in human retinal pigment epithelium. *Ophthalmologica*, 1989;199(2-3):116-21.

45. Delori, FC, Dorey, CK, Staurenghi, G, Arend, O, Goger, DG, and Weiter, JJ, In vivo fluorescence of the ocular fundus exhibits retinal pigment epithelium lipofuscin characteristics. *Invest Ophthalmol Vis Sci*, 1995;36(3):718-29.

46. Delori, FC, Goger, DG, and Dorey, CK, Age-related accumulation and spatial distribution of lipofuscin in RPE of normal subjects. *Invest Ophthalmol Vis Sci*, 2001;42(8):1855-66.

47. Eldred, GE and Katz, ML, Fluorophores of the human retinal pigment epithelium: separation and spectral characterization. *Exp Eye Res*, 1988;47(1):71-86.

48. Ng, KP, Gugiu, B, Renganathan, K, Davies, MW, Gu, X, Crabb, JS, Kim, SR, Rozanowska, MB, Bonilha, VL, Rayborn, ME, Salomon, RG, Sparrow, JR, Boulton, ME, Hollyfield, JG, and Crabb, JW, Retinal pigment epithelium lipofuscin proteomics. *Mol Cell Proteomics*, 2008;7(7):1397-405.

49. Cuervo, AM and Dice, JF, When lysosomes get old. *Exp Gerontol*, 2000;35(2):119-31.

50. Katz, ML, Drea, CM, Eldred, GE, Hess, HH, and Robison, WG, Jr., Influence of early photoreceptor degeneration on lipofuscin in the retinal pigment epithelium. *Exp Eye Res*, 1986;43(4):561-73.

51. Katz, ML, Gao, CL, and Rice, LM, Formation of lipofuscin-like fluorophores by reaction of retinal with photoreceptor outer segments and liposomes. *Mech Ageing Dev*, 1996;92(2-3):159-74.

52. Eldred, GE and Lasky, MR, Retinal age pigments generated by self-assembling lysosomotropic detergents. *Nature*, 1993;361(6414):724-6.

53. von Ruckmann, A, Fitzke, FW, and Bird, AC, Distribution of fundus autofluorescence with a scanning laser ophthalmoscope. *Br J Ophthalmol*, 1995;79(5):407-12.

54. von Ruckmann, A, Fitzke, FW, and Bird, AC, Fundus autofluorescence in age-related macular disease imaged with a laser scanning ophthalmoscope. *Invest Ophthalmol Vis Sci*, 1997;38(2):478-86.

55. Feeney-Burns, L, Hilderbrand, ES, and Eldridge, S, Aging human RPE: morphometric analysis of macular, equatorial, and peripheral cells. *Invest Ophthalmol Vis Sci*, 1984;25(2):195-200.

56. Wing, GL, Blanchard, GC, and Weiter, JJ, The topography and age relationship of lipofuscin concentration in the retinal pigment epithelium. *Invest Ophthalmol Vis Sci*, 1978;17(7):601-7.

57. Weiter, JJ, Delori, FC, Wing, GL, and Fitch, KA, Retinal pigment epithelial lipofuscin and melanin and choroidal melanin in human eyes. *Invest Ophthalmol Vis Sci*, 1986;27(2):145-52.

58. Dorey, CK, Wu, G, Ebenstein, D, Garsd, A, and Weiter, JJ, Cell loss in the aging retina. Relationship to lipofuscin accumulation and macular degeneration. *Invest Ophthalmol Vis Sci*, 1989;30(8):1691-9.

59. Eldred, GE, Lipofuscin fluorophore inhibits lysosomal protein degradation and may cause early stages of macular degeneration. *Gerontology*, 1995;41 Suppl 2:15-28.

60. Wihlmark, U, Wrigstad, A, Roberg, K, Nilsson, SE, and Brunk, UT, Lipofuscin accumulation in cultured retinal pigment epithelial cells causes enhanced sensitivity to blue light irradiation. *Free Radic Biol Med*, 1997;22(7):1229-34.

61. Schutt, F, Davies, S, Kopitz, J, Holz, FG, and Boulton, ME, Photodamage to human RPE cells by A2-E, a retinoid component of lipofuscin. *Invest Ophthalmol Vis Sci*, 2000;41(8):2303-8.

62. Gaillard, ER, Atherton, SJ, Eldred, G, and Dillon, J, Photophysical studies on human retinal lipofuscin. *Photochem Photobiol*, 1995;61(5):448-53.

63. Suter, M, Reme, C, Grimm, C, Wenzel, A, Jaattela, M, Esser, P, Kociok, N, Leist, M, and Richter, C, Age-related macular degeneration. The lipofusion component N-retinyl-N-retinylidene ethanolamine detaches proapoptotic proteins from mitochondria and induces apoptosis in mammalian retinal pigment epithelial cells. *J Biol Chem*, 2000;275(50):39625-30.

64. Parish, CA, Hashimoto, M, Nakanishi, K, Dillon, J, and Sparrow, J, Isolation and one-step preparation of A2E and iso-A2E, fluorophores from human retinal pigment epithelium. *Proc Natl Acad Sci U S A*, 1998;95(25):14609-13.

65. Ben-Shabat, S, Parish, CA, Vollmer, HR, Itagaki, Y, Fishkin, N, Nakanishi, K, and Sparrow, JR, Biosynthetic studies of A2E, a major fluorophore of retinal pigment epithelial lipofuscin. *J Biol Chem*, 2002;277(9):7183-90.

66. Mata, NL, Weng, J, and Travis, GH, Biosynthesis of a major lipofuscin fluorophore in mice and humans with ABCR-mediated retinal and macular degeneration. *Proc Natl Acad Sci U S A*, 2000;97(13):7154-9.

67. Liu, J, Itagaki, Y, Ben-Shabat, S, Nakanishi, K, and Sparrow, JR, The biosynthesis of A2E, a fluorophore of aging retina, involves the formation of the precursor, A2-PE, in the photoreceptor outer segment membrane. *J Biol Chem*, 2000;275(38):29354-60.

68. Sparrow, JR and Boulton, M, RPE lipofuscin and its role in retinal pathobiology. *Exp Eye Res*, 2005;80(5):595-606.

69. Fishkin, NE, Sparrow, JR, Allikmets, R, and Nakanishi, K, Isolation and characterization of a retinal pigment epithelial cell fluorophore: an all-trans-retinal dimer conjugate. *Proc Natl Acad Sci U S A*, 2005;102(20):7091-6.

70. Sparrow, JR, Parish, CA, Hashimoto, M, and Nakanishi, K, A2E, a lipofuscin fluorophore, in human retinal pigmented epithelial cells in culture. *Invest Ophthalmol Vis Sci*, 1999;40(12):2988-95.

71. Sparrow, JR, Fishkin, N, Zhou, J, Cai, B, Jang, YP, Krane, S, Itagaki, Y, and Nakanishi, K, A2E, a byproduct of the visual cycle. *Vision Res*, 2003;43(28):2983-90.

72. De, S and Sakmar, TP, Interaction of A2E with model membranes. Implications to the pathogenesis of age-related macular degeneration. *J Gen Physiol*, 2002;120(2):147-57.

73. Holz, FG, Schutt, F, Kopitz, J, Eldred, GE, Kruse, FE, Volcker, HE, and Cantz, M, Inhibition of lysosomal degradative functions in RPE cells by a retinoid component of lipofuscin. *Invest Ophthalmol Vis Sci*, 1999;40(3):737-43.

74. Sparrow, JR, Nakanishi, K, and Parish, CA, The lipofuscin fluorophore A2E mediates blue light-induced damage to retinal pigmented epithelial cells. *Invest Ophthalmol Vis Sci*, 2000;41(7):1981-9.

75. Bergmann, M, Schutt, F, Holz, FG, and Kopitz, J, Inhibition of the ATP-driven proton pump in RPE lysosomes by the major lipofuscin fluorophore A2-E may contribute to the pathogenesis of age-related macular degeneration. *FASEB J*, 2004;18(3):562-4.

76. Finnemann, SC, Leung, LW, and Rodriguez-Boulan, E, The lipofuscin component A2E selectively inhibits phagolysosomal degradation of photoreceptor phospholipid by the retinal pigment epithelium. *Proc Natl Acad Sci U S A*, 2002;99(6):3842-7.

77. Boulton, M, Rozanowska, M, and Rozanowski, B, Retinal photodamage. *J Photochem Photobiol B*, 2001;64(2-3):144-61.

78. Arend, O, Weiter, JJ, Goger, DG, and Delori, FC, [In vivo fundus fluorescence measurements in patients with age related macular degeneration]. *Ophthalmologe*, 1995;92(5):647-53.

79. Marmorstein, AD, Marmorstein, LY, Sakaguchi, H, and Hollyfield, JG, Spectral profiling of autofluorescence associated with lipofuscin, Bruch's Membrane, and sub-RPE deposits in normal and AMD eyes. *Invest Ophthalmol Vis Sci*, 2002;43(7):2435-41.

80. Spaide, R, Autofluorescence from the outer retina and subretinal space: hypothesis and review. *Retina*, 2008;28(1):5-35.

81. Staudt, S, Bellman, C, Schutt, F, Losch, A, and Holz, FG, Various Intra- and extracellular fluorophores other than RPE lipofuscin contribute to intensity in topographic fundus autofluorescence images. *Invest Ophthalmol Vis Sci*, 2000;41:Abstract 873.

82. Holz, FG, Bellmann, C, Margaritidis, M, Schutt, F, Otto, TP, and Volcker, HE, Patterns of increased in vivo fundus autofluorescence in the junctional zone of geographic atrophy of the retinal pigment epithelium associated with age-related macular degeneration. *Graefes Arch Clin Exp Ophthalmol*, 1999;237(2):145-52.

83. Delori, FC, Fleckner, MR, Goger, DG, Weiter, JJ, and Dorey, CK, Autofluorescence distribution associated with drusen in age-related macular degeneration. *Invest Ophthalmol Vis Sci*, 2000;41(2):496-504.

84. Lois, N, Owens, SL, Coco, R, Hopkins, J, Fitzke, FW, and Bird, AC, Fundus autofluorescence in patients with age-related macular degeneration and high risk of visual loss. *Am J Ophthalmol*, 2002;133(3):341-9.

85. Bindewald, A, Schmitz-Valckenberg, S, Jorzik, JJ, Dolar-Szczasny, J, Sieber, H, Keilhauer, C, Weinberger, AW, Dithmar, S, Pauleikhoff, D, Mansmann, U, Wolf, S, and Holz, FG, Classification of abnormal fundus autofluorescence patterns in the junctional zone of geographic atrophy in patients with age related macular degeneration. *Br J Ophthalmol*, 2005;89(7):874-8.

86. Solbach, U, Keilhauer, C, Knabben, H, and Wolf, S, Imaging of retinal autofluorescence in patients with age-related macular degeneration. *Retina*, 1997;17(5):385-9.

87. Holz, FG, Bellman, C, Staudt, S, Schutt, F, and Volcker, HE, Fundus autofluorescence and development of geographic atrophy in age-related macular degeneration. *Invest Ophthalmol Vis Sci*, 2001;42(5):1051-6.

88. Smith, RT, Chan, JK, Busuoic, M, Sivagnanavel, V, Bird, AC, and Chong, NV, Autofluorescence characteristics of early, atrophic, and high-risk fellow eyes in age-related macular degeneration. *Invest Ophthalmol Vis Sci*, 2006;47(12):5495-504.

89. Sunness, JS, Ziegler, MD, and Applegate, CA, Issues in quantifying atrophic macular disease using retinal autofluorescence. *Retina*, 2006;26(6):666-72.

90. Karadimas, P and Bouzas, EA, Fundus autofluorescence imaging in serous and drusenoid pigment epithelial detachments associated with age-related macular degeneration. *Am J Ophthalmol*, 2005;140(6):1163-5.

91. Scholl, HP, Bellmann, C, Dandekar, SS, Bird, AC, and Fitzke, FW, Photopic and scotopic fine matrix mapping of retinal areas of increased fundus autofluorescence in patients with age-related maculopathy. *Invest Ophthalmol Vis Sci*, 2004;45(2):574-83.

92. Schmitz-Valckenberg, S, Bultmann, S, Dreyhaupt, J, Bindewald, A, Holz, FG, and Rohrschneider, K, Fundus autofluorescence and fundus perimetry in the junctional zone of geographic atrophy in patients with age-related macular degeneration. *Invest Ophthalmol Vis Sci*, 2004;45(12):4470-6.

93. Garron, LK, The Ultrastructure of the Retinal Pigment Epithelium with Observations on the Choriocapillaris and Bruch's Membrane. *Trans Am Ophthalmol Soc*, 1963;61:545-88.

94. Hogan, MJ, Alvarado, JA, and Weddell, JE, Histology of the human eye; an atlas and textbook. 1971, Philadelphia,: Saunders. xiii, 687 p.

95. Nakaizumi, Y, Hogan, MJ, and Feeney, L, The Ultrastructure of Bruch's Membrane. 3. The Macular Area of the Human Eye. *Arch Ophthalmol*, 1964;72:395-400.

96. Chong, NH, Keonin, J, Luthert, PJ, Frennesson, CI, Weingeist, DM, Wolf, RL, Mullins, RF, and Hageman, GS, Decreased thickness and integrity of the macular elastic layer of Bruch's membrane correspond to the distribution of lesions associated with age-related macular degeneration. *Am J Pathol*, 2005;166(1):241-51.

97. Hewitt, AT, Nakazawa, K, and Newsome, DA, Analysis of newly synthesized Bruch's membrane proteoglycans. *Invest Ophthalmol Vis Sci*, 1989;30(3):478-86.

98. Nakaizumi, Y, The Ultrastructure of Bruch's Membrane. I. Human, Monkey, Rabbit, Guinea Pig, and Rat Eyes. *Arch Ophthalmol*, 1964;72:380-7.

99. Hayreh, SS, The choriocapillaris. *Albrecht Von Graefes Arch Klin Exp Ophthalmol*, 1974;192(3):165-79.

100. Yoneya, S, Tso, MO, and Shimizu, K, Patterns of the choriocapillaris. A method to study the choroidal vasculature of the enucleated human eye. *Int Ophthalmol*, 1983;6(2):95-9.

101. Taubold, RD, Studies on chemical nature of lipofusion (age pigment) isolated from normal human brain. *Lipids*, 1975;10(7):383-90.

102. Green, WR and Enger, C, Age-related macular degeneration histopathologic studies. The 1992 Lorenz E. Zimmerman Lecture. *Ophthalmology*, 1993;100(10):1519-35.

103. Bonilha, VL, Age and disease-related structural changes in the retinal pigment epithelium. *Clin Ophthalmol*, 2008;2(2):413-24.

104. Olver, JM, Functional anatomy of the choroidal circulation: methyl methacrylate casting of human choroid. *Eye*, 1990;4 (Pt 2):262-72.

105. Ramrattan, RS, van der Schaft, TL, Mooy, CM, de Bruijn, WC, Mulder, PG, and de Jong, PT, Morphometric analysis of Bruch's membrane, the choriocapillaris, and the choroid in aging. *Invest Ophthalmol Vis Sci*, 1994;35(6):2857-64.

106. van der Schaft, TL, Mooy, CM, de Bruijn, WC, Oron, FG, Mulder, PG, and de Jong, PT, Histologic features of the early stages of age-related macular degeneration. A statistical analysis. *Ophthalmology*, 1992;99(2):278-86.

107. Friedman, E and Smith, TR, Macular Diseases: Senile Changes of the Choriocapillaris of the Posterior Pole. *Trans Am Acad Ophthalmol Otolaryngol*, 1965;69:652-61.

108. Olver, J, Pauleikhoff, D, and Bird, A, Morphometric analysis of age changes in the choriocapillaris. *Invest Ophthalmol Vis Sci.* , 1991;31((suppl):47).

109. Yamamoto, T and Yamashita, H, Scanning electron microscopic observation of Bruch's membrane with the osmium tetroxide treatment. *Br J Ophthalmol*, 1989;73(3):162-7.

110. Newsome, DA, Hewitt, AT, Huh, W, Robey, PG, and Hassell, JR, Detection of specific extracellular matrix molecules in drusen, Bruch's membrane, and ciliary body. *Am J Ophthalmol*, 1987;104(4):373-81.

111. Hogan, MJ and Alvarado, J, Studies on the human macula. IV. Aging changes in Bruch's membrane. *Arch Ophthalmol*, 1967;77(3):410-20.

112. Karwatowski, WS, Jeffries, TE, Duance, VC, Albon, J, Bailey, AJ, and Easty, DL, Preparation of Bruch's membrane and analysis of the age-related changes in the structural collagens. *Br J Ophthalmol*, 1995;79(10):944-52.

113. Marshall, J, The ageing retina: physiology or pathology. *Eye*, 1987;1 (Pt 2):282-95.

114. Hewitt, AT and Newsome, DA, Altered synthesis of Bruch's membrane proteoglycans associated with dominant retinitis pigmentosa. *Curr Eye Res*, 1985;4(3):169-74.

115. Marshall, GE, Konstas, AG, Reid, GG, Edwards, JG, and Lee, WR, Collagens in the aged human macula. *Graefes Arch Clin Exp Ophthalmol*, 1994;232(3):133-40.

116. Herbst, TJ, McCarthy, JB, Tsilibary, EC, and Furcht, LT, Differential effects of laminin, intact type IV collagen, and specific domains of type IV collagen on endothelial cell adhesion and migration. *J Cell Biol*, 1988;106(4):1365-73.

117. Kliffen, M, Mooy, CM, Luider, TM, Huijmans, JG, Kerkvliet, S, and de Jong, PT, Identification of glycosaminoglycans in age-related macular deposits. *Arch Ophthalmol*, 1996;114(8):1009-14.

118. Alexander, RA and Garner, A, Elastic and precursor fibres in the normal human eye. *Exp Eye Res*, 1983;36(2):305-15.

119. Loffler, KU and Lee, WR, Basal linear deposit in the human macula. *Graefes Arch Clin Exp Ophthalmol*, 1986;224(6):493-501.

120. Spraul, CW, Lang, GE, Grossniklaus, HE, and Lang, GK, Histologic and morphometric analysis of the choroid, Bruch's membrane, and retinal pigment epithelium in postmortem eyes with age-related macular degeneration and histologic examination of surgically excised choroidal neovascular membranes. *Surv Ophthalmol*, 1999;44 Suppl 1:S10-32.

121. Snow, KK and Seddon, JM, Do age-related macular degeneration and cardiovascular disease share common antecedents? *Ophthalmic Epidemiol*, 1999;6(2):125-43.

122. Marshall, GE, Konstas, AG, Reid, GG, Edwards, JG, and Lee, WR, Type IV collagen and laminin in Bruch's membrane and basal linear deposit in the human macula. *Br J Ophthalmol*, 1992;76(10):607-14.

123. Killingsworth, MC, Age-related components of Bruch's membrane in the human eye. *Graefes Arch Clin Exp Ophthalmol*, 1987;225(6):406-12.

124. Ruberti, JW, Curcio, CA, Millican, CL, Menco, BP, Huang, JD, and Johnson, M, Quick-freeze/deep-etch visualization of age-related lipid accumulation in Bruch's membrane. *Invest Ophthalmol Vis Sci*, 2003;44(4):1753-9.

125. Curcio, CA, Millican, CL, Bailey, T, and Kruth, HS, Accumulation of cholesterol with age in human Bruch's membrane. *Invest Ophthalmol Vis Sci*, 2001;42(1):265-74.

126. Li, CM, Chung, BH, Presley, JB, Malek, G, Zhang, X, Dashti, N, Li, L, Chen, J, Bradley, K, Kruth, HS, and Curcio, CA, Lipoprotein-like particles and cholesteryl esters in human Bruch's membrane: initial characterization. *Invest Ophthalmol Vis Sci*, 2005;46(7):2576-86.

127. Huang, JD, Presley, JB, Chimento, MF, Curcio, CA, and Johnson, M, Age-related changes in human macular Bruch's membrane as seen by quick-freeze/deep-etch. *Exp Eye Res*, 2007;85(2):202-18.

128. Curcio, CA, Presley, JB, Millican, CL, and Medeiros, NE, Basal deposits and drusen in eyes with age-related maculopathy: evidence for solid lipid particles. *Exp Eye Res*, 2005;80(6):761-75.

129. Pauleikhoff, D, Barondes, MJ, Minassian, D, Chisholm, IH, and Bird, AC, Drusen as risk factors in age-related macular disease. *Am J Ophthalmol*, 1990;109(1):38-43.

130. Fisher, RF, The influence of age on some ocular basement membranes. *Eye*, 1987;1 (Pt 2):184-9.

131. Starita, C, Hussain, AA, Pagliarini, S, and Marshall, J, Hydrodynamics of ageing Bruch's membrane: implications for macular disease. *Exp Eye Res*, 1996;62(5):565-72.

132. Holz, FG, Sheraidah, G, Pauleikhoff, D, and Bird, AC, Analysis of lipid deposits extracted from human macular and peripheral Bruch's membrane. *Arch Ophthalmol*, 1994;112(3):402-6.

133. Sheraidah, G, Steinmetz, R, Maguire, J, Pauleikhoff, D, Marshall, J, and Bird, AC, Correlation between lipids extracted from Bruch's membrane and age. *Ophthalmology*, 1993;100(1):47-51.

134. Bird, AC and Marshall, J, Retinal pigment epithelial detachments in the elderly. *Trans Ophthalmol Soc U K*, 1986;105 (Pt 6):674-82.

135. Lusis, AJ, Atherosclerosis. *Nature*, 2000;407(6801):233-41.

136. Ross, R, Atherosclerosis--an inflammatory disease. *N Engl J Med*, 1999;340(2):115-26.

137. Williams, KJ and Tabas, I, The response-to-retention hypothesis of early atherogenesis. *Arterioscler Thromb Vasc Biol*, 1995;15(5):551-61.

138. Williams, KJ and Tabas, I, The response-to-retention hypothesis of atherogenesis reinforced. *Curr Opin Lipidol*, 1998;9(5):471-4.

139. Skalen, K, Gustafsson, M, Rydberg, EK, Hulten, LM, Wiklund, O, Innerarity, TL, and Boren, J, Subendothelial retention of atherogenic lipoproteins in early atherosclerosis. *Nature*, 2002;417(6890):750-4.

140. Segrest, JP, Jones, MK, De Loof, H, and Dashti, N, Structure of apolipoprotein B-100 in low density lipoproteins. *J Lipid Res*, 2001;42(9):1346-67.

141. Farese, RV, Jr., Veniant, MM, Cham, CM, Flynn, LM, Pierotti, V, Loring, JF, Traber, M, Ruland, S, Stokowski, RS, Huszar, D, and Young, SG, Phenotypic analysis of mice expressing exclusively apolipoprotein B48 or apolipoprotein B100. *Proc Natl Acad Sci U S A*, 1996;93(13):6393-8.

142. Greeve, J, Altkemper, I, Dieterich, JH, Greten, H, and Windler, E, Apolipoprotein B mRNA editing in 12 different mammalian species: hepatic expression is reflected in low concentrations of apoB-containing plasma lipoproteins. *J Lipid Res*, 1993;34(8):1367-83.

143. Chan, L, Apolipoprotein B, the major protein component of triglyceride-rich and low density lipoproteins. *J Biol Chem*, 1992;267(36):25621-4.

144. Young, SG, Bertics, SJ, Scott, TM, Dubois, BW, Curtiss, LK, and Witztum, JL, Parallel expression of the MB19 genetic polymorphism in apoprotein B-100 and apoprotein B-48. Evidence that both apoproteins are products of the same gene. *J Biol Chem*, 1986;261(7):2995-8.

145. NIH, Second report of the Expert Panel on Detection, Evaluation, and Treatment of High Blood Cholesterol in Adults (Adult Treatment Panel II), in National Cholesterol Education Program. 1993, National Heart, Lung, and Blood Institute: *Bethesda, Md.*

146. Wight, TN, Cell biology of arterial proteoglycans. *Arteriosclerosis*, 1989;9(1):1-20.

147. Chait, A and Wight, TN, Interaction of native and modified low-density lipoproteins with extracellular matrix. *Curr Opin Lipidol*, 2000;11(5):457-63.

148. Wight, TN, The extracellular matrix and atherosclerosis. *Curr Opin Lipidol*, 1995;6(5):326-34.

149. Cardoso, LE and Mourao, PA, Glycosaminoglycan fractions from human arteries presenting diverse susceptibilities to atherosclerosis have different binding affinities to plasma LDL. *Arterioscler Thromb*, 1994;14(1):115-24.

150. Camejo, G, Olofsson, SO, Lopez, F, Carlsson, P, and Bondjers, G, Identification of Apo B-100 segments mediating the interaction of low density lipoproteins with arterial proteoglycans. *Arteriosclerosis*, 1988;8(4):368-77.

151. Hollmann, J, Schmidt, A, von Bassewitz, DB, and Buddecke, E, Relationship of sulfated glycosaminoglycans and cholesterol content in normal and arteriosclerotic human aorta. *Arteriosclerosis*, 1989;9(2):154-8.

152. Hurt-Camejo, E, Olsson, U, Wiklund, O, Bondjers, G, and Camejo, G, Cellular consequences of the association of apoB lipoproteins with proteoglycans. Potential contribution to atherogenesis. *Arterioscler Thromb Vasc Biol*, 1997;17(6):1011-7.

153. Tannock, LR, Olin, KL, Barrett, PH, Wight, TN, and Chait, A, Triglyceride-rich lipoproteins from subjects with type 2 diabetes do not demonstrate increased binding to biglycan, a vascular proteoglycan. *J Clin Endocrinol Metab*, 2002;87(1):35-40.

154. Sartipy, P, Bondjers, G, and Hurt-Camejo, E, Phospholipase A2 type II binds to extracellular matrix biglycan: modulation of its activity on LDL by colocalization in glycosaminoglycan matrixes. *Arterioscler Thromb Vasc Biol*, 1998;18(12):1934-41.

155. Riessen, R, Isner, JM, Blessing, E, Loushin, C, Nikol, S, and Wight, TN, Regional differences in the distribution of the proteoglycans biglycan and decorin in the extracellular matrix of atherosclerotic and restenotic human coronary arteries. *Am J Pathol*, 1994;144(5):962-74.

156. Salisbury, BG and Wagner, WD, Isolation and preliminary characterization of proteoglycans dissociatively extracted from human aorta. *J Biol Chem*, 1981;256(15):8050-7.

157. Little, PJ, Osman, N, and O'Brien, KD, Hyperelongated biglycan: the surreptitious initiator of atherosclerosis. *Curr Opin Lipidol*, 2008;19(5):448-54.

158. Bianco, P, Fisher, LW, Young, MF, Termine, JD, and Robey, PG, Expression and localization of the two small proteoglycans biglycan and decorin in developing human skeletal and non-skeletal tissues. *J Histochem Cytochem*, 1990;38(11):1549-63.

159. Asundi, V, Cowan, K, Matzura, D, Wagner, W, and Dreher, KL, Characterization of extracellular matrix proteoglycan transcripts expressed by vascular smooth muscle cells. *Eur J Cell Biol*, 1990;52(1):98-104.

160. Ruoslahti, E and Yamaguchi, Y, Proteoglycans as modulators of growth factor activities. *Cell*, 1991;64(5):867-9.

161. Camejo, G, Fager, G, Rosengren, B, Hurt-Camejo, E, and Bondjers, G, Binding of low density lipoproteins by proteoglycans synthesized by proliferating and quiescent human arterial smooth muscle cells. *J Biol Chem*, 1993;268(19):14131-7.

162. Baker, SM, Sugars, RV, Wendel, M, Smith, AJ, Waddington, RJ, Cooper, PR, and Sloan, AJ, TGF-beta/extracellular matrix interactions in dentin matrix: a role in regulating sequestration and protection of bioactivity. *Calcif Tissue Int*, 2009;85(1):66-74.

163. Schmidt, G, Hausser, H, and Kresse, H, Interaction of the small proteoglycan decorin with fibronectin. Involvement of the sequence NKISK of the core protein. *Biochem J*, 1991;280 (Pt 2):411-4.

164. Schonherr, E, Witsch-Prehm, P, Harrach, B, Robenek, H, Rauterberg, J, and Kresse, H, Interaction of biglycan with type I collagen. *J Biol Chem*, 1995;270(6):2776-83.

165. Whinna, HC, Choi, HU, Rosenberg, LC, and Church, FC, Interaction of heparin cofactor II with biglycan and decorin. *J Biol Chem*, 1993;268(6):3920-4.

166. O'Brien, KD, Olin, KL, Alpers, CE, Chiu, W, Ferguson, M, Hudkins, K, Wight, TN, and Chait, A, Comparison of apolipoprotein and proteoglycan deposits in human coronary atherosclerotic plaques: colocalization of biglycan with apolipoproteins. *Circulation*, 1998;98(6):519-27.

167. Kunjathoor, VV, Chiu, DS, O'Brien, KD, and LeBoeuf, RC, Accumulation of biglycan and perlecan, but not versican, in lesions of murine models of atherosclerosis. *Arterioscler Thromb Vasc Biol*, 2002;22(3):462-8.

168. Gianturco, SH and Bradley, WA, Pathophysiology of triglyceride-rich lipoproteins in atherothrombosis: cellular aspects. *Clin Cardiol*, 1999;22(2 Suppl):II-7-II-14.

169. Camejo, G, Rosengren, B, Olson, U, Lopez, F, Olofson, SO, Westerlund, C, and Bondjers, G, Molecular basis of the association of arterial proteoglycans with low density lipoproteins: its effect on the structure of the lipoprotein particle. *Eur Heart J*, 1990;11 Suppl E:164-73.

170. Weisgraber, KH and Rall, SC, Jr., Human apolipoprotein B-100 heparin-binding sites. *J Biol Chem*, 1987;262(23):11097-103.

171. Hirose, N, Blankenship, DT, Krivanek, MA, Jackson, RL, and Cardin, AD, Isolation and characterization of four heparin-binding cyanogen bromide peptides of human plasma apolipoprotein B. *Biochemistry*, 1987;26(17):5505-12.

172. Schwenke, DC and Carew, TE, Initiation of atherosclerotic lesions in cholesterol-fed rabbits. II. Selective retention of LDL vs. selective increases in LDL permeability in susceptible sites of arteries. *Arteriosclerosis*, 1989;9(6):908-18.

173. Schwenke, DC and Carew, TE, Initiation of atherosclerotic lesions in cholesterol-fed rabbits. I. Focal increases in arterial LDL concentration precede development of fatty streak lesions. *Arteriosclerosis*, 1989;9(6):895-907.

174. Chisolm, GM, 3rd, Antioxidants and atherosclerosis: a current assessment. *Clin Cardiol*, 1991;14(2 Suppl 1):I25-30.

175. Witztum, JL and Steinberg, D, Role of oxidized low density lipoprotein in atherogenesis. *J Clin Invest*, 1991;88(6):1785-92.

176. Cushing, SD, Berliner, JA, Valente, AJ, Territo, MC, Navab, M, Parhami, F, Gerrity, R, Schwartz, CJ, and Fogelman, AM, Minimally modified low density lipoprotein induces monocyte chemotactic protein 1 in human endothelial cells and smooth muscle cells. *Proc Natl Acad Sci U S A*, 1990;87(13):5134-8.

177. Quinn, MT, Parthasarathy, S, Fong, LG, and Steinberg, D, Oxidatively modified low density lipoproteins: a potential role in recruitment and retention of monocyte/macrophages during atherogenesis. *Proc Natl Acad Sci U S A*, 1987;84(9):2995-8.

178. Autio, I, Jaakkola, O, Solakivi, T, and Nikkari, T, Oxidized low-density lipoprotein is chemotactic for arterial smooth muscle cells in culture. *FEBS Lett*, 1990;277(1-2):247-9.

179. McMurray, HF, Parthasarathy, S, and Steinberg, D, Oxidatively modified low density lipoprotein is a chemoattractant for human T lymphocytes. *J Clin Invest*, 1993;92(2):1004-8.

180. Navab, M, Berliner, JA, Watson, AD, Hama, SY, Territo, MC, Lusis, AJ, Shih, DM, Van Lenten, BJ, Frank, JS, Demer, LL, Edwards, PA, and Fogelman, AM, The Yin and Yang of oxidation in the development of the fatty streak. A review based on the 1994 George Lyman Duff Memorial Lecture. *Arterioscler Thromb Vasc Biol*, 1996;16(7):831-42.

181. Griendling, KK and Alexander, RW, Oxidative stress and cardiovascular disease. *Circulation*, 1997;96(10):3264-5.

182. Rajavashisth, TB, Andalibi, A, Territo, MC, Berliner, JA, Navab, M, Fogelman, AM, and Lusis, AJ, Induction of endothelial cell expression of granulocyte and macrophage colony-stimulating factors by modified low-density lipoproteins. *Nature*, 1990;344(6263):254-7.

183. Fuster, V, Ross, R, and Topol, EJ, Atherosclerosis and coronary artery disease. 1996, Philadelphia: Lippincott-Raven. 2 v. (xxv, 1661, 42 p.).

184. Vijayagopal, P, Srinivasan, SR, Radhakrishnamurthy, B, and Berenson, GS, Lipoprotein-proteoglycan complexes from atherosclerotic lesions promote cholesteryl ester accumulation in human monocytes/macrophages. *Arterioscler Thromb*, 1992;12(2):237-49.

185. Hurt, E, Bondjers, G, and Camejo, G, Interaction of LDL with human arterial proteoglycans stimulates its uptake by human monocyte-derived macrophages. *J Lipid Res*, 1990;31(3):443-54.

186. O'Brien, KD, Gordon, D, Deeb, S, Ferguson, M, and Chait, A, Lipoprotein lipase is synthesized by macrophage-derived foam cells in human coronary atherosclerotic plaques. *J Clin Invest*, 1992;89(5):1544-50.

187. Katsuda, S, Coltrera, MD, Ross, R, and Gown, AM, Human atherosclerosis. IV. Immunocytochemical analysis of cell activation and proliferation in lesions of young adults. *Am J Pathol*, 1993;142(6):1787-93.

188. Raines, EW, Rosenfeld, ME, and Ross, R, The role of macrophages. , in *Atherosclerosis and coronary artery disease*, V. Fuster, R. Ross, and E.J. Topol, Editors. 1996, Lippincott-Raven: Philadelphia. 539-55.

189. Stemme, S, Faber, B, Holm, J, Wiklund, O, Witztum, JL, and Hansson, GK, T lymphocytes from human atherosclerotic plaques recognize oxidized low density lipoprotein. *Proc Natl Acad Sci U S A*, 1995;92(9):3893-7.

190. Ismail, NA, Alavi, MZ, and Moore, S, Lipoprotein-proteoglycan complexes from injured rabbit aortas accelerate lipoprotein uptake by arterial smooth muscle cells. *Atherosclerosis*, 1994;105(1):79-87.

191. Hansson, GK, Jonasson, L, Seifert, PS, and Stemme, S, Immune mechanisms in atherosclerosis. *Arteriosclerosis*, 1989;9(5):567-78.

192. Tertov, VV, Orekhov, AN, Ryong, LH, and Smirnov, VN, Intracellular cholesterol accumulation is accompanied by enhanced proliferative activity of human aortic intimal cells. *Tissue Cell*, 1988;20(6):849-54.

193. Merrilees, MJ, Campbell, JH, Spanidis, E, and Campbell, GR, Glycosaminoglycan synthesis by smooth muscle cells of differing phenotype and their response to endothelial cell conditioned medium. *Atherosclerosis*, 1990;81(3):245-54.

194. Jonasson, L, Bondjers, G, and Hansson, GK, Lipoprotein lipase in atherosclerosis: its presence in smooth muscle cells and absence from macrophages. *J Lipid Res*, 1987;28(4):437-45.

195. Ylä-Herttuala, S, Lipton, BA, Rosenfeld, ME, Goldberg, IJ, Steinberg, D, and Witztum, JL, Macrophages and smooth muscle cells express lipoprotein lipase in human and rabbit atherosclerotic lesions. *Proc Natl Acad Sci U S A*, 1991;88(22):10143-7.

196. Glagov, S, Weisenberg, E, Zarins, CK, Stankunavicius, R, and Kolettis, GJ, Compensatory enlargement of human atherosclerotic coronary arteries. *N Engl J Med*, 1987;316(22):1371-5.

197. Hansson, GK and Libby, P, The role of the lymphocyte., in *Atherosclerosis and coronary artery disease*, V. Fuster, R. Ross, and E.J. Topol, Editors. 1996, Lippincott-Raven: Philadelphia. 557-68.

198. Hajjar, DP and Haberland, ME, Lipoprotein trafficking in vascular cells. Molecular Trojan horses and cellular saboteurs. *J Biol Chem*, 1997;272(37):22975-8.

199. Curcio, CA, Johnson, M, Huang, JD, and Rudolf, M, Aging, Age-related Macular Degeneration, and the Response-to-Retention of Apolipoprotein B-Containing Lipoproteins. *Prog Retin Eye Res*, 2009.

200. Bocan, TM, Schifani, TA, and Guyton, JR, Ultrastructure of the human aortic fibrolipid lesion. Formation of the atherosclerotic lipid-rich core. *Am J Pathol*, 1986;123(3):413-24.

201. Guyton, JR, Bocan, TM, and Schifani, TA, Quantitative ultrastructural analysis of perifibrous lipid and its association with elastin in nonatherosclerotic human aorta. *Arteriosclerosis*, 1985;5(6):644-52.

202. Haimovici, R, Gantz, DL, Rumelt, S, Freddo, TF, and Small, DM, The lipid composition of drusen, Bruch's membrane, and sclera by hot stage polarizing light microscopy. *Invest Ophthalmol Vis Sci*, 2001;42(7):1592-9.

203. Rudolf, M and Curcio, CA, Esterified cholesterol is highly localized to Bruch's membrane, as revealed by lipid histochemistry in wholemounts of human choroid. *J Histochem Cytochem*, 2009;57(8):731-9.

204. Gulcan, HG, Alvarez, RA, Maude, MB, and Anderson, RE, Lipids of human retina, retinal pigment epithelium, and Bruch's membrane/choroid: comparison of macular and peripheral regions. *Invest Ophthalmol Vis Sci*, 1993;34(11):3187-93.

205. Pauleikhoff, D, Sheraidah, G, Marshall, J, Bird, AC, and Wessing, A, [Biochemical and histochemical analysis of age related lipid deposits in Bruch's membrane]. *Ophthalmologe*, 1994;91(6):730-4.

206. Spaide, RF, Ho-Spaide, WC, Browne, RW, and Armstrong, D, Characterization of peroxidized lipids in Bruch's membrane. *Retina*, 1999;19(2):141-7.

207. Malek, G, Li, CM, Guidry, C, Medeiros, NE, and Curcio, CA, Apolipoprotein B in cholesterol-containing drusen and basal deposits of human eyes with age-related maculopathy. *Am J Pathol*, 2003;162(2):413-25.

208. Campochiaro, PA, Jerdon, JA, and Glaser, BM, The extracellular matrix of human retinal pigment epithelial cells in vivo and its synthesis in vitro. *Invest Ophthalmol Vis Sci*, 1986;27(11):1615-21.

209. Korte, GE and D'Aversa, G, The elastic tissue of Bruch's membrane. Connections to choroidal elastic tissue and the ciliary epithelium of the rabbit and human eyes. *Arch Ophthalmol*, 1989;107(11):1654-8.

210. Das, A, Frank, RN, Zhang, NL, and Turczyn, TJ, Ultrastructural localization of extracellular matrix components in human retinal vessels and Bruch's membrane. *Arch Ophthalmol*, 1990;108(3):421-9.

211. Call, TW and Hollyfield, JG, Sulfated proteoglycans in Bruch's membrane of the human eye: localization and characterization using cupromeronic blue. *Exp Eye Res*, 1990;51(4):451-62.

212. Augustin, AJ and Kirchhof, J, Inflammation and the pathogenesis of age-related macular degeneration. *Expert Opin Ther Targets*, 2009;13(6):641-51.

213. Xu, H, Chen, M, and Forrester, JV, Para-inflammation in the aging retina. *Prog Retin Eye Res*, 2009;28(5):348-68.

214. Chen, H, Liu, B, Lukas, TJ, and Neufeld, AH, The aged retinal pigment epithelium/choroid: a potential substratum for the pathogenesis of age-related macular degeneration. *PLoS ONE*, 2008;3(6):e2339.

215. Hageman, GS, Mullins, RF, Russell, SR, Johnson, LV, and Anderson, DH, Vitronectin is a constituent of ocular drusen and the vitronectin gene is expressed in human retinal pigmented epithelial cells. *FASEB J*, 1999;13(3):477-84.

216. Johnson, LV, Ozaki, S, Staples, MK, Erickson, PA, and Anderson, DH, A potential role for immune complex pathogenesis in drusen formation. *Exp Eye Res*, 2000;70(4):441-9.

217. Mullins, RF, Russell, SR, Anderson, DH, and Hageman, GS, Drusen associated with aging and age-related macular degeneration contain proteins common to extracellular deposits associated with atherosclerosis, elastosis, amyloidosis, and dense deposit disease. *FASEB J*, 2000;14(7):835-46.

218. Sakaguchi, H, Miyagi, M, Shadrach, KG, Rayborn, ME, Crabb, JW, and Hollyfield, JG, Clusterin is present in drusen in age-related macular degeneration. *Exp Eye Res*, 2002;74(4):547-9.

219. Ishibashi, T, Patterson, R, Ohnishi, Y, Inomata, H, and Ryan, SJ, Formation of drusen in the human eye. *Am J Ophthalmol*, 1986;101(3):342-53.

220. Feeney-Burns, L and Ellersieck, MR, Age-related changes in the ultrastructure of Bruch's membrane. *Am J Ophthalmol*, 1985;100(5):686-97.

221. Hageman, GS and Mullins, RF, Molecular composition of drusen as related to substructural phenotype. *Mol Vis*, 1999;5:28.

222. Burns, RP and Feeney-Burns, L, Clinico-morphologic correlations of drusen of Bruch's membrane. *Trans Am Ophthalmol Soc*, 1980;78:206-25.

223. Penfold, PL, Killingsworth, MC, and Sarks, SH, Senile macular degeneration: the involvement of immunocompetent cells. *Graefes Arch Clin Exp Ophthalmol*, 1985;223(2):69-76.

224. Killingsworth, MC, Sarks, JP, and Sarks, SH, Macrophages related to Bruch's membrane in age-related macular degeneration. *Eye*, 1990;4 (Pt 4):613-21.

225. Oh, H, Takagi, H, Takagi, C, Suzuma, K, Otani, A, Ishida, K, Matsumura, M, Ogura, Y, and Honda, Y, The potential angiogenic role of macrophages in the formation of choroidal neovascular membranes. *Invest Ophthalmol Vis Sci*, 1999;40(9):1891-8.

226. Dastgheib, K and Green, WR, Granulomatous reaction to Bruch's membrane in age-related macular degeneration. *Arch Ophthalmol*, 1994;112(6):813-8.

227. Penfold, PL, Killingsworth, MC, and Sarks, SH, Senile macular degeneration. The involvement of giant cells in atrophy of the retinal pigment epithelium. *Invest Ophthalmol Vis Sci*, 1986;27(3):364-71.

228. Penfold, PL, Liew, SC, Madigan, MC, and Provis, JM, Modulation of major histocompatibility complex class II expression in retinas with age-related macular degeneration. *Invest Ophthalmol Vis Sci*, 1997;38(10):2125-33.

229. Flood, C, Gustafsson, M, Richardson, PE, Harvey, SC, Segrest, JP, and Boren, J, Identification of the proteoglycan binding site in apolipoprotein B48. *J Biol Chem*, 2002;277(35):32228-33.

230. Sanan, DA, Newland, DL, Tao, R, Marcovina, S, Wang, J, Mooser, V, Hammer, RE, and Hobbs, HH, Low density lipoprotein receptor-negative mice expressing human apolipoprotein B-100 develop complex atherosclerotic lesions on a chow diet: no accentuation by apolipoprotein(a). *Proc Natl Acad Sci U S A*, 1998;95(8):4544-9.

231. Purcell-Huynh, DA, Farese, RV, Jr., Johnson, DF, Flynn, LM, Pierotti, V, Newland, DL, Linton, MF, Sanan, DA, and Young, SG, Transgenic mice expressing high levels of human apolipoprotein B develop severe atherosclerotic lesions in response to a high-fat diet. *J Clin Invest*, 1995;95(5):2246-57.

232. Veniant, MM, Pierotti, V, Newland, D, Cham, CM, Sanan, DA, Walzem, RL, and Young, SG, Susceptibility to atherosclerosis in mice expressing exclusively apolipoprotein B48 or apolipoprotein B100. *J Clin Invest*, 1997;100(1):180-8.

233. ETDRS_Research_Group, Grading diabetic retinopathy from stereoscopic color fundus photographs--an extension of the modified Airlie House classification. ETDRS report number 10. Early Treatment Diabetic Retinopathy Study Research Group. *Ophthalmology*, 1991;98(5 Suppl):786-806.

234. Scholl, HP, Peto, T, Dandekar, S, Bunce, C, Xing, W, Jenkins, S, and Bird, AC, Inter- and intra-observer variability in grading lesions of age-related maculopathy and macular degeneration. *Graefes Arch Clin Exp Ophthalmol*, 2003;241(1):39-47.

235. Sallo, FB, Peto, T, Leung, I, Xing, W, Bunce, C, and Bird, AC, The International Classification system and the progression of age-related macular degeneration. *Curr Eye Res*, 2009;34(3):238-40.

236. Fitzke, FW, Crabb, DP, McNaught, AI, Edgar, DF, and Hitchings, RA, Image processing of computerised visual field data. *Br J Ophthalmol*, 1995;79(3):207-12.

237. Fitzke, FW and Kemp, CM, Probing visual function with psychophysics and photochemistry. *Eye*, 1989;3 (Pt 1):84-9.

238. Westcott, MC, McNaught, AI, Crabb, DP, Fitzke, FW, and Hitchings, RA, High spatial resolution automated perimetry in glaucoma. *Br J Ophthalmol*, 1997;81(6):452-9.

239. Guymer, RH, Gross-Jendroska, M, Owens, SL, Bird, AC, and Fitzke, FW, Laser treatment in subjects with high-risk clinical features of age-related macular degeneration. Posterior pole appearance and retinal function. *Arch Ophthalmol*, 1997;115(5):595-603.

240. Wu, D, Bird, AC, McNaught, A, Buckland, MS, and Fitzke, FW, Fine matrix mapping of the macular region in normal subjects. *Zhonghua Yan Ke Za Zhi*, 1995;31(4):243-9.

241. Culham, LE, Fitzke, FW, Timberlake, G, and Marshall, J, Assessment of fixation stability in normal subjects and patients using a scanning laser ophthalmoscope. *Clin. Vision. Sci.*, 1993;8:551-561.

242. Steinman, RM, Effect of target size, luminance, and color on monocular fixation. *J. Opt. Soc. Am.*, 1965;55:1158-1165.

243. Bjelik, A, Bereczki, E, Gonda, S, Juhasz, A, Rimanoczy, A, Zana, M, Csont, T, Pakaski, M, Boda, K, Ferdinandy, P, Dux, L, Janka, Z, Santha, M, and Kalman, J, Human apoB overexpression and a high-cholesterol diet differently modify the brain APP metabolism in the transgenic mouse model of atherosclerosis. *Neurochem Int*, 2006;49(4):393-400.

244. Callow, MJ, Stoltzfus, LJ, Lawn, RM, and Rubin, EM, Expression of human apolipoprotein B and assembly of lipoprotein(a) in transgenic mice. *Proc Natl Acad Sci U S A*, 1994;91(6):2130-4.

245. Hogan, B, Manipulating the mouse embryo : a laboratory manual. 2nd ed. 1994, Plainview, N.Y.: Cold Spring Harbor Laboratory Press. xvii, 497 p.

246. Sambrook, J and Russell, DW, Molecular cloning : a laboratory manual. 3rd ed. 2001, Cold Spring Harbor, N.Y.: Cold Spring Harbor Laboratory Press.

247. Bjelik, A, Pakaski, M, Bereczki, E, Gonda, S, Juhasz, A, Rimanoczy, A, Zana, M, Janka, Z, Santha, M, and Kalman, J, APP mRNA splicing is upregulated in the brain of biglycan transgenic mice. *Neurochem Int*, 2007;50(1):1-4.

248. Csont, T, Bereczki, E, Bencsik, P, Fodor, G, Gorbe, A, Zvara, A, Csonka, C, Puskas, LG, Santha, M, and Ferdinandy, P, Hypercholesterolemia increases myocardial oxidative and nitrosative stress thereby leading to cardiac dysfunction in apoB-100 transgenic mice. *Cardiovasc Res*, 2007;76(1):100-9.

249. Bonnet, M, Pingault, C, and Tapissier, J, [Gradual disappearance of macular hyalin verrucosities]. *Arch Ophtalmol (Paris)*, 1976;36(6-7):465-74.

250. Leibrock, CS, Reuter, T, and Lamb, TD, Molecular basis of dark adaptation in rod photoreceptors. *Eye*, 1998;12 (Pt 3b):511-20.

251. Haig, C, Hecht, S, and Patek, AJ, Jr., Vitamin a and Rod-Cone Dark Adaptation in Cirrhosis of the Liver. *Science*, 1938;87(2267):534-536.

252. Seeliger, MW, Biesalski, HK, Wissinger, B, Gollnick, H, Gielen, S, Frank, J, Beck, S, and Zrenner, E, Phenotype in retinol deficiency due to a hereditary defect in retinol binding protein synthesis. *Invest Ophthalmol Vis Sci*, 1999;40(1):3-11.

253. Saari, JC, Biochemistry of visual pigment regeneration: the Friedenwald lecture. *Invest Ophthalmol Vis Sci*, 2000;41(2):337-48.

254. Dowling, JE and Wald, G, Vitamin a Deficiency and Night Blindness. *Proc Natl Acad Sci U S A*, 1958;44(7):648-61.

255. Katz, ML, Gao, CL, and Stientjes, HJ, Regulation of the interphotoreceptor retinoid-binding protein content of the retina by vitamin A. *Exp Eye Res*, 1993;57(4):393-401.

256. Katz, ML, Kutryb, MJ, Norberg, M, Gao, CL, White, RH, and Stark, WS, Maintenance of opsin density in photoreceptor outer segments of retinoid-deprived rats. *Invest Ophthalmol Vis Sci*, 1991;32(7):1968-80.

257. Li, T, Sandberg, MA, Pawlyk, BS, Rosner, B, Hayes, KC, Dryja, TP, and Berson, EL, Effect of vitamin A supplementation on rhodopsin mutants threonine-17 --> methionine and proline-347 --> serine in transgenic mice and in cell cultures. *Proc Natl Acad Sci U S A*, 1998;95(20):11933-8.

258. Redmond, TM, Yu, S, Lee, E, Bok, D, Hamasaki, D, Chen, N, Goletz, P, Ma, JX, Crouch, RK, and Pfeifer, K, Rpe65 is necessary for production of 11-cis-vitamin A in the retinal visual cycle. *Nat Genet*, 1998;20(4):344-51.

259. Mata, NL, Radu, RA, Clemmons, RC, and Travis, GH, Isomerization and oxidation of vitamin a in cone-dominant retinas: a novel pathway for visual-pigment regeneration in daylight. *Neuron*, 2002;36(1):69-80.

260. Kemp, CM, Jacobson, SG, Faulkner, DJ, and Walt, RW, Visual function and rhodopsin levels in humans with vitamin A deficiency. *Exp Eye Res*, 1988;46(2):185-97.

261. Sunness, JS, Johnson, MA, Massof, RW, and Marcus, S, Retinal sensitivity over drusen and nondrusen areas. A study using fundus perimetry. *Arch Ophthalmol*, 1988;106(8):1081-4.

262. Chuang, EL, Sharp, DM, Fitzke, FW, Kemp, CM, Holden, AL, and Bird, AC, Retinal dysfunction in central serous retinopathy. *Eye*, 1987;1 (Pt 1):120-5.

263. Miceli, MV, Newsome, DA, Tate, DJ, Jr., and Sarphie, TG, Pathologic changes in the retinal pigment epithelium and Bruch's membrane of fat-fed atherogenic mice. *Curr Eye Res*, 2000;20(1):8-16.

264. Dithmar, S, Sharara, NA, Curcio, CA, Le, NA, Zhang, Y, Brown, S, and Grossniklaus, HE, Murine high-fat diet and laser photochemical model of basal deposits in Bruch membrane. *Arch Ophthalmol*, 2001;119(11):1643-9.

265. Cousins, SW, Espinosa-Heidmann, DG, Alexandridou, A, Sall, J, Dubovy, S, and Csaky, K, The role of aging, high fat diet and blue light exposure in an experimental mouse model for basal laminar deposit formation. *Exp Eye Res*, 2002;75(5):543-53.

266. Cousins, SW, Marin-Castano, ME, Espinosa-Heidmann, DG, Alexandridou, A, Striker, L, and Elliot, S, Female gender, estrogen loss, and Sub-RPE deposit formation in aged mice. *Invest Ophthalmol Vis Sci*, 2003;44(3):1221-9.

267. Dithmar, S, Curcio, CA, Le, NA, Brown, S, and Grossniklaus, HE, Ultrastructural changes in Bruch's membrane of apolipoprotein E-deficient mice. *Invest Ophthalmol Vis Sci*, 2000;41(8):2035-42.

268. Kliffen, M, Lutgens, E, Daemen, MJ, de Muinck, ED, Mooy, CM, and de Jong, PT, The APO(*)E3-Leiden mouse as an animal model for basal laminar deposit. *Br J Ophthalmol*, 2000;84(12):1415-9.

269. Espinosa-Heidmann, DG, Sall, J, Hernandez, EP, and Cousins, SW, Basal laminar deposit formation in APO B100 transgenic mice: complex interactions between dietary fat, blue light, and vitamin E. *Invest Ophthalmol Vis Sci*, 2004;45(1):260-6.

270. Malek, G, Johnson, LV, Mace, BE, Saloupis, P, Schmechel, DE, Rickman, DW, Toth, CA, Sullivan, PM, and Bowes Rickman, C, Apolipoprotein E allele-dependent pathogenesis: a model for age-related retinal degeneration. *Proc Natl Acad Sci U S A*, 2005;102(33):11900-5.

271. Schmidt-Erfurth, U, Rudolf, M, Funk, M, Hofmann-Rummelt, C, Franz-Haas, NS, Aherrahrou, Z, and Schlotzer-Schrehardt, U, Ultrastructural changes in a murine model of graded Bruch membrane lipoidal degeneration and corresponding VEGF164 detection. *Invest Ophthalmol Vis Sci*, 2008;49(1):390-8.

272. Winkler, BS, Boulton, ME, Gottsch, JD, and Sternberg, P, Oxidative damage and age-related macular degeneration. *Mol Vis*, 1999;5:32.

273. van der Schaft, TL, Mooy, CM, de Bruijn, WC, Bosman, FT, and de Jong, PT, Immunohistochemical light and electron microscopy of basal laminar deposit. *Graefes Arch Clin Exp Ophthalmol*, 1994;232(1):40-6.

274. Bretillon, L, Thuret, G, Gregoire, S, Acar, N, Joffre, C, Bron, AM, Gain, P, and Creuzot-Garcher, CP, Lipid and fatty acid profile of the retina, retinal pigment epithelium/choroid, and the lacrimal gland, and associations with adipose tissue fatty acids in human subjects. *Exp Eye Res*, 2008;87(6):521-8.

275. Tserentsoodol, N, Gordiyenko, NV, Pascual, I, Lee, JW, Fliesler, SJ, and Rodriguez, IR, Intraretinal lipid transport is dependent on high density lipoprotein-like particles and class B scavenger receptors. *Mol Vis*, 2006;12:1319-33.

276. Li, CM, Presley, JB, Zhang, X, Dashti, N, Chung, BH, Medeiros, NE, Guidry, C, and Curcio, CA, Retina expresses microsomal triglyceride transfer protein: implications for age-related maculopathy. *J Lipid Res*, 2005;46(4):628-40.

277. Tserentsoodol, N, Sztein, J, Campos, M, Gordiyenko, NV, Fariss, RN, Lee, JW, Fliesler, SJ, and Rodriguez, IR, Uptake of cholesterol by the retina occurs primarily via a low density lipoprotein receptor-mediated process. *Mol Vis*, 2006;12:1306-18.

278. Eyden, B, Yamazaki, K, Menasce, LP, Charchanti, A, and Agnantis, NJ, Basement-membrane-related peri-vascular matrices not organised as a basal lamina: distribution in malignant tumours and benign lesions. *J Submicrosc Cytol Pathol*, 2000;32(4):515-23.

279. Eyden, B and Tzaphlidou, M, Structural variations of collagen in normal and pathological tissues: role of electron microscopy. *Micron*, 2001;32(3):287-300.

280. Bereczki, E, Gonda, S, Csont, T, Korpos, E, Zvara, A, Ferdinandy, P, and Santha, M, Overexpression of biglycan in the heart of transgenic mice: an antibody microarray study. *J Proteome Res*, 2007;6(2):854-61.

281. Westergren-Thorsson, G, Schmidtchen, A, Sarnstrand, B, Fransson, LA, and Malmstrom, A, Transforming growth factor-beta induces selective increase of proteoglycan production and changes in the copolymeric structure of dermatan sulphate in human skin fibroblasts. *Eur J Biochem*, 1992;205(1):277-86.

282. Westermann, D, Mersmann, J, Melchior, A, Freudenberger, T, Petrik, C, Schaefer, L, Lullmann-Rauch, R, Lettau, O, Jacoby, C, Schrader, J, Brand-Herrmann, SM, Young, MF, Schultheiss, HP, Levkau, B, Baba, HA, Unger, T, Zacharowski, K, Tschope, C, and Fischer, JW, Biglycan is required for adaptive remodeling after myocardial infarction. *Circulation*, 2008;117(10):1269-76.

283. Bereczki, E and Santha, M, The role of biglycan in the heart. *Connect Tissue Res*, 2008;49(3):129-32.

284. Westergren-Thorsson, G, Hernnas, J, Sarnstrand, B, Oldberg, A, Heinegard, D, and Malmstrom, A, Altered expression of small proteoglycans, collagen, and transforming growth factor-beta 1 in developing bleomycin-induced pulmonary fibrosis in rats. *J Clin Invest*, 1993;92(2):632-7.

285. Hunzelmann, N, Anders, S, Sollberg, S, Schonherr, E, and Krieg, T, Co-ordinate induction of collagen type I and biglycan expression in keloids. *Br J Dermatol*, 1996;135(3):394-9.

286. Sime, PJ, Sarnstrand, B, Xing, Z, Graham, F, Fisher, L, and Gauldie, J, Adenovirus-mediated gene transfer of the proteoglycan biglycan induces fibroblastic responses in the lung. *Chest*, 1997;111(6 Suppl):137S.

287. Rada, JA, Achen, VR, Penugonda, S, Schmidt, RW, and Mount, BA, Proteoglycan composition in the human sclera during growth and aging. *Invest Ophthalmol Vis Sci*, 2000;41(7):1639-48.

288. Ihanamaki, T, Salminen, H, Saamanen, AM, Pelliniemi, LJ, Hartmann, DJ, Sandberg-Lall, M, and Vuorio, E, Age-dependent changes in the expression of matrix components in the mouse eye. *Exp Eye Res*, 2001;72(4):423-31.

289. Nakashima, Y, Fujii, H, Sumiyoshi, S, Wight, TN, and Sueishi, K, Early human atherosclerosis: accumulation of lipid and proteoglycans in intimal thickenings followed by macrophage infiltration. *Arterioscler Thromb Vasc Biol*, 2007;27(5):1159-65.

290. Pentikainen, MO, Oorni, K, Lassila, R, and Kovanen, PT, The proteoglycan decorin links low density lipoproteins with collagen type I. *J Biol Chem*, 1997;272(12):7633-8.

291. Wagner, WD, Goldberg, IJ, Parthasarathy, N, and Bottoms, JD, Lipoprotein lipase enhances binding of decorin but not biglycan to low density lipoprotein. *Circulation.*, 1997;96:I-39-I-40.

LIST OF OWN PUBLICATIONS

Publications and presentations related to this thesis

1) Peer-reviewed publications

Sallo FB, Rechtman E, Peto T, Stanescu-Segall D, Vogt G, Bird AC, Fitzke FW. Functional aspects of drusen regression in Age-Related Macular Degeneration. Br J Ophthalmol. 2009 Jun 18. [Epub ahead of print] PMID: 19535356 [PubMed - as supplied by publisher] (IF 2.859)

Sallo FB, Bereczki E, Csont T, Luthert PJ, Munro P, Ferdinandy P, Sántha M, Lengyel I. Bruch's membrane changes in transgenic mice overexpressing the human biglycan and apolipoprotein b-100 genes. Exp Eye Res. 2009 Aug;89(2):178-86. Epub 2009 Mar 24. PMID: 19324038 (IF 2.579)

2) Presentations at national congresses

Sallo FB, Rechtman E, Peto T, Luong V, Bird AC, Fitzke FW. Functional testing of the macula in age-related macular disease. Poster presentation at the Annual Congress of the Hungarian Ophthalmological Society, Szeged, Hungary, June 9-11 2005.

3) Presentations at international congresses

Sallo FB, Luthert PJ, Munro P, Santha M, Bereczki E, Lengyel I. Changes in Bruch's Membrane of transgenic mice overexpressing ApoB100 and Biglycan proteins - implications for Age-Related Macular Degeneration. Annual Meeting of ARVO Ft. Lauderdale, April 27 - May 1, 2008 (Poster presentation)

Sallo FB, Rechtman E, Peto T, Luong V, Bird AC, Fitzke FW: Fine Matrix Mapping of Drusen and Non-Drusen Retinal Areas in Age-Related Maculopathy. Poster presentation (1399/B168), Annual Meeting of ARVO in Ft. Lauderdale, May 1-5, 2005.

4) Citable abstracts

F. B. Sallo, P. J. Luthert, P. Munro, M. Santha, E. Bereczki, and I. Lengyel: Changes in Bruch's Membrane of Transgenic Mice Overexpressing ApoB100 and Biglycan Proteins - Implications for Age-Related Macular Degeneration. Invest. Ophthalmol. Vis. Sci. 2008 49: E-Abstract 1754.

Sallo FB, Peto T, Rechtman E, Bird AC, Fitzke FW: A macula lutea funkcionális vizsgálata idoskori maculadegenerációban Szemészet, 142. Évfolyam (2005) I. Supplementum 1-140.

F.B. Sallo, E. Rechtman, T. Peto, V. Luong, A.C. Bird, and F.W. Fitzke: Fine Matrix Mapping of Drusen and Non–Drusen Retinal Areas in Age–Related Maculopathy. Invest. Ophthalmol. Vis. Sci. 2005 46: E-Abstract 1399.

Publications and presentations not immediately related to this thesis

1) Peer-reviewed publications

Sallo FB, Peto T, Leung I, Xing W, Bunce C, Bird AC. The International Classification system and the progression of age-related macular degeneration. Curr Eye Res. 2009 Mar;34(3):238-40. PMID: 19274532 (IF 1.519)

2) Presentations at national congresses

Hatvani I, **Sallo FB**. Ophthalmological aspects of dirofilarioses. Lecture at the CME conference of St Istvan University, Budapest, Hungary, November 6, 2004.

Hatvani I, **Sallo FB**: Living filarioid in the human vitreous. Congress of the Hungarian Ophthalmological Society 2002, Miskolc, Hungary

Bausz M, Sényi K, **Sallo FB**, Süveges I: Our conclusions from 15 years follow up of children operated with bilateral congenital cataract, SHIOL Keszthely, Hungary 2002

Sallo FB, Hatvani I: Pigment epithelial cysts of the pupillary rim of the iris causing transient blindness. SHIOL (Societas Hungarica ad Implantandam Oculi Lenticulam), 2002, Keszthely, Hungary

Hatvani I, **Sallo FB**, Axmann Á, Fok É, Albert M, Baska F: A case of intravitreal filarioidosis in Hungary. Joint Congress of the Hungarian Society of Parasitologists and the Hungarian Zoological Society 2002 Budapest, Hungary

Hatvani I, **Sallo FB:** Reposition of an encaptured IOL haptic SHIOL 2002, Keszthely, Hungary

Hatvani I, Czvikovszky Gy, **Sallo FB:** Refractive surgical procedures following penetrating corneal grafts. SHIOL 2001 Kaposvár, Hungary

Hatvani I., **Sallo FB**., Current place of glaucoma implants in our practice The 2nd National Congress of Ophthalmology of the Romanian Society of Ophthalmology, Sinaia, Romania 2001

Hatvani I, **Sallo FB**., A newly designed multifunctional intravitreal instrument The Congress of the Retina Section of the Hungarian Ophthalmological Society, 2001, Pécs, Hungary

Sallo FB, Czvikovszky Gy, Hatvani I Intraoperative examination of the retina using a rigid endoscope following removal of a luxated lens due to blunt trauma – „in vivo Miyake view" The Millennial Session of the Retina Section of the Hungarian Ophthalmological Society, 2000 Tihany, Hungary

3) Presentations at international congresses

Stanescu DM, Rechtman E, **Sallo FB**, O'Toole L, Luong V, Fitzke FW (4077/B435) The Photopic and Scotopic Visual Thresholds in Eyes With Solar Retinopathy: A Comparison With the Anatomical Damage. Poster presentation at the Annual Meeting of ARVO in Ft. Lauderdale, May 1-5, 2005

Stanescu D, Bonnel S, **Sallo FB**, Sahel J: CMV retinitis in Good Syndrome, EVER 2004. (poster presentation)

Sallo FB, Peto T, Dandekar S, Leung I, Bird AC: The International Classification System and progression of AMD, Annual Meeting of ARVO, Ft. Lauderdale, USA, May 4-8, 2003 (poster presentation)

4) Citable abstracts

D.M. Stanescu, E. Rechtman, **F. Sallo**, L. O'Toole, V. Luong, and F. Fitzke. The Photopic and Scotopic Visual Thresholds in Eyes With Solar Retinopathy: A Comparison With the Anatomical Damage. Invest. Ophthalmol. Vis. Sci. 2005 46: E-Abstract 4077.

F.B. Sallo, T. Peto, S. Dandekar, I. Leung, and A.C. Bird. The International Classification System and Progression of AMD. Invest. Ophthalmol. Vis. Sci. 2003 44: E-Abstract 1811.

Hatvani I, **Sallo FB**, Fok É, Baska F, Albert M: Élő filarioid az üvegtestben. Szemészet, 139. Évfolyam (2002) II. Supplementum 1-136.

ACKNOWLEDGEMENTS

I am deeply grateful to my Supervisor, Professor György Salacz for his unerring guidance, to Drs Tunde Peto and Imre Lengyel for their friendship, help and patronage through many years, to Professor Idlikó Süveges, the coordinator of the Ophthalmology Programme of the School of Doctoral Studies and Professor János Németh, Head of the Department of Ophthalmology of Semmelweis University for supporting this work. I would like to thank all my co-authors including Professors Alan C Bird, Philip J Luthert, Frederick W Fitzke and Glen Jeffery; Mr Peter Munro, Ms Irene Leung, Dr Erika Bereczki, Dr Miklós Sántha, Dr Dinu Stanescu-Segall, Dr Ehud Rechtman, Dr Gábor Vogt, Professor Péter Ferdinandy, Dr Tamás Csont, Ms Wen Xi, Ms Catey Bunce and Mr Vy Luong; working with you has indeed been an honour as well as a pleasure. Many thanks to Professor Edward M Rubin at the Life Sciences Division, Lawrence Berkeley Laboratory, University of California, Berkeley, CA, USA for his kind bequest of the transgenes used in our study and to Dr Rita Vámos, Ms Eszter Zaláni Kiss, Ms Tatiana Mansour, Ms Delna Mariner, Mr Dániel Somfai, Mr Tibor Fermon, Mr Istvan Toth for their technical and general support. And last but not least, I would like to thank God, my Family and all my Friends for making this possible!

APPENDIX

Coding Manual for the AMD Study Colour Photographs				
1. Photo quality	**2. Drusen size**	**ANSWER FOR DRUSEN SIZE Grade separately for each size Drusen**	**ZONE 1-3**	**ZONE 1 ONLY**
	Size	**Number**	**Crystalline Drusen**	**Serogranular Drusen**
	0. Absent	0. Absent	0. Absent	0. Absent
1. Perfect image (Perfect stereo)	1. Questionable	1. Questionable	1. Questionable	1. Questionable
2. Reasonable image (reasonable stereo)	2. **< 63µm** (hard drusen)	2. 1-9	2. 1-9	2. Present
3. Acceptable image (acceptable stereo)	3. **63µm-125µm** intermediate soft drusen	3. 10-19	3. >10	
4. Poor, but main features still gradable (Poor stereo)	**125-250 µm** 41 large semisolid distinct 42 large semisolid subconfluent 43 large semisolid confluent	4. 20-50		
5. Very poor image, no grading possible (no stereo)	**250-500 µm** 51 large semisolid distinct 52 large semisolid subconfluent 53 large semisolid confluent	5. >50		
6. Not centred, but grading of at least one zone possible	**>500 µm** 61 large semisolid distinct 62 large semisolid subconfluent 63 large semisolid confluent			
	7. Cannot grade - obscuring lesions	7. Cannot grade - obscuring lesions	7. Cannot grade - obscuring lesions	7. Cannot grade - obscuring lesions
	8. Cannot grade - photo quality	8. Cannot grade - photo quality	8. Cannot grade - photo quality	8. Cannot grade - photo quality
9. Missing	9. Missing	9. Missing	9. Missing	9. Missing

Coding Manual for the AMD Study Colour Photographs					
3. Hyper-pigmentation		**4. Hypo-pigmentation**	**Zone 1-3**	**5. Geographic Atrophy**	
Presence	**Type**	**Presence**	**Total area covered by drusen**	**5.1 presence: Zones 1, 2 and 3**	**5.3 Total area covered**
0. Absent	0. Absent	0. Absent	0. Absent	0. Absent	0. Absent
1. Questionable	1.Questionable	1.questionable	1. Questionable	1. Questionable	1. < 250µm
2. Present, < 63µm	2. linear	2. < 63µm	2. < 10%	2. Present	2. 250µm-500µm
3. Present, > 63µm	3. punctate	3. > 63µm	3. < 25%		3. 500µm -1000µm
	4. Mixed		4. < 50%		4. 1000µm-3000µm
	5. Peripapillary		5. ≥ 50%		5. 3000µm-6000µm
	6. Artefact				6. > 6000µm
7. Cannot grade - obscuring lesions	7. Cannot grade - obscuring lesions	7. Cannot grade - obscuring lesions	7. Cannot grade - obscuring lesions	7. Cannot grade - obscuring lesions	7. Cannot grade - obscuring lesions
8. Cannot grade - photo quality	8. Cannot grade - photo quality	8. Cannot grade - photo quality	8. Cannot grade - photo quality	8. Cannot grade - photo quality	8. Cannot grade - photo quality
9. Missing	9. Missing	9. Missing	9. Missing	9. Missing	9. Missing

Coding Manual for the AMD Study Colour Photographs					
6. Neovascular AMD					
6.1 presence	**6.2 Features**	**6.3 Scar/fibrous**	**6.4 Retinal haemorrhage**	**6.5 TOTAL area of Neovascular lesion**	**7.0 Predominant Phenotype**
0. Absent	0. Absent	0. Absent	0. Absent	0. Absent	0. Normal
1. Questionable	1. Questionable	1. Questionable	1. Questionable	1. < 250µm	1. Hard drusen only
2. Present	2. Hard exudates	2. Subretinal	2. Subretinal	2. 250µm-500µm	2. Soft drusen
	3. Serous neruro-retinal detachment	3. Preretinal	3. In plane of retina	3. 500µm -1000µm	3. GA
	4. Serous RPE detachment	4. Neovascular membrane	4. Sub-hyaloid	4. 1000µm-3000µm	4. Pigment Epithelial Detachment
	5. Haemorrhagic RPE detachment		5. Intravitreal	5. 3000µm-6000µm	5. CNV
				6. > 6000µm	6. Other
7. Cannot grade - obscuring lesions	7. Cannot grade - obscuring lesions	7. Cannot grade - obscuring lesions	7. Cannot grade - obscuring lesions	7. Cannot grade - obscuring lesions	7. Cannot grade - obscuring lesions
8. Cannot grade - photo quality	8. Cannot grade - photo quality	8. Cannot grade - photo quality	8. Cannot grade - photo quality	8. Cannot grade - photo quality	8. Cannot grade - photo quality
9. Missing	9. Missing	9. Missing	9. Missing	9. Missing	9. Missing

Coding Manual for the AMD Study FAF (cSLO) images				
1. Photo quality	**2. Predominant phenotype**	**3. Decreased Autofluorescence**	**4. Decreased Autofluorescence (total area)**	**5. Corresponding decreased Autofluorescence (colour)**
	0. Normal	0. Absent	0. Absent	0. Absent
1. Perfect image	1. Hard drusen only	1. Questionable	1. < 250µm	1. Geographic Atrophy
2. Reasonable image	2. Soft drusen	Unifocal well defined border 21. Homogeneous 22. Heterogeneous	2. 250µm-500µm	2. Neovascular lesion
3. Acceptable image	3. GA	Unifocal indistinct border 31. Homogeneous 32. Heterogeneous	3. 500µm-1000µm	3. Soft drusen
4. Poor, but main features still gradable	4. Pigment Epithelial Detachment	Multifocal well defined border 41. Homogeneous 42. Heterogeneous	4. 1000µm-3000µm	4. blood
5. Very poor image, no grading possible	5. CNV	Multifocal indistinct border 51. Homogeneous 52. Heterogeneous	5. 3000µm-6000µm	5. exudates
6. Not centred, but grading of at least one zone possible	6. Other	6. Normal decreased FAF at fovea	6. > 6000µm	6.edge
	7. Cannot grade - obscuring lesions	7. Cannot grade - obscuring lesions	7. Cannot grade - obscuring lesions	7. Cannot grade - obscuring lesions
	8. Cannot grade - photo quality	8. Cannot grade - photo quality	8. Cannot grade - photo quality	8. Cannot grade - photo quality
9. Missing	9. Missing	9. Missing	9. Missing	9. Missing

Coding Manual for the AMD Study FAF (cSLO) images			
6. Fovea involved in lesion	**7. Increased Autofluorescence**	**8. Corresponding increased autofluorescence (colour)**	**9. Background fluorescence**
0. Absent	0. Absent	0. Absent: no correspondence	0. Homogeneous
1. Questionable	1. Questionable	Corresponds with: 11. Scattered Drusen 12. Parafoveal drusen	1. Questionable
2. Yes	Within lesion/drusen 21: mottled 22: well defined focus 23: reticular pattern	2. Corresponds with RPE changes	2. Diffusely irregular
	Around lesion 31: focal 32: partial band (<50%) 33: band (>50%)	3. Edge of lesion	3. Focal increases
		4. Scar / fibrous	
		5. Detached retina (SRF)	
		6. Exudates	
7. Cannot grade - obscuring lesions	7. Cannot grade - obscuring lesions	7. Cannot grade - obscuring lesions	7. Cannot grade - obscuring lesions
8. Cannot grade - photo quality	8. Cannot grade - photo quality	8. Cannot grade - photo quality	8. Cannot grade - photo quality
9. Missing	9. Missing	9. Missing	9. Missing